DEVELOPMENT OF A NEW TENSILE STRESS

MODEL FOR EXPANSIVE SOILS

By

LIZHOU CHEN

Bachelor of Science in Geotechnical Engineering
Tongji University
Shanghai, China
1996

Master of Science in Civil Engineering
Michigan State University
East Lansing, Michigan
2007

Submitted to the Faculty of the
Graduate College of the
Oklahoma State University
in partial fulfillment of
the requirements for
the Degree of
DOCTOR OF PHILOSOPHY
December, 2015

DEVELOPMENT OF A NEW TENSILE STRESS

MODEL FOR EXPANSIVE SOILS

Dissertation Approved:

Dr. Rifat Bulut

Dissertation Adviser

Dr. Wilber Gregory

Dr. Xiaoming Yang

Dr. Qi Cheng

ACKNOWLEDGEMENTS

First of all, I would like to express my sincere thanks to Dr. Bulut, my advisor, for his invaluable advice, guidance and patience through my whole time at Oklahoma State University. I would have never developed a strong interest in research without his continuous help. His great support and kindness will be remembered deeply through my life.

Besides my advisor, I would like to thank the rest of my dissertation committee: Dr. Yang, Dr. Gregory, and Dr. Cheng, for their insightful comments and encouragement, but also for the hard questions which incented me to widen my research from various perspectives.

Last but not least, I thank my fellow researchers Yi Tian, Sruthi Mantri, Omar M. Amer and Er Yue for their help. My deepest gratitude goes to my parents, my wife, my daughter and son for their loves.

Name: Lizhou Chen

Date of Degree: DECEMBER, 2015

Title of Study: DEVELOPMENT OF A NEW TENSILE STRESS MODEL FOR EXPANSIVE SOILS

Major Field: Civil Engineering

Abstract: The problems associated with drying shrinkage are worldwide, and cause great damage to highways and buildings constructed on expansive soils. Literature review indicates that the development of shrinkage crack is governed by the principle of unsaturated soil mechanics. Suction increases as water content decreases. This leads to the increase of tensile stress, and cracks occur when tensile stress exceeds tensile strength. Currently, there is not an available model which describes the relationship between suction and tensile stress directly.

In this research, a new model for predicting tensile stress from suction is developed based on the Summarac's model (2004), Mitchell's model (1979) and assumption that soil is elastic and isotropic before cracking. The validity of the new model is demonstrated using finite element method (FEM) and experiment. In the analysis of FEM, the "Heat Transfer Model" in Abaqus is applied to calculate the profile of suction, and the "3-D Stress Model" is used to predict the distribution of tensile stress in the subgrade. The soil specimens were tested using two initial moisture boundary conditions for their drying shrinkage characteristics. The objectives in selecting the two initial moisture cases were to simulate the field conditions. In the first case, the specimens were tested in the drying experiment from close to a saturated moisture content. The purpose was to simulate a heavy rainfall in the subgrade soil. In the second case, the specimens were tested in the drying experiment from an initial optimum moisture content. The objective was to simulate the subgrade soil condition after compaction.

There are several applications of the new model in geotechnical practice such as the prediction of crack initiation from the soil water characteristic curve (SWCC), the estimation of crack depth for a given drying time, and the estimation of drying time for a specific crack depth. In this research, the depth of crack developing outside the pavement slab is estimated using the new model, and the performances of vertical moisture barrier and horizontal moisture barrier in presence of outside crack are analyzed and compared.

The new model incorporates the principles of unsaturated soil mechanics for the analysis of the formation of cracks in expansive soils, and provides theoretical foundation for future design and treatment of subgrade soils.

.

TABLE OF CONTENTS

Chapter Page

Chapter Page

Chapter Page

LIST OF TABLES

Table Page

Table Page

Table Page

LIST OF FIGURES

Figure Page

Figure Page

Figure Page

Figure Page

CHAPTER I

INTRODUCTION

1.1 Background

Expansive soils are found worldwide including the United States, Canada, Australia, China, India, and many other countries. In the United States, expansive soils cover approximately 20% of national area (Krohn and Slosson 1980). Distribution of expansive soils across the United State is shown in Figure 1.1 (Olive et al. 1989). The most important characteristic of expansive soils is the shrinkage during drying seasons and swelling in wetting seasons. The main reasons behind volume change with season are the mineral type, structure of expansive soils and moisture variations.

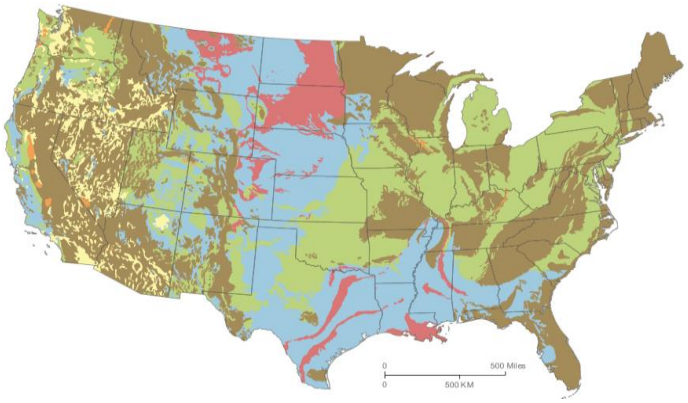

Note: Red color is the area with high concentration of expansive soils

Figure 1.1 Distribution of Expansive Soils in the U.S.A. (Olive et al. 1989)

The minerals contained in expansive soils are illite, kaolinite and montmorillonite which are the weathering products of two parent rocks: igneous rocks such as basalt and dolerite and sedimentary rocks like shale and marl (Donaldson 1973, Chen 1988). The main characteristic of those minerals is the large specific surface area. Chen (1988) presented that the specific surface areas of illite, kaolinite and montmorillonite are 65-180 m^2/g, 10-20 m^2/g and 50-840 m^2/g, respectively. It is noted that montmorillonite has the highest specific surface area, so the amount of the montmorillonite mineral directly controls the degree of expansion and shrinkage. The other characteristic is the negatively charged clay particle surfaces which can attract exchangeable ions and water molecules in the solution.

Due to its unique characteristics, expansive soils cause many problems. During the wetting seasons, the uplift pressure caused by the swelling of expansive soils could be more than 250kPa which can easily damage lightly-loaded or wood-frame structures (Rogers et al. 1993). In these cases, the soil movement at the edge of the foundation is usually larger than the movement in the center due to uneven distribution of water content. This uneven movement exacerbates the damage of foundations (Rogers et al. 1993). See Figure 1.2.

During the drying season, the shrinkage of expansive soils is the main reason behind the longitudinal cracks that initiate and propagate in the pavement. The soil under the pavement slab is much wetter than the soil outside the slab because the water movement is prevented across the pavement slab. The uneven distribution of the water content contributes to the uneven settlement of pavement during drying season, and leads to the development of longitudinal cracks (Jayatilaka et al. 1993; Puppala et al. 2010, and Bulut et al. 2014). See Figure 1.3.

In the United States, the cost to seal and repair cracks in road pavements is about $7-$15 billion annually by the reports published by Nuhfer et al. (1993) and Wray and Meyer (2004). The economic

loss due to expansive soils is as twice as the combined loss of hurricanes, tornados, floods and earthquakes (Wyoming Multi-Hazard Mitigation Plan 2011).

Figure 1.2 Structure Damage Due to Uneven Settlement (Retrieved from http://www.usinspect.com/insights/guides/expansive-soils US Inspect)

Figure 1.3 Cracks at Lake Hefner Site in Oklahoma City (Bulut et al. 2014)

1.2 Mechanism of the Development of Cracks

As shown in Figure 1.2 and Figure 1.3, cracks develop during the process of shrinkage or swelling in expansive soils, and leads to the reduction of serviceability life and the increase of maintenance cost. The field observations show that most of cracks initiate at the edge of the pavement or foundation where water content variations are great with the season. The shrinkage cracks in expansive soils have been an important topic in geotechnical engineering since 1930's (Chen 1988), and remarkable progress has been achieved since that time. Now, it is well established in the literature that the initiation of shrinkage cracks can be explained in the light of unsaturated soil mechanics (Ayad et al. 1997, Lytton et al. 2005, Luo and Prozzi 2008, Bulut et al. 2014).

In unsaturated soil mechanics, the three key parameters governing the development of cracks are water content, suction and tensile stress. The relationships among those parameters are introduced in the following sections.

1.2.1 Water Content

The reason behind the development of shrinkage cracks lies in the uneven distribution of water content. The water content of the soil below the groundwater table is constant (i.e., saturated water content), while it changes with the season for the soil above the groundwater table due to precipitation and evaporation. In addition, the existence of the pavement or foundation slab changes the pathway of water evaporation or infiltration because the pavement or foundation is usually regarded as an impermeable layer because of its low permeability. Usually, the water content below the pavement or foundation is higher than the water content outside pavement slab (EI-Garhy and Wray 2004, Luo and Prozzi 2009). Other surface covering conditions, such as vegetation, ditch and pre-existing crack, play a big role in the change of water content. All of those factors result in the non-uniform distribution of water content, which leads to the initiation of cracks when pavement or foundation is not strong enough to resist the uneven soil movement.

1.2.2 Soil Suction

Soil suction consists of two components: matric suction and osmotic suction. Soil suction is the negative stress in the pore water. The relationship between water content and suction has been widely investigated, and is described in terms of soil water characteristic curve (SWCC) in unsaturated soil mechanics (Gardner 1958, Brooks and Corey 1964, Van Genuchten 1980, Fredlund and Xing 1994). Based on experimental data and theoretical analysis, many models have been put forward by researchers such as Brooks and Corey (1964), Brutsaert (1967), Van Genuchten (1980) and Fredlund and Xing (1994). Some of the models are applied for a specific range of suction, and others are suitable for the whole range of suction (0.0 kPa to 10^6 kPa).

Suction reaches its maximum value in the drying season and minimum value in the wetting season. Figure 1.4 shows the suction envelope which includes three lines. The left line is the drying suction profile, the right line is the wetting suction profile and the middle one is the equilibrium suction line. Expansive soils swell in wetting season and shrink in drying season, so it leads to change of stress state in soil.

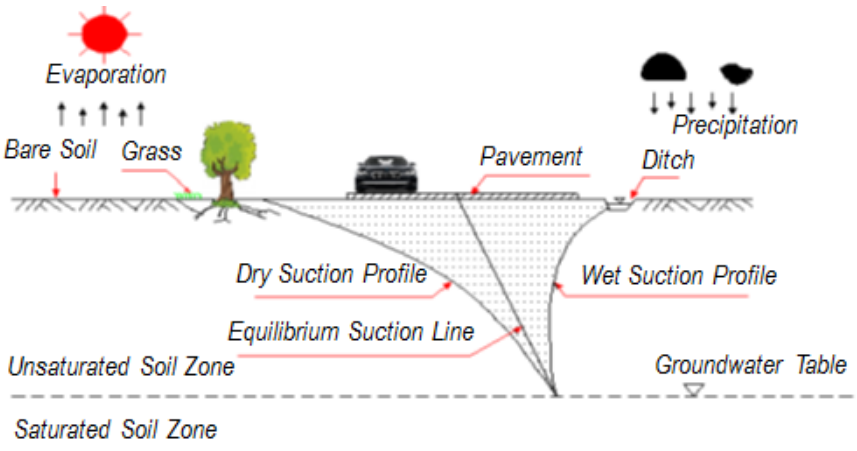

Figure 1.4 Suction Envelopes

1.2.3 Tensile Stress

The increase in suction causes the volume decrease of expansive soil. Correspondingly, tensile stress is induced. According to the model given in Lytton et al. (2005), the volumetric strain of expansive soils is due to two factors: overburden pressure (i.e., mechanical stress) and suction. Different from saturated soils, overburden pressure is small compared to suction that it can be ignored for the shallow depths of expansive soils (Luo and Prozzi 2009). Thus, the dominant factor to govern tensile stress in unsaturated expansive soils at shallow depths is suction.

Besides suction, other factors governing tensile stress in the soil are boundary conditions. Tensile stresses are not produced in the case where the soil can deform freely. Peron et al. (2009) confirms that the cracks do not initiate if the soil sample is not constrained during the process of desiccation. Similar conclusions were made by Luo and Prozzi (2009) and Kodikara et al. (1999). However, as stated by Kodikara et al. (2002) and Bulut et al. (2014), the shrinkage is restrained due to various factors, so the generation of tensile stress is unavoidable.

The reduction of water content leads to the increase of suction which causes the increase of tensile stress. Shrinkage crack develops when tensile stress exceeds the tensile strength of the soil.

1.3 Problem Statement

Expansive soils have been widely investigated in geotechnical engineering because of their great damages to pavements and foundations (Chen 1988), and significant progress has been achieved in many aspects of problems associated with expansive soils. Up to date, the relationship between water content and suction has been investigated and many models have been proposed. New techniques and devices have been developed to measure the suction from very low value (1.0pF) to high value (5.5pF). The effect of suction on tensile strength, the change of volume with suction, and various treatments have been widely studied.

However, there are still many problems in engineering practice dealing with expansive soils. In this research, the following two problems are investigated.

(1) The first problem is the relation between suction and tensile stress. The literature review reveals that little research is conducted to analyze the tensile stress in the soil. Currently, few models are available, and all of those models have their limitations. For example, Summarac (2004) proposed a model to calculate the tensile stress from water content. However, the decisive factor governing tensile stress is suction instead of water content. For instance, the increase of suction may be 50kPa for clay soils when water content is reduced by 1%, while it may be only 5kPa for sandy soils for the same reduction of water content. Another example is from Sih et al. (1968) who suggested that tensile stress is caused by overburden pressure and the changes in temperature and water content, but the effect of suction is still ignored in their model.

    Based on a comprehensive literature review, no direct work has been devoted to quantify the relationship between tensile stress and suction. As discussed above, suction and tensile stress are the two fundamental variables describing the crack development in expansive soils. To better understand the development of cracks, it is very important to establish a bridge between suction and tensile stress.

(2) The second problem is the effect of cracks developing outside the pavement slab on the performance of pavement in presence of moisture barriers. Due to its low cost and rapid construction, moisture barrier is one of the popular methods to deal with expansive soils. However, the performances of moisture barriers are not as good as our expectations in some cases. One of the reasons lies in the numerous outside cracks which become the pathways of infiltration and evaporation of the moisture in the soil. Hence, it is critical to investigate the damage due to outside cracks.

1.4 Objectives of Research

The purpose of the dissertation is to develop a new model which can be used to predict the tensile stress from suction. The tasks are listed as follows:

(1) Develop a new model to predict tensile stress from suction. The new model is based on the assumption that soil is an elastic and isotropic material before cracking (Sih et al 1968). The prediction of suction contained in the new model is obtained by the model proposed by Mitchell (1979).

(2) Verify the new model using finite element method. The validation includes two steps. Firstly, heat diffusion and moisture diffusion are governed by the same partial diffusion equation, so the "Heat Transfer Model" in Abaqus (finite element analysis software) is capable for calculating the distribution of suction. Secondly, using the output file containing the suctions from "Heat Transfer Model" as input file, the profile of tensile stress in subgrade is calculated by "3-D Stress Model" in Abaqus.

(3) Verify the new model by experiment. In order to adequately investigate the relation between suction and tensile stress, the designed experimental protocal consists of two parts. First part is to measure suction and tensile stress from the state close to saturation to the initiation of cracks. The purpose is to simulate the situation after heavy rainstorm. The second part is to measure suction and tensile stress from optimum water content to the initiation of cracks. Its purpose is to simulate the soil after compaction.

(4) Apply the new model to analyze the effect of outside cracks on the performance of pavement in presence of vertical moisture barriers and horizontal moisture barriers. If the parameters involved are given, then the distribution of tensile stress with depth can be obtained using the new model, and the crack depth can be determined. Then, the outside crack with known depth

and location is generated in the finite element model, and the changes of suction, tensile stress and displacement due to the crack are analyzed.

1.5 Significance of Research

(1) The new model will incorporate the principles of unsaturated soil mechanics for the analysis of the formation of cracks in expansive soils. As stated above, there is still no model available to depict the relation between suction and tensile stress directly. Therefore, the three fundamental variables (i.e., water content, suction and tensile stress) in unsaturated soil mechanics will be integrated together for the development of the new model.

(2) The new model can be applied to predict the initiation of crack using the SWCC of the soil. Tensile stress can also be predicted using the same SWCC. The location of crack initiation can then be obtained if the tensile strength of the soil is known.

(3) The new model can be used to estimate the drying time required for a specific crack depth or the crack depth for a specific drying time. In the new model, tensile stress is a function of the depth and drying time. Drying time can be estimated when the crack depth is known. Similarly, the crack depth can be obtained if the drying time is given.

(4) The application of the new model in analyzing the effect of outside crack on the performance of pavement in presence of vertical moisture barrier and horizontal moisture barrier shows that the new model can be used to guide the future design of pavement on expansive soils.

1.6 Organization of Dissertation

Chapter II reviews the basic terminologies in unsaturated soil mechanics and the state-of the-art methods to measure tensile stress. At first, the concept of soil suction and its component, moisture diffusion coefficient, suction compression index, soil water characteristic curve (SWCC) and the techniques for measuring suction are introduced. Secondly, this chapter reviews the advantages and

disadvantages of current methods for measuring tensile stress in soils. Those methods include Thin Film Test, Bench Scale Test, Temperature-Stress Testing Machine and Restrained Ring Test.

The objective of Chapter III is to develop a new model which setups the bridge between suction and tensile stress. Based on the Summarac's model (2004), Mitchell's model (1979) and the assumptions that soil is elastic and isotropic before cracking, the new model is put forward. The parameters affecting the profiles of suction and tensile stress are analyzed, and the main applications of the new model are presented.

In Chapter IV, Abaqus, a finite element analysis software, is used to verify the new model developed in Chapter III. The validation includes two steps. The first step is to use "Heat Transfer Model" to calculate the profile of suction under different boundary conditions, and the second step is to apply "3-D Stress Model" to predict the distribution of tensile stress with depth in subgrade.

Chapter V summarizes the experimental protocal which is designed to verify the new model. The experimental protocal includes two parts which simulate the two moisture states in geotechnical practice: soil after heavy rain and soil after compaction. The soil properties, specimen preparation and experiment setups are described. The techniques for measuring suctions and tensile stress are illustrated.

Chapter VI analyzes the data and results of experiments obtained from restrained ring testing. The chapter mainly includes two comparisons. The first comparison is between the measured suctions by filter method or tensiometer and the theoretical suction by Mitchell's model. The purpose is to verify that the suction from Mitchell's model is reasonable. The second comparison is between the measured tensile stress and the tensile stress predicted by the new model. The purpose is to verify the new model. In the end, the relationship between cracking time and diffusion coefficient, the validity of restrained ring method, and the change of diffusion coefficient with time are studied.

The purpose of Chapter VII is to study the effects of outside cracks on the performance of pavement

in presence of moisture barrier by means of finite element method. The depth of outside crack is predicted using the new model, and then the changes in suction, settlement and tensile stress with various crack depths are analyzed in the pavement with vertical moisture or horizontal moisture barrier. Also, the performance of horizontal moisture barrier is compared to the performance of vertical moisture barrier in the case of the same crack depth and the same moisture length.

Finally, Chapter VIII summarizes the main findings and contributions of the dissertation, and the recommendations for future research are also given.

CHAPTER II

LITERATURE REVIEW

2.1 Terminologies in Unsaturated Soil Mechanics

2.1.1 Total Soil Suction

The theory of soil suction was developed in the early of 20th century by Buckingham (1907), and its original purpose was to deal with the problems associated with soil-water-plant system. In 1950's, the Road Research Laboratory in England emphasized the importance of soil suction in explaining the behavior of unsaturated soil (Chen 1988). Since then, the concept of soil suction has been gradually accepted in geotechnical engineering.

Soil suction is defined as the free energy state of soil-water system, and is the negative stress in the pore water. The gradient of soil suction is the force which drives moisture from low suction zone to high suction zone. Based on the principle of thermodynamics, soil suction can be calculated in terms of partial vapor pressure proposed by Kelvin. See Equation [2.1].

$$h_t = \frac{RT}{V} ln(\frac{p}{p_o}) \qquad [2.1]$$

Where h_t= total suction; T= absolute temperature; R= universal gas constant; V= molar volume of the water; p= partial vapor pressure, and p_0= saturated vapor pressure of pure water.

Soil suction is usually represented in pF unit ($pF = log_{10}$ /$suction\ in\ cm\ of\ water$/). Table 2.1 lists the relationship between suction and typical consistency levels of the soil (Aubeny et al. 2003).

Table 2.1 Suction Levels at Typical Cases (Aubeny et al. 2003)

Case	Suction (pF)
Liquid limit	1.0 *
Wet limit for clays	2.5 *
Plastic limit for clays	3.5 *
Wilting point of vegetation	4.5 *
Tensile strength of confined water	5.3 *
Air dry	6.0 *
Oven dry	7.0

Note: * The suctions in the table are approximate values.

2.1.2 Matric Suction

Total suction consists of matric suction and osmotic suction. The development of matric suction is due to the meniscus at the air-soil interface caused by surface tension. There are several factors affecting matric suction which include the radius of meniscus curvature, the other is the degree of saturation and surface adsorptive forces. Matric suction increases with the increase of surface adsorptive forces, the decrease of soil particle size and the degree of saturation because all of them reduce the partial vapor pressure.

Matric suction can be conceptually described in terms of a capillary model. As shown in Figure 2.1, the upward capillary force is equal to the downward gravity of the water in the tube. The

height of capillary rise can be obtained by Equation [2.2]. Then, matric suction is the product of the height and water density. See Equation [2.3].

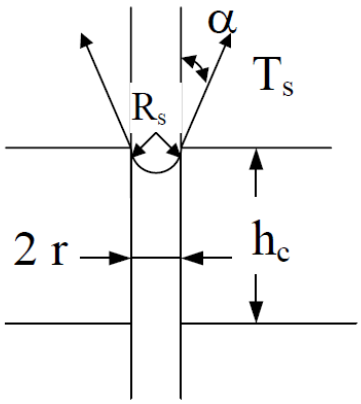

Figure 2.1 Capillary Force Model (Fredlund et al. 1993)

$$h_c = \frac{2T_s \cos\alpha}{\rho_w g r} \qquad [2.2]$$

Where h_c = height of capillary rise; T_s = surface tension; ρ_w = mass density of water; g = acceleration due to gravity; r = radius of capillary tube, and α = contact angle between tube and water.

Theoretically, matric suction can be obtained by Equation [2.3]. In engineering practice, it is impossible to measure millions of radii of soil particles and the contact angle α due to the complexity of soil structure. Usually, matric suction is measured in the soil using different methods such as filter paper, tensiometer, and thermocouple psychrometer.

$$u_a - u_w = \rho_w g h = \frac{2T_s \cos\alpha}{r} \qquad [2.3]$$

where $(u_a - u_w)$ =matric suction; u_a=pore-air pressure, and u_w=pore-water pressure.

2.1.3 Osmotic Suction

The other component of total suction is osmotic suction. Soil is the weathering product of rocks, so various ions, such as Na^{+} and Ca^{2+}, are unavoidably dissolved in soil solution. As the concentration of the ions in the soil solution increases, the vapor pressure of the soil solution decreases. This leads to the increase of osmotic suction.

Figure 2.2 shows a conceptual model to illustrate how osmotic suction is generated (Tindall and Kunkel 1999). The container in the middle of Figure 2.2 is divided into two parts by semi-permeable membrane. The left side is soil solution and the right side is pure water. In the case without any external pressure, pure water flows to soil solution through semi-permeable membrane due to the presence of ions in soil solution. In order to prevent the flow, excessive gas pressure, P, is exerted to the left side. The exerted pressure is equal to osmotic suction.

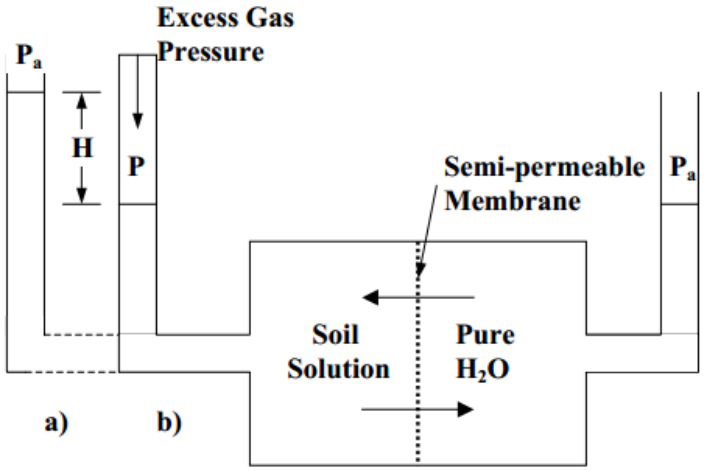

Figure 2.2 Osmotic Suction (Tindall and Kunkel 1999)

Osmotic suction values of different salt solutions at 25^0C are listed in Table 2.2 (Bulut et al. 2001). This table can be used to establish the calibration curve for the filter paper which will be used in the experimental program designed for this research.

Table 2.2 Osmotic Suctions for Salt Solutions in kPa (Bulut et al. 2001)

Osmotic Suctions at 25 °C							
Molality (m)	**NaCl**	**KCl**	**NH_4Cl**	**Na_2SO_4**	**$CaCl_2$**	**$Na_2S_2O_3$**	**$MgCl_2$**
0.001	5	5	5	7	7	7	7
0.002	10	10	10	14	14	14	14
0.005	24	24	24	34	34	34	35
0.010	48	48	48	67	67	67	68
0.020	95	95	95	129	132	130	133
0.050	234	233	233	306	320	310	324
0.100	463	460	460	585	633	597	643
0.200	916	905	905	1115	1274	1148	1303
0.300	1370	1348	1348	1620	1946	1682	2000
0.400	1824	1789	1789	2108	2652	2206	2739
0.500	2283	2231	2231	2582	3396	2722	3523
0.600	2746	2674	2671	3045	4181	3234	4357
0.700	3214	3116	3113	3498	5008	3744	5244
0.800	3685	3562	3558	3944	5882	4254	6186
0.900	4159	4007	4002	4384	6799	4767	7187
1.000	4641	4452	4447	4820	7767	5285	8249
1.200	5616	5354	5343	…	…	…	…
1.400	6815	6261	6247	…	…	…	…
1.500	…	…	…	6998	13397	7994	14554
1.600	7631	7179	7155	…	…	…	…
1.800	8683	8104	8076	…	…	…	…
2.000	9757	9043	9003	9306	20457	1021	22682
2.500	12556	11440	11366	11901	29115	14489	32776

2.1.4 Moisture Diffusion Coefficient

Moisture diffusion coefficient is an important parameter which governs the movement rate of moisture in unsaturated soils. One of the popular methods to measure diffusion coefficient in the laboratory was proposed by Mitchell (1979). Based on one dimensional flow, Mitchell (1979) measured the change of suction over time at a specific location of cylindrical soil sample whose surface was covered and one end was open to air. See Figure 2.3.

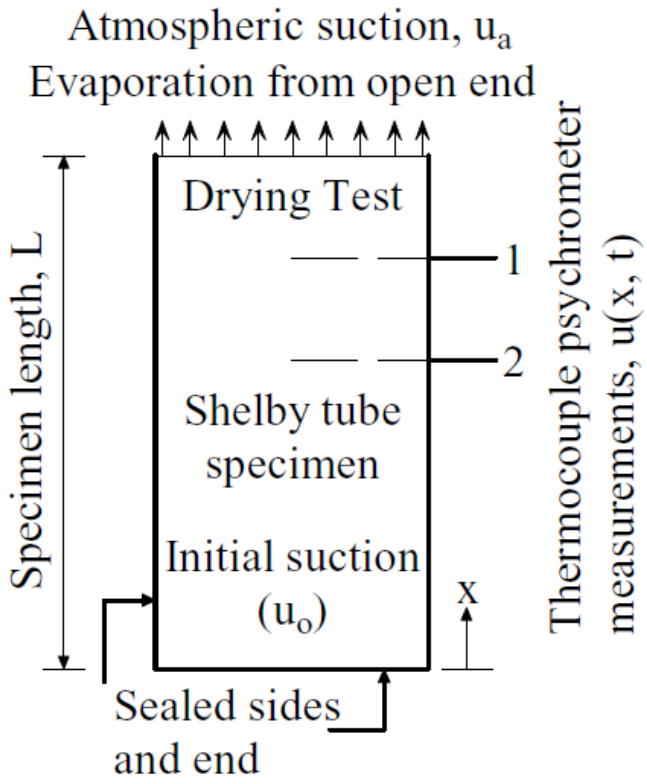

Figure 2.3 Drying Test of Mitchell's Method (Mabirizi and Bulut 2010)

Mitchell (1979) solved the one dimensional diffusion equation with known boundary conditions. See Equation [2.4]. The main limitation of Mitchell's method is that the diffusion coefficient is assumed constant over a small suction change, while Brooks and Corey (1964) suggested that the diffusion coefficient is a variable which changes with drying time and suction.

$$u(x,t) = u_a + \sum_0^\infty \frac{2(u_0 - u_a) sin z_n}{z_n + sin z_n cos z_n} exp\left(\frac{z_n{}^2 \alpha t}{L^2}\right) cos\left(\frac{z_n x}{L}\right) \quad [2.4]$$

where $u\,(x, t)$ = suction which is the function of time and position; x = distance from closed end; t = measured time; u_a = atmospheric suction; α = diffusion coefficient; z_n= solution of cot z_n = (z_n/h_eL); L= length of soil sample, and h_e = evaporation coefficient.

Diffusion coefficient can also be expressed as a function of the saturated permeability of the soil and the slope of soil water characteristic curve (Mitchell 1979). See Equation [2.5].

$$\alpha = \frac{k_0 h_0}{c} \frac{\gamma_w}{\gamma_d} \quad [2.5]$$

where k_o = permeability of saturated soil; h_o = a constant value of suction equal to 100 cm; γ_d = unit weight of dry soil; γ_w = unit weight of water, and c = slope of soil water characteristic curve (suction is displayed by logarithmic scale).

2.1.5 Suction Compression Index

Suction compression index describes the linear relationship between volumetric strain and change in suction in logarithmic suction. Based on the analysis of unsaturated soils, Fredlund and Rahardjo (1993) present that volume changes nonlinearly with suction, but does change linealy with the logarithmic suction. The model given in Lytton et al. (2005) also describes the linear relationship between volumetric strain and logarithm of stress and logarithm of suction. See Equation [2.6].

$$\frac{\Delta V}{V} = -\gamma_h log_{10}\left(\frac{u_f}{u_i}\right) - \gamma_\sigma log_{10}\left(\frac{\sigma_f}{\sigma_i}\right) - \gamma_\pi og_{10}\left(\frac{\pi_f}{\pi_i}\right) \quad [2.6]$$

where $\frac{\Delta V}{V}$ = volumetric strain; u_f, u_i = final matric suction and initial matric suction, respectively; σ_f, σ_i = final mechanical stress and initial mechanical stress, respectively; π_f, π_i = final osmotic suction and initial osmotic suction, respectively; γ_h = matric suction compression index; γ_σ = mechanical stress compression index, and γ_π = osmotic suction compression index.

Luo and Prozzi (2009) assumed that the volumetric strain due to mechanical stress could be ignored for pavements at shallow depths because it is small compared to matric suction. Also, the salt concentration of the soil solution is very low in most cases, so the volume change caused by osmotic suction can be neglected. In that case, the matric suction component plays a predominant role in the volume change of expansive soils at shallow depths. In this research, suction compression index is referred to matric suction compression index.

The suction compression index may be estimated by the chart developed by Mckeen (1981) as shown in Figure 2.4. In the method proposed by Mckeen (1981), Equation [2.7] and Equation [2.8] are applied to calculate activity ratio and cation exchange capacity, respectively. As shown in Figure 2.4, in total there are nine zones, and there is a specific volume change guide number (γ_0) for every zone. Volume change guide number is the suction compression index when clay content is 100%. Then the actual suction compression index is calculated by Equation [2.9].

$$A_c = \frac{PI\%}{\frac{\%-2micron}{\%-No.200\ sieve}\times 100} \quad [2.7]$$

$$CEC_c = \frac{CEC\frac{miliequivalents}{100\ gm\ of\ dry\ soils}}{\frac{\%-2\ micron}{\%-No.200\ sieve}\times 100} \quad [2.8]$$

$$\gamma_h = \gamma_0 \times \frac{\%-2micron}{\%-No.200\ sieve} \quad [2.9]$$

where A_c =activity ratio; $PI\%$ = plasticity index in percent; CEC = cation exchange capacity; γ_0 = volume change guide number of suction compression index, and γ_h = actual suction compression index.

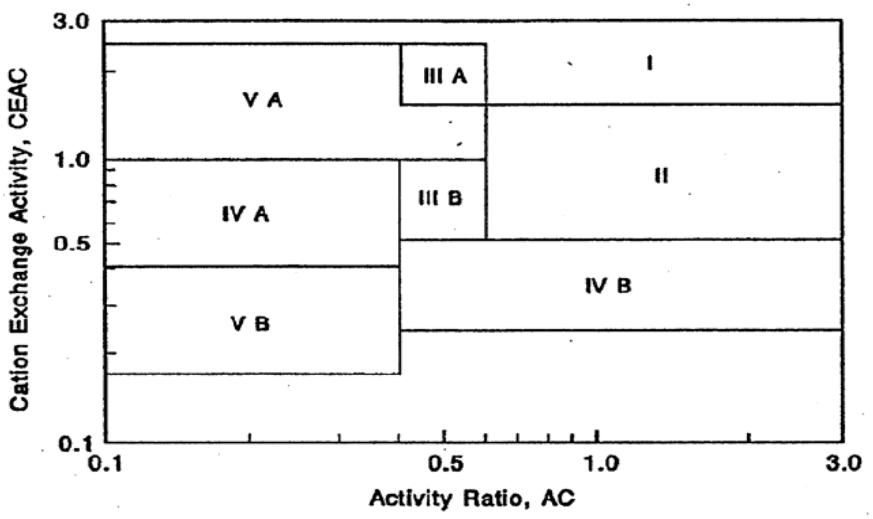

Figure 2.4 Prediction of Suction Compression Index (Mckeen 1981)

Covar and Lytton (2001) improved the Mckeen's method based on the analysis of 6500 soil data from Soil Survey Laboratory (SSL) of the National Soil Survey Center. Eight zones are created on the Casagrande's plasticity chart based on plasticity index and liquid limit of the soil (Figure 2.5), and a corresponding figure for every zone is generated to determine volume change guide number. For example, Figure 2.6 is the chart to determine γ_0 in Zone I. The actual suction compression index is obtained by Equation [2.9].

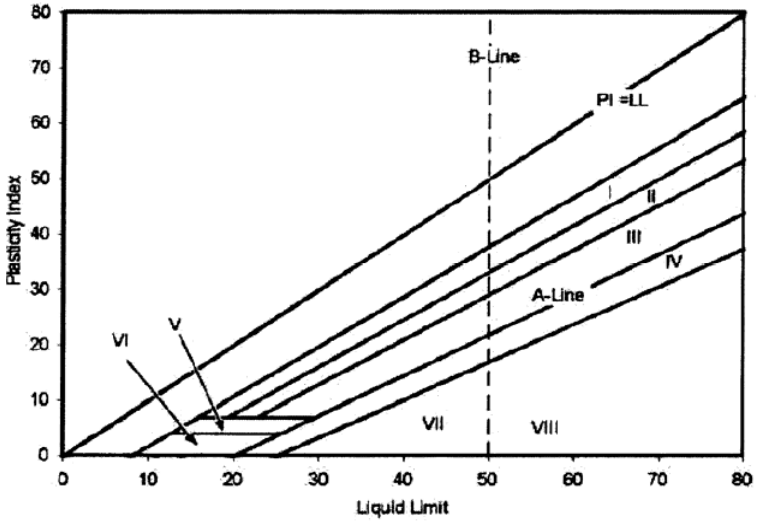

Figure 2.5 Soil Regions for Suction Compression Index (Covar and Lytton 2001)

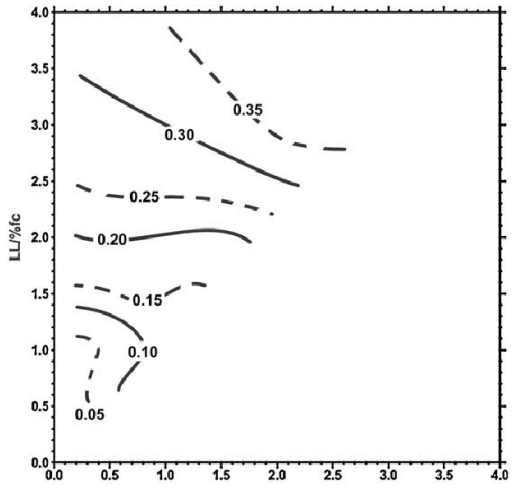

Figure 2.6 Zone I Chart for Determining γ_0 (Covar and Lytton 2001)

2.1.6 Soil Water Characteristic Curve (SWCC)

Soil water characteristic curve (SWCC) describes the change of suction with water content (Williams 1982). Usually, water content refers to gravimetric water content in geotechnical engineering, while it is mostly volumetric water content in soil science (Fredlund and Xing 1994). In some cases, the degree of saturation is used instead of water content in SWCC. Suction is matric suction or total suction in SWCC.

Figure 2.7 shows a typical soil water characteristic curve (Fredlund et al. 2011), and is divided into three zones: boundary effect zone, transitional zone and residual zone. All the pores in the soil are filled with water and the soil is in the state of saturation in the boundary effect zone, while the water content begins to gradually decrease and leads to the increase of suction in transitional zone, and the pore water is very difficult to remove in the residual zone (Vanapalli et al. 1996).

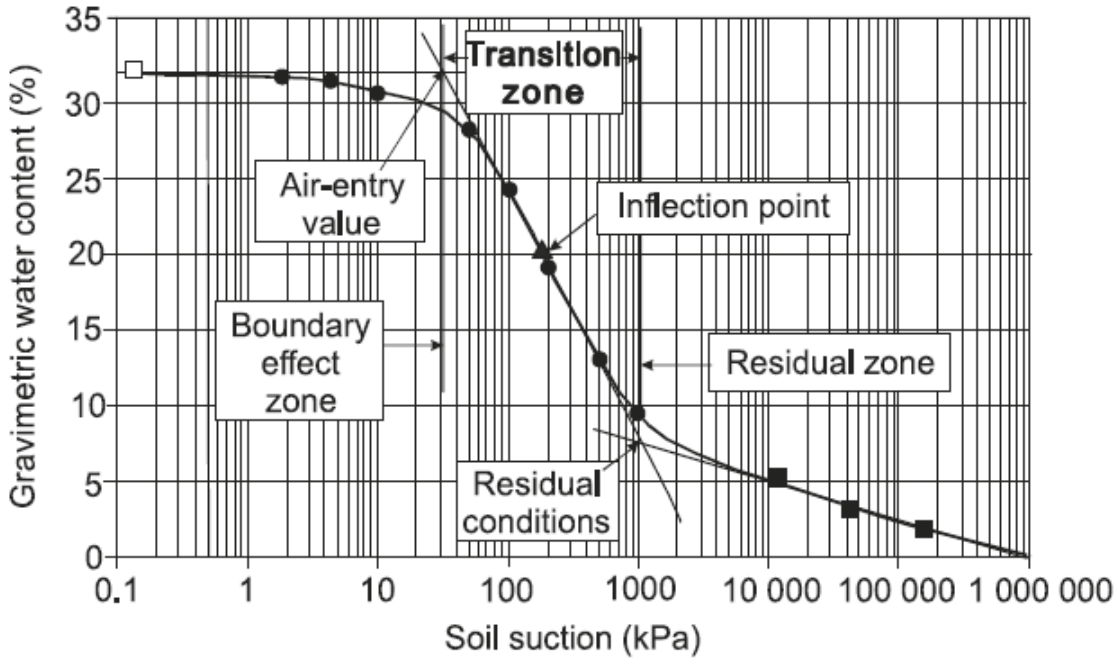

Figure 2.7 A Typical SWCC (Fredlund et al. 2011)

SWCC can be used in determining the shear strength, permeability and volume change of unsaturated soils (Fredlund and Xing 1994). Up to date, a large number of empirical models have been developed, and they can be grouped under three categories depending on the range of suction (Fredlund et al 2011). The first category is from zero suction to completely dry condition 10^6kPa; the second one is from air-entry value to residual value, and the last one is from air-entry value to completely dry. One model for every category is presented in the following paragraphs.

For the first category, the representative model, proposed by Pham and Fredlund (2005), is a combination of three phases which are from zero suction to air entry value, from air entry value to residual value, and from residual suction to theoretical maximum suction 10^6kPa. See Equation [2.10].

$$\begin{cases} w_1(\psi) = w_u - S_1 log(\psi) & 1 \le \psi \le \psi_a \\ w_2(\psi) = w_a - S_2 log\left(\frac{\psi}{\psi_a}\right) & \psi_a \le \psi \le \psi_r \\ w_3(\psi) = S_3 log\left(\frac{10^6}{\psi}\right) & \psi_r \le \psi \le 10^6 \end{cases} \quad [2.10]$$

where $w_1(\psi), w_2(\psi)$ and $w_3(\psi)$ = water content at boundary effect zone, transitional zone and residual zone, respectively; w_u *and* w_a = water content at 1kPa and air-entry value, respectively; S_1, S_2 *and* S_3 = slope of SWCC at boundary effect zone, transitional zone and residual zone, respectively, and ψ =suction.

The representative model of the second category is Gardner's model (1958) which is also one of the earliest models. See Equation [2.11].

$$\theta_w = \theta_r + \frac{\theta_s - \theta_r}{1 + (\frac{u_a - u_w}{a})^b} \quad [2.11]$$

where θ_w= volumetric water content; θ_r=residual water content; θ_s= saturated water content; a, b = matric suction value at a volumetric water content of $(\frac{\theta_r + \theta_s}{2})$ and the slope, respectively.

The representative model of the last category is also developed by Fredlund and Xing (1994). See Equation [2.12]. This model is one of the most widely accepted models in geotechnical engineering.

$$\theta(\psi, a_f, n_f, m_f) = C(\psi)\frac{\theta_s}{(\ln(e+\left(\psi/a_f\right)^{n_f})^{m_f}} \quad [2.12]$$

$$C(\psi) = 1 - \frac{ln(1+\psi/\psi_r)}{ln[1+(10^6/\psi_r)]}$$

where ψ =suction; θ = volumetric water content; θ_s = saturated water content; e= constant 2.718; $a_f, n_f \; and \; m_f$= three fitting parameters, and ψ_r = suction at residual value which varies from 1500kPa to 3000kPa depending on soil types.

2.2 Measurement of Soil Suction

To date, many techniques and devices have been developed to measure suction by researchers and geotechnical engineers. Table 2.3 lists suction component, measured range and equilibrium time for common techniques. However, suction measurement is still a challenging issue and almost every technique or method has its own limitation or shortcomings such as accuracy, cost or application range and so on. In this section, the basic working principles of tensiometer and filter paper are introduced subsequently because both of them are used in the experimental protocal designed to verify the new model in this research.

Table 2.3 The Summary of Suction Measurement
(Fredlund et al. 1993, Bulut et al 2001, Bulut and Leong 2008)

Suction	Techniques / Devices	Suction (kPa)	Equilibrium Time
Matric Suction	Jet-fill tensiometer	0-90	Several minutes
	UMS T5-10 tensiometer	0-160	Several minutes
	Null-typeaxis translation apparatus	0-1500	Several hours to days
	Electrical conductivity sensor	0-1500	6-50 hours
	Thermal conductivity sensor	10-1500	Hours to days
	In-contact filter paper	50-30000 (or higher)	5-14 days
Total Suction	Thermocouple psychrometer	300-7000	1hour
	Chilled-mirror hygrometer	500-30000	10 minutes
	Non-contact filter paper	50-30000 (or higher)	5-14 days
Osmotic suction	Pore-fluid squeezer	Entire range	days

2.2.1 Tensiometer

Tensiometer is a device which measures matric suction directly. As shown in Figure 2.8, a typical tensiometer consists of a high air-entry ceramic cup or porous cup, a tube and vacuum gauge. At first, the tube is filled with deaired water and the ceramic cup is fully saturated, and then the ceramic cup is slowly inserted into the soil. Matric suction can be read directly from the vacuum gauge when the ceramic cup and the tested soil reach equilibrium. There are sevaral advantages of using a tensiometer. First of all, unlike other methods such as the filter paper which is only used in the laboratory, the tensiometer can be used both in the laboratory and in field (UMS T5/T5x User Manual, Fredlund and Rahardjo 1993). Tensiometer does not require any calibration. Finally, suction can be obtained in a few minutes. As far as the limitation is

concerned, the air bubbles trapped in the tube result in the decrease of accuracy. Also, the tensiometer is only used in the wet soil due to its low measuring range. For example, the range of jet-fill tensiometer is 0-90kPa, and the range of UMS T5-10 tensiometer is 0-160kPa.

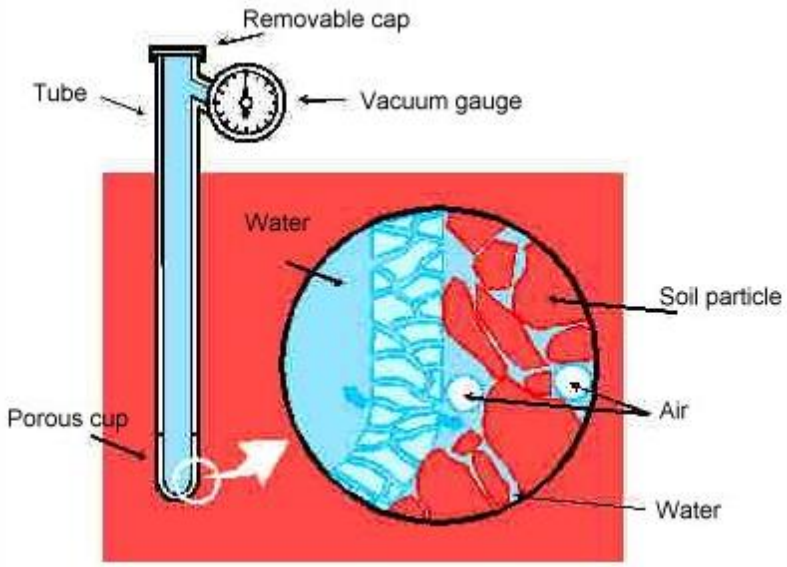

Figure 2.8 Tensiometer (Hegney and Hoffman 2005)

2.2.2 Filter Paper

Filter paper is another widely used technique which can measure total suction and matric suction depending on the condition of contact between the filter paper and soil. If the filter paper is not in contact with the soil sample, as shown in the top of Figure 2.9, then the water is exchanged in the vapor phase between the soil sample and filter paper. When they reach equilibrium, total suction is obtained by using the calibration curve which is established using the relation between osmotic suction and relative humidity (Bulut et al. 2001). If the filter paper is in contact with the soil sample, as shown in the bottom of Figure 2.9, then the filter paper can exchange the water in the liquid phase with the soil sample freely. Matric suction is obtained by the calibration curve when the filter paper and soil reach equilibrium. Due to the direct contact of the filter paper with the

soil, the time for matric suction is generally faster than the time for total suction (Rahardjo and Leong 2006). The main advantages of the filter paper method include the large range of measurement (50-30000kPa), reliability and low cost. The drawback is that filter paper is a time-consuming technique which often takes 7-14 days.

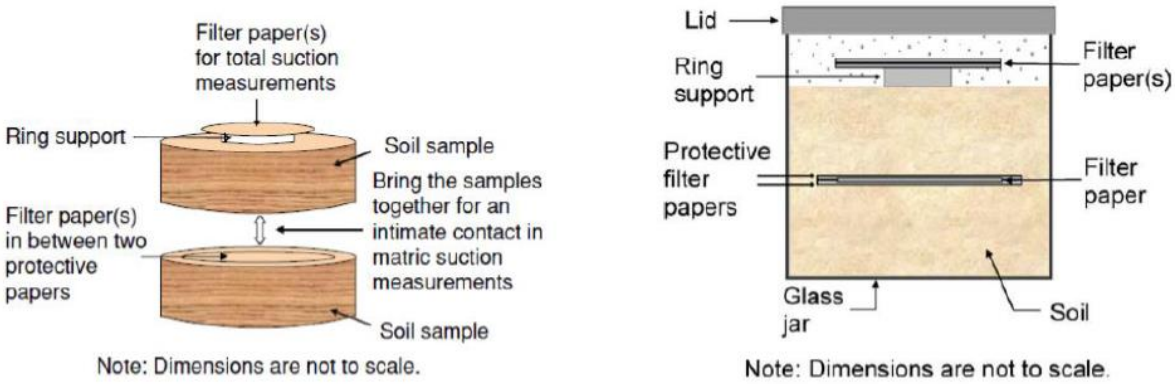

Figure 2.9 Filter Paper Method (Bulut and Wray 2005)

2.3 Measurement of Tensile Stress

The measurement of tensile stress is an important component for studying the relationship between suction and tensile stress in soils. There are four main methods to measure tensile stress based on a comprehensive literature review, and their working principles, advantages and limitations are introduced below.

2.3.1 Thin Film Test

Shinde et al. (2012) tested the tensile stress of expansive soils by measuring the deflection angle of a silicon wafer caused by the shrinkage of a thin clay layer with the help of laser beam. If the tensile stress induced by the shrinkage of thin film exceeds the critical value (tensile strength of the soil), then cracks nucleate and ultimately lead to the failure of the thin film. The apparatus is

depicted in Figure 2.10 in which L1 and L2 are incident and reflected laser rays, respectively.

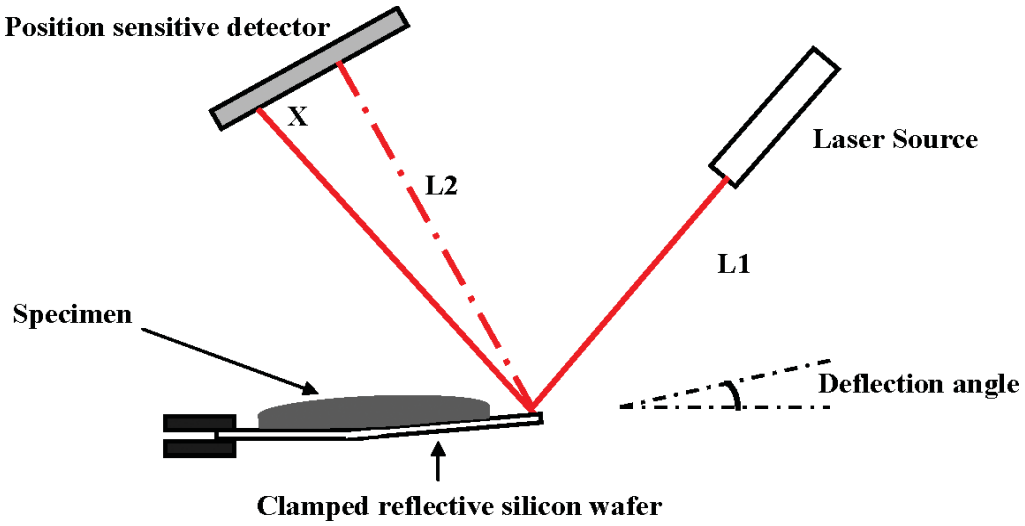

Figure 2.10 Thin film Test (Shinde et al. 2012)

A thin layer of clay (approximately 1.0mm) with different water contents is put on a thin silicon wafer with 15 mm length, 4.5 mm width and 158 um thickness. One end of the wafer is fixed and the other end is free, so the behavior of the wafer is similar to a cantilever beam. An incident laser beam (L1) is reflected by the wafer and then collected by a sensitive detector. The bending of the silicon wafer due to the shrinkage of the thin clay specimen causes a small movement of the reflected beam (L2) on the surface of the detector. Then, the small displacement is correlated to tensile stress which can be calculated by Equation [2.13].

$$\sigma_t = \frac{E_s t_s^3}{12 t_f(t) L_f [t_s + t_f(t)]} \tan^{-1}\left[\frac{X(t)}{L_{laser}}\right] \qquad [2.13]$$

where E_s = elastic modulus of silicon wafer; L_f = length of clay film; L_{laser} = length of the initially reflected laser ray; $X(t)$ = displacement of the laser beam on the surface of detector; $t_f(t)$ = thickness of clay film which decreases as time increases, t_s = thickness of silicon wafer, and t = time.

It seems that the thin film test is a complicated method because it is difficult to make a 1.0 mm thick sample and attach it to a small silicon wafer. Also, how the thickness of sample affects the testing results was not presented. The most important drawback of the thin film test lies probably in the difficulty in measuring the change of suction with water content or tensile stress due to the very small thickness of sample.

2.3.2 Bench Scale Test

Varsei et al. (2014) developed a new method to measure tensile stress during the desiccation of expansive soils at the University of Oklahoma. In the experiment, the soil sample is placed in a desiccation box with 25cm width and 30.5cm length. The rectangular box is divided into two equal halves: one half is fixed and the other half sits on some small ball bearings which are used to reduce the friction between the box and the supporting table. Some screws, placed at the end of the box wall and embedded into the soil, are used to prevent the soil from pulling away from the end during the drying process, and a teflon sheet is put under the soil bed to reduce the friction between the soil sample and box. Two load cells are installed to measure the tensile stress generated during the experiment. See Figure 2.10.

(a) Panorama of experiment

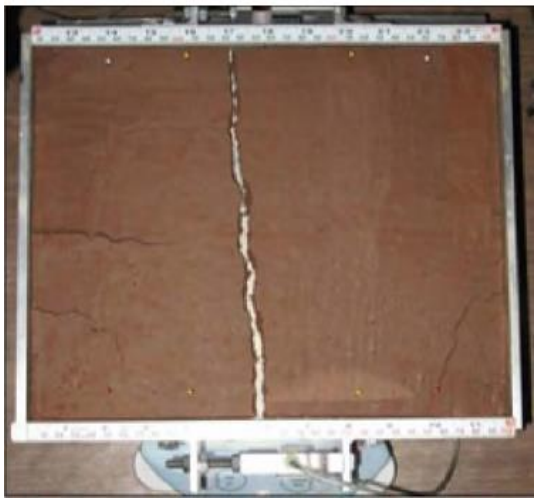

(b) Typical crack

Figure 2.11 Bench Scale Test (Varsei et al. 2014)

The desiccation box sits upon a large digital scale which is used to measure the change of water content. A high resolution camera, installed at the top of the sample, records the development of the cracks, weight of the soil sample and load cell readout. See Figure 2.11 (a). Because the soil sample is not allowed to move freely at the end of the box due to the installation of screws, a linear crack is expected to occur in the middle of the box where tensile stress reachs its maximum value. Figure 2.11 (b) shows a typical desiccation crack.

Bench scale test can measure the change of water content and tensile stress change with time. Its main limitation is that the accuracy cannot be guaranteed because the cross sectional area of the soil sample is taken as constant. As we know, the development of crack is a gradual process. At the very beginning, a shallow crack occurs at the surface of soil sample, and then the crack depth increases with drying time. Thus, the actual area subjected to tensile stress decrease as the time increases, and the measured tensile stress should be lower than the actual tensile stress. Another drawback is the assumption that the tensile stress along the path of the crack reaches its maximum value and is distributed uniformly everywhere at the time of the crack occurrence.

2.3.3 Temperature-Stress Testing Machine (TSTM)

TSTM has been widely used to test tensile stress of concrete since 1930's. For example, Davis et al.(1937), Blanks et al. (1938), Carlson (1938), Paillére et al. (1976) and Springenschmid et al. (1984) used TSTM to test tensile stress with different restraint conditions and cooling- heating temperature cycles. Figure 2.12 depicts a schematic drawing of a typical TSTM equipment.

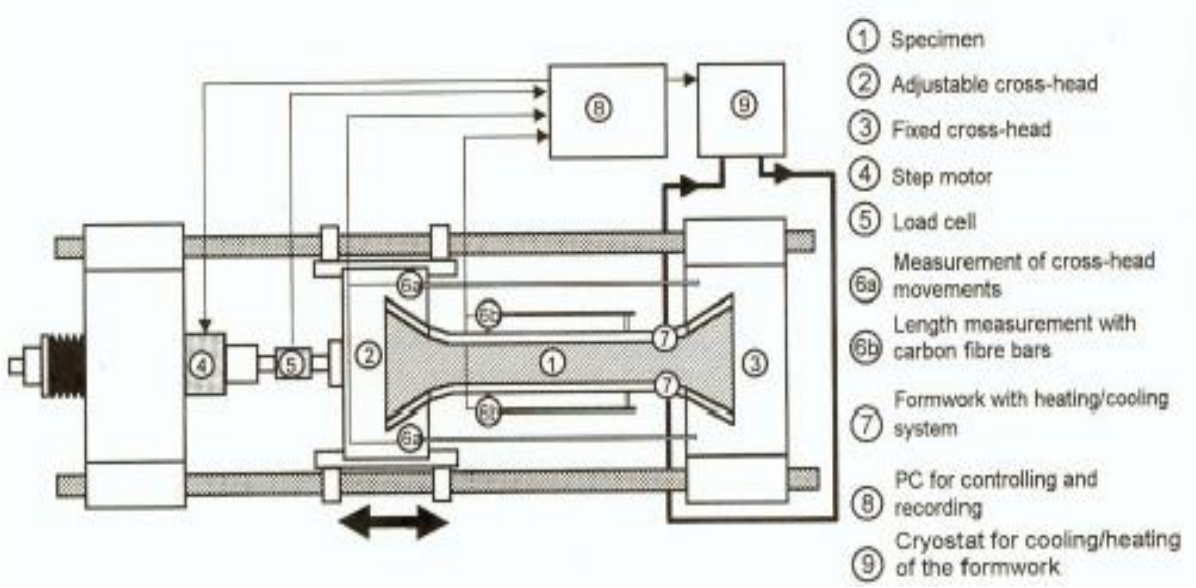

Figure 2.12 TSTM Equipment (Springenschmid et al. 1994)

A concrete specimen with cylindrical middle part and enlarged end parts is placed in TSTM. One end of the specimen is fixed, and the other end can move freely with the adjustable cross head. A load cell and LVDT are installed to measure the stress and the deformation caused by the change of temperature, respectively. The stress reaches its maximum value when cracks develop and the specimen fails.

It is found that the behavior of the expansive soil during drying is similar to the behavior of concrete which is subjected to the change of temperature since moisture diffusion in expansive soil is the same as the heat diffusion in concrete. If the soil sample has enough bending strength, then TSTM is an alternative way to measure the change of tensile stress in expansive soil.

2.3.4 Restrained Ring Test

Like TSTM, the restrained ring has been widely applied to assess the potential for early-age cracking in concrete, and now becomes a standard method of AASHTO and ASTM. The behavior of early-age concrete shrinkage is very similar to the desiccation of expansive soils, so the restrained ring is an alternative way to measure the change of tensile stress. Literature review reveals that Najm et al. (2009), Costa (2010), Amarisiri (2013) and Shannon et al (2015) are the forerunners to widen its application from early-age concrete to unsaturated soils, and they proposed that the restrained ring method might be the only effective method to depict the stress evolution due to natural load such as changes in temperature or water content.

The process of the restrained ring test is relatively simple. An inner restrained ring with specific dimension is made, and then the soil sample is placed into the ring. Minimum two strain gauges suggested by ASTM C-1581 or four strain gauges suggested by AASHTO are installed in the mid-height of the inside ring, and their directions of installation should be parallel to the circumference of the ring. Also, an outer ring is installed to hold the soil specimen. See Figure 2.13.

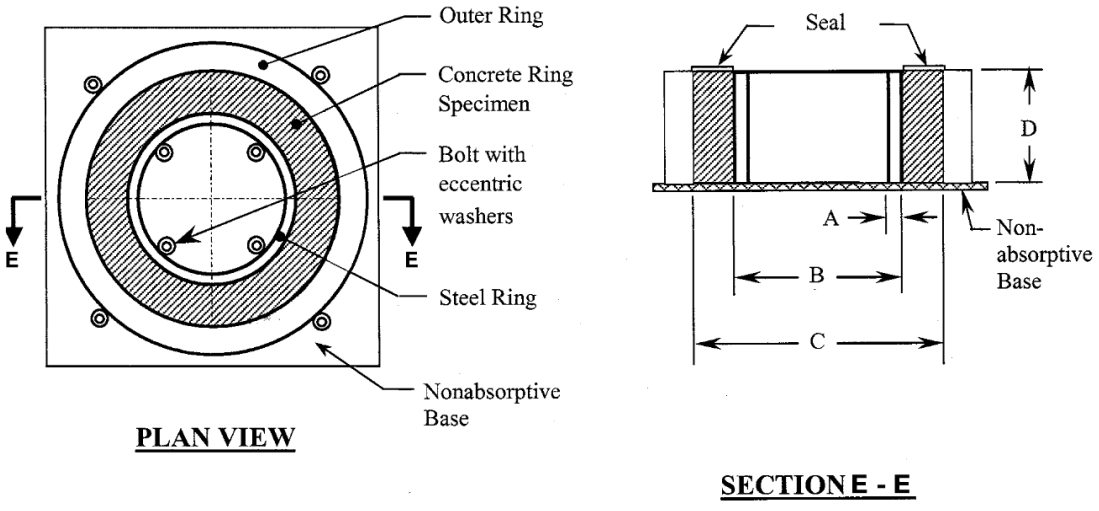

Figure 2.13 Restrained Ring (ASTM C-1581)

The pressure is induced between the soil sample and the inner restrained ring during the process of desiccation because the restrained ring prevents the shrinkage of the expansive soil. The stress in the inner restrained ring is measured by strain gauges, and then the tensile stress in the soil specimen can be back calculated by the solution of an elastic cylinder subjected to compressive stress (Weiss and Furgeson 2001).

The restrained ring testing method has several advantages. First of all, the device is simple and the preparation of the specimen is easy. Also, the mechanical concept of the model is clear and the equations to calculate tensile stress are simple and available. Most importantly, the restrained ring is a widely accepted method to evaluate the tensile stress of early-age concrete, and has become a standard method of AASHTO and ASTM, and has been used by several researchers for measuring the tensile stress generated in shrinking soils. Therefore, it is a very promising method in measuring tensile stress due to the similarity between early-age concrete and expansive soils.

2.3.5 Summary of Available Methods

The objectives of the experiment program in this research are to establish a relationship between tensile stress and suction, record the development of cracks, and investigate how suction and water content change with time. Thus, the desired experiment method should be able to measure tensile stress, suction, water content and record the development of cracks simultaneously.

As stated above, four main methods to measure tensile stress are thin film test, bench scale test, TSTM and restrained ring method. In this research, the restrained ring method is chosen due to the following reasons:

a) Thin film test. Sample preparation is difficult, and it is impossible to insert a 5.0mm tensiometer to a 1.0mm thick clay layer to measure suction.
b) Bench scale test. The measured tensile stress deviates from the actual tensile stress due to two reasons. One is that the area subjected to tensile stress is not constant, and the other

is that the distributions of tensile stress along the vertical direction and horizontal direction of the crack are not uniform.

c) TSTM. The specimen should have enough bending strength. Otherwise the specimen would possibly collapse or produce large deformation during the experiment. The other drawback is that there is no experience available with this device in expansive soils.

d) The restrained ring method. Due to its simple device, clear mathematical model, and available AASHTO and ASTM standards, the restrained ring method is selected. Also, it seems that the restrained ring method is the only method which can meet all of the requirements of this experiment (i.e., tensile stress, suction, water content and crack).

Different from previous researchers like Najm et al. (2009), Costa (2010) or Amarisiri (2013), the restrained ring method is modified to incorporate the measurement of suction in this research. For a soil sample close to the state of saturation, suction can be obtained directly from the tensiometer which is inserted into the soil sample. For a soil sample at optimum water content, suction can be obtained from the SWCC developed from the filter paper method.

2.4 Measurement of Tensile Strength

Compared to the measurement of tensile stress, the measurement of tensile strength is a relatively matured field and many methods have been developed. For instance, Bishop & Garga (1969) employed a triaxial testing apparatus to test the tensile strength of soils. As shown in Figure 2.14, the middle part of the specimen is cylindrical and two ends are enlarged. When compressive stress is applied, the specimen is pulled apart from the two enlargement ends, and it fails when the tensile strength is reached.

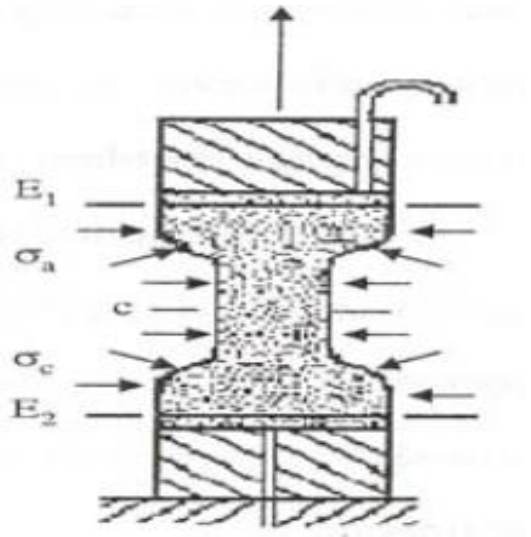

Figure 2.14 The Triaxial Device for Tensile Strength (Bishop and Garga 1969)

Another method to test for tensile strength is the Brazilian method proposed by Carneiro and Barcellos (1953). A cylindrical specimen is placed horizontally between two plane frames through which a compression load is exerted along the diameter. The tensile stress is generated inside the soil sample, and then tensile strength can be calculated by the load value and specimen geometry when the soil fails. See Figure 2.15.

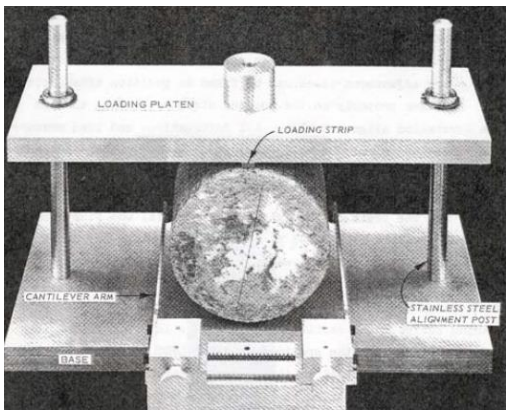

Figure 2.15 Brazilian Device for Tensile Strength (Carneiro and Barcellos 1953)

Also, Tang and Graham (2000) developed a direct method to test tensile strength of the soil. As shown in Figure 2.16, the soil sample is glued to a pair of special molds. The two halves of molds are pulled apart when tensile load is exerted, and then tensile strength is obtained when the soil sample is failed

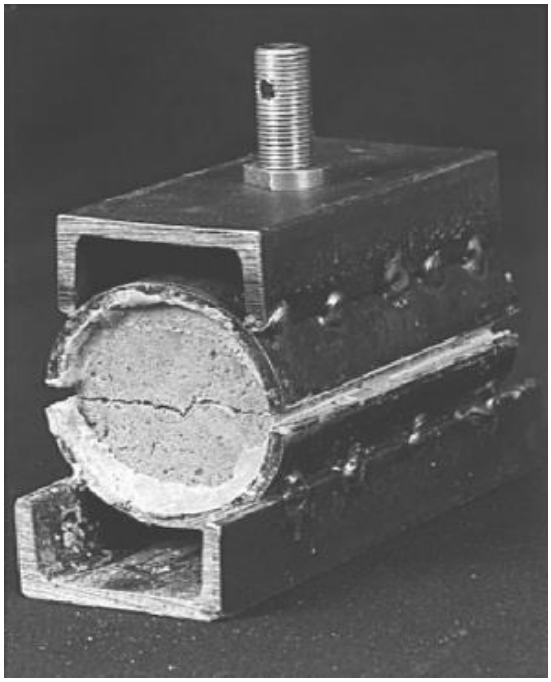

Figure 2.16 Direct Test of Tensile Strength by Tang and Graham (2000)

Based on the working principles described above, it is found that the common characteristic of those methods for tensile strength is to apply external load, and compressive stress or tensile stress is generated in the soil sample, and the sample is failed when tensile stress exceeds tensile strength.

One may wonder whether it is possible to use those tensile strength methods mentioned above to measure tensile stress or not. However, tensile stress is different from tensile strength in that tensile stress is an internal stress which is induced by the change of suction, and its nature is the

same as temperature stress. As Najm et al. (2009) stated, any method applying external load cannot measure the tensile stress due to the internal factor such as temperature and suction. Thus, those methods (i.e., triaxial device, Brazilian device and direct test) applying external loads are not suitable for measuring the tensile stress in expansive soils.

CHAPTER III

DEVELOPMENT AND APPLICATION OF A NEW MODEL

3.1 Introduction

In this dissertation study, a new mechanistic model is proposed for predicting tensile stresses from suction measurements. The comprehensive literature review indicates that the existing models are not devoted to quantifying the relationship between tensile stress and suction directly. Similar models proposed by Sih et al. (1968) and Summarac (2004) are based on water content and tensile stress relationship.

Sih et al. (1968) present that tensile stress is caused by the changes of temperature, water content and overburden pressure, and the model is based on the assumptions that soil is an elastic and isotropic material. Tensile stresses in y-direction and z-direction, shear stress in the yz-plane, as shown in Figure 3.1, can be obtained by Equation [3.1], Equation [3.2] and Equation [3.3], respectively (Sih et al. 1968). The coordinate system in the analysis is shown in Figure 3.1 where x-axis is longitudinal (traffic direction), y-axis is transverse and z-axis is vertical direction.

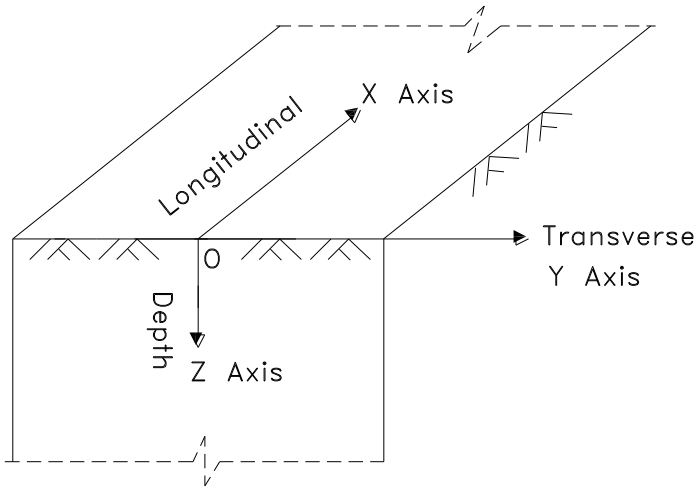

Figure 3.1 Coordinate System in the Model

$$\sigma_y = \frac{E}{1-\nu^2}[\varepsilon_y + \nu\varepsilon_z - \eta(1+\nu)(T-T_0) - \beta(1+\nu)(C-C_0)] \quad [3.1]$$

$$\sigma_z = \frac{E}{1-\nu^2}[\varepsilon_z + \nu\varepsilon_y - \eta(1+\nu)(T-T_0) - \beta(1+\nu)(C-C_0)] \quad [3.2]$$

$$\tau_{yz} = \frac{E}{2(1+\nu)}\gamma_{yz} \quad [3.3]$$

where $E\ and\ \nu$ = elastic modulus and Poisson's ratio, respectively;

$\varepsilon_y, \varepsilon_z\ and\ \gamma_{yz}$ = strain in y-axis, z-axis and yz-plane, respectively;

$\sigma_y, \sigma_z\ and\ \sigma_{yz}$ = stress in y-axis, z-axis, and yz-plane, respectively;

$T\ and\ T_0$ = final temperature and initial temperature, respectively;

$C\ and\ C_0$ = final water content and initial water content, respectively;

$\eta\ and\ \beta$ = thermal dilation coefficient and moisture shrinkage coefficient, respectively.

The strains in y-axis and z-axis would be zero (i.e., $\varepsilon_y = \varepsilon_z = 0$) if the half plane is initially unstrained (Summarac 2004). Also, T is equal to T_0 if there is no temperature change. Based on

the assumptions given above, the Sih's model was simplified into Equation [3.4] by Summarac (2004).

$$\sigma_y = \sigma_z = \frac{E}{1-\nu}\beta(C - C_0) \quad [3.4]$$

Carslaw and Jeger (1959) suggest that the distribution of moisture is governed by Equation [3.5] in terms of error function.

$$C = C_0\left(1 - erf\frac{z}{2\sqrt{\alpha t}}\right) \quad [3.5]$$

Summarac's model, given in Equation [3.6], is obtained by substituting Equation [3.5] into Equation [3.4].

$$\sigma_x = \frac{E}{1-\nu}C_0\beta\left(1 - erf\frac{x}{2\sqrt{\alpha t}}\right) \quad [3.6]$$

where α = coefficient of moisture diffusion in soil; x = depth; t = time, and $E,\ \nu,\ \beta\ and\ C_0$ = the same as above.

The Summarac's model describes the increase in tensile stress with the decrease of water content in the soil. However, based on the principles of unsaturated soil mechanics, the change in tensile stress must be represented in terms of suction instead of water content. For example, the increase of suction could reach 50kPa when the reduction of water content is only 1% in a clay soil, while it may only be 5kPa for the same reduction of water content in a sandy soil. Therefore, it is more desirable to establish the relationship between tensile stress and suction.

3.2 Development of the Tensile Stress Model

At any point in a soil layer, the state of stresses caused by mechanical pressure can be expressed in the matrix form below (Harry and Edward 1974).

$$\begin{bmatrix} \sigma_x & \tau_{xy} & \tau_{xz} \\ \tau_{yx} & \sigma_y & \tau_{yz} \\ \tau_{zx} & \tau_{zy} & \sigma_z \end{bmatrix}$$

where σ_x = normal mechanical stress in x-axis; σ_y = normal mechanical stress in y-axis; σ_z= normal mechanical stress in z-axis, $\tau_{xy}, \tau_{xz}\ and\ \tau_{yz}$ are shear stresses in xy-plane, xz-plane and yz-plane, respectively.

Besides mechanical stresses due to overburden pressure and external loads, there is another component of stress caused by matric suction in unsaturated soils. Similar to temperature stress, suction generates normal stresses, and do not generate shear stresses. The matrix below gives the suction stress u_w (Fredlund and Rahardjo 1993).

$$\begin{bmatrix} u_w & 0 & 0 \\ 0 & u_w & 0 \\ 0 & 0 & u_w \end{bmatrix}$$

Like the temperature strain, the strain due to suction can be expressed in Equation [3.7] (Mckeen 1981).

$$\varepsilon_u = \gamma_h \Delta u \qquad [3.7]$$

where, ε_u= strain due to suction, γ_h = suction compression index, and Δu = the change of suction.

Corresponding to two components of stresses (i.e., mechanical stress and suction), there are two components of strains in unsaturated soils which are mechanical strain and suction strain. The mechanical strain can be obtained using Hooke's law, and the suction strain can be obtained by Equation [3.7]. The total strain is the sum of the mechanical strain and suction strain, and can be obtained by Equation [3.8], [3.9] and [3.10] (Lai et al. 2009).

$$\varepsilon_x = \frac{1}{E}\left(\sigma_x - \nu\sigma_y - \nu\sigma_z\right) + \gamma_h \Delta u \qquad [3.8]$$

$$\varepsilon_y = \frac{1}{E}\left(\sigma_y - \nu\sigma_x - \nu\sigma_z\right) + \gamma_h \Delta u \quad [3.9]$$

$$\varepsilon_z = \frac{1}{E}\left(\sigma_z - \nu\sigma_x - \nu\sigma_y\right) + \gamma_h \Delta u \quad [3.10]$$

Luo and Prozzi (2009) states that the strains in horizontal directions (i.e., $\varepsilon_x \; and \; \varepsilon_y$) remain zero before the development of cracking due to the lateral constraints. This conclusion is confirmed by Konrad et al. (1997) based on the field observations. Therefore, Equation [3.8] can be rewritten as Equation [3.11].

$$\varepsilon_x = \frac{1}{E}\left(\sigma_x - \nu\sigma_y - \nu\sigma_z\right) + \gamma_h \Delta u = 0 \quad [3.11]$$

Based on the assumption that soil is an elastic and isotropic material before cracking, the stress in x-axis is equal to the stress in y-axis in a horizontal plane (i.e., $\sigma_x = \sigma_y$). Substituting $\sigma_y = \sigma_x$into Equation [3.11], the tensile stress in unsaturated soils is obtained. See Equation [3.12].

$$\frac{1}{E}(\sigma_x - \nu\sigma_x - \nu\sigma_z) + \gamma_h \Delta u = 0$$

$$\sigma_x = \frac{\nu\sigma_z}{1-\nu} - \frac{E}{1-\nu}\gamma_h \Delta u \quad [3.12]$$

The change of suction in Equation [3.12] can be obtained by Mitchell's model as shown in Equation [3.13].

$$\Delta u = u - u_0 = (u_f - u_0)(1 - erf\,\frac{z}{2\sqrt{\alpha t}}) \quad [3.13]$$

Finally, the tensile stress in unsaturated soils, given in Equation [3.14], is obtained by substituting Equation [3.13] into Equation [3.12].

$$\sigma_x = -\frac{\nu\sigma_z}{1-\nu} + \frac{E}{1-\nu}\gamma_h \Delta u = -\frac{\nu\sigma_z}{1-\nu} + \frac{E}{1-\nu}\gamma_h (u_f - u_0)(1 - erf\,\frac{z}{2\sqrt{\alpha t}}) \quad [3.14]$$

Where, σ_x=tensile stress, ν= Poisson's ratio; σ_z= mechanical stress due to overburden pressure ($\sigma_z = \gamma z$, γ= unit weight of the soil), z = depth, E = elastic modulus, u_f= final surface suction, u_0 = initial suction, γ_h= suction compression index, α= diffusion coefficient, and t= drying time.

The new model, Equation [3.14], consists of two terms. The first term is to calculate the tensile stress from mechanical stress, and the second term is to calculate the tensile stress from suction. It must be noted that the sign of the first term is negative and the sign of the second term is positive. This means that overburden pressure reduces tensile stress while suction increases tensile stress. In other words, overburden pressure is helpful to prevent the development of crack.

On the other hand, cracks always initiate at shallow depths during the process of desiccation in clay soils. In this case, the contribution of mechanical stress to tensile stress is very small while the contribution of suction is dominant.

For example, given that ν =0.3, $\gamma = 18\,kN/m^3$, $z = 0.5m$, $(u_f - u_0)\left(1 - erf\frac{z}{2\sqrt{\alpha t}}\right) = 0.2$, $E = 5000kPa$, and $\gamma_h = 0.03$. As shown in the following calculations, the tensile stress is $-3.9kPa$ due to mechanical stress, while it is +42.9kPa due to suction. The tensile stress due to overburden pressure is only 9% of the stress due to suction (i.e. $3.9kPa$/ $42.9kPa$=9 %). Therefore, for the cases where soils are located at shallow depths, the first term can be ignored for practical purposes and the result is on the safe side.

$$\sigma_x = -\frac{\nu\sigma_z}{1-\nu} = -\frac{0.3\times 18kN/m^3\times 0.5m}{1-0.3} = -3.9kPa$$

$$\sigma_x = \frac{E}{1-\nu}\gamma_h \Delta u = \frac{5000}{1-0.3}\times 0.03 \times 0.2 = 42.9kPa$$

Another point worth to point out is that elastic modulus is assumed as constant in calculating tensile stress. Many researchers, like Varsei et al (2014) and Chertkov (2002), present that cracks start to occur when water content is slightly changed from close to saturated moisture state. The

purpose of Equation [3.14] is used to calculate the tensile stress before cracking, so it is reasonable to assume that elastic modulus and Poisson's ratio stay constant during the small range of water content.

3.3 Effect of Parameters on the Suction Profile

The new model, Equation [3.14], depicts the relationship between suction and tensile stress. Before fully understanding the change of tensile stress, it is necessary to understand the change of suction. The main parameters in Mitchell's model (i.e., Equation 3.13) for obtaining suction profile include final surface suction and initial suction, drying time and diffusion coefficient. In the parametric analysis, initial suction is assumed to be 3.5pF, and the other parameters are varied from maximum values to minimum values as shown in Table 3.1.

Table 3.1 The Ranges of Parameters in Suction Analysis

Parameters	Minimum	Maximum	Unit
Final surface suction	3.5	4.5	pF
Drying time	1	6	month
Diffusivity coefficient	1.0×10^{-7}	1.0×10^{-3}	cm^2/sec

Figure 3.2 gives the suction profile using Equation [3.13] by increasing the final surface suction from 3.5pF to 4.5pF in 0.2pF increments when diffusion coefficient is $5.0 \times 10^{-5}\, cm^2/s$ and drying time is 3 months. It can be seen in Figure 3.2 that suction greatly reduces with the increase of depth. The depth to constant suction is around 0.8m, and is not significantly affected by final surface suction. Also, it is found that the final surface suction only affects the suction values at shallow depths.

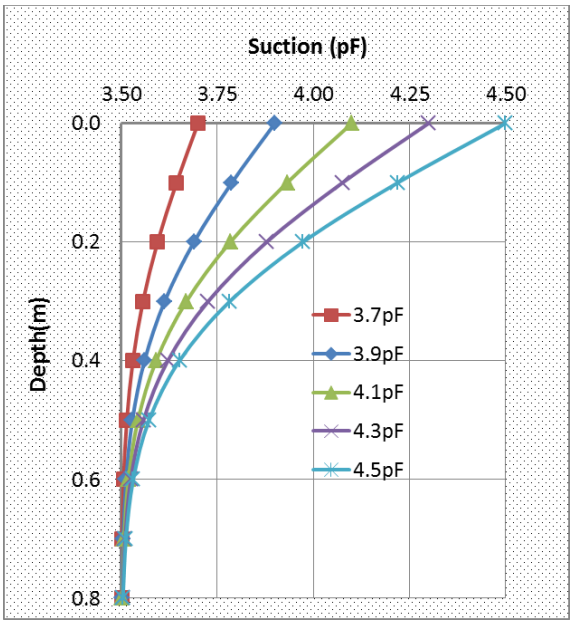

Figure 3.2 Suction Distributions with Depth at Different Final Suctions

Figure 3.3 depicts the influence of drying time on the profiles of suction while considering a constant surface suction of 4.5pF and a diffusion coefficient of $5.0 \times 10^{-5} cm^2/s$. In this analysis, the drying time increases from 1 month to 6 months in 1 month increment. Figure 3.3 shows that the envelopes of suction expand laterally with the increase of the drying time. Also, the depth to constant suction increases with the drying time. For instance, the depth to constant suction is 0.40m for 1 month drying time, while it increases to 1.0m for 6 months drying time.

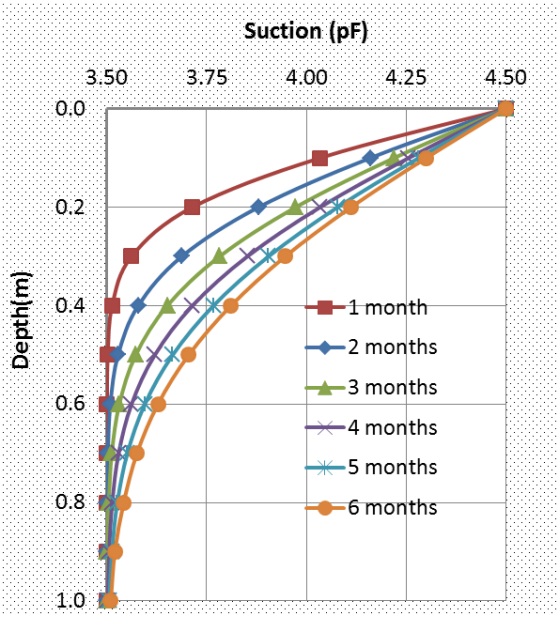

Figure 3.3 Suction Distributions with Depth at Different Drying Times

The last parameter studied here is the diffusion coefficient. The effect of the diffusion coefficient on the profile of suction is undertaken at constant final surface suction of 4.5pF and 3 months drying time. Diffusion coefficient increases from $1.0 \times 10^{-7}\, cm^2/s$, which represents a tight and uncracked soil, to $1.0 \times 10^{-3}\, cm^2/s$, which represents a loose or cracked soil, with the increment of 10 times. Figure 3.4 describes the change of suction with diffusion coefficient.

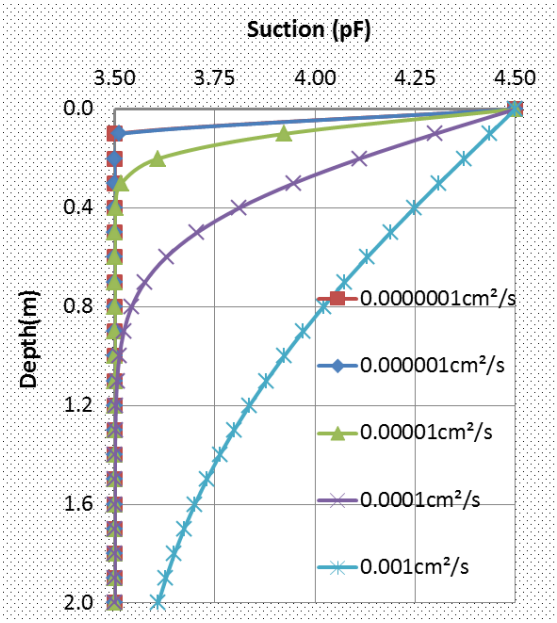

Figure 3.4 Suction Distributions with Depth at Different Diffusion Coefficients.

As shown in Figure 3.4, diffusion coefficient exerts the greatest influence on the profiles of suction among the three parameters (i.e., drying time, final surface suction and diffusion coefficient). The depth to constant suction is 0.10m for $1.0 \times 10^{-6}\, cm^2/s$ diffusion coefficient, while it is greater than 2.0m for $1.0 \times 10^{-3}\, cm^2/s$ diffusion coefficient. As we know, the development of cracks can significantly increase the diffusion coefficient. This leads to the increase of the depth to constant suction. Therefore, it is critical to control the development of cracks in pavements.

3.4 Effect of Parameters on the Profile of Tensile Stress

A parametric study is undertaken to evaluate Equation [3.14] for predicting the tensile stress profiles in the subgrade soils. The first term in Equation [3.14] is the tensile stress which is caused by overburden pressure. As stated above, the tensile stress due to overburden pressure is very small for shallow soil depths. In this parametricanalysis, the first term in Equation [3.14] is not considered.

The main parameters in the second term of Equation [3.14] are the diffusion coefficient, drying time, elastic modulus, Poisson's ratio, suction compression index, final surface suction and initial suction. Initial suction is fixed at 3.5pF and Poisson's ratio is 0.3 in the analysis, and the other parameters change over minimum and maximum ranges as shown in Table 3.2.

Table 3.2 The Range of Parameters in the Analysis of Tensile Stress

Variable	Minimum	Maximum	Unit
u_f	3.7	4.5	pF
t	1	6	month
α	1.0×10^{-7}	1.0×10^{-3}	cm^2/sec
E	3000	10000	kPa
γ_h	0.01	0.08	N/A

Furthermore, rather than analyzing the effect of each parameter in Equation [3.14] independently, some of the parameters are combined to reduce the number of variables in the parametric study. Therefore, the "$\frac{E}{1-\nu}\gamma_h(u_f - u_0)$" is taken as a single variable "k", and the "αt" term is considered another term "m".

One may question that the sensitivity analyses of "m" and "k" parameters will be affected if the two variables are dependent. As discussed above, the elastic modulus and Poisson's ratio are assumed to be constant, so the variable "k" including the elastic modulus and Poisson's ratio does not change with the variable "m" containing the drying time. In other words, k and m are independent.

The minimum and maximum values of "k" and "m" parameters can be obtained by substituting the values of the variables in Table 3.2 as shown in the calculations below.

$$\mathrm{k_{min}} = \frac{E\gamma_h}{1-\nu}(u_f - u_0) = \frac{3000*0.01}{0.7} \times 0.2 \approx 9 \text{ kPa}$$

$$\mathrm{k_{max}} = \frac{E\gamma_h}{1-\nu}(u_f - u_0) = \frac{10000*0.08}{0.7} \times 1.0 \approx 1143\ kPa$$

$$\mathrm{m_{min}} = \alpha \mathrm{t} = 1.0 * \frac{10^{-7}\mathrm{cm}^2}{\mathrm{sec}} * 1\ \text{month or}\ (1 * 30 * 24 * 3600)\mathrm{sec} = 0.2592\mathrm{cm}^2$$

$$\mathrm{m_{max}} = \alpha \mathrm{t} = 1.0 * \frac{10^{-3}\mathrm{cm}^2}{\mathrm{sec}} * 6\ \text{month or}\ (6 * 30 * 24 * 3600)\mathrm{sec} = 15552\mathrm{cm}^2$$

Figure 3.5 gives the profile of tensile stress using Equation [3.14] by increasing the "k" value from 10kPa to 1000kPa while the "m" value is fixed at 389 cm^2 which is the product of 3 months drying time and 5.0 × 10^{-5} cm^2/sec diffusion coefficient. Figure 3.5 shows that the maximum tensile stress increases from 10kPa to 1000kPa when the "k" value increases from 10kPa to 1000kPa. This means that the combination of suction compression index, the difference between final surface suction and initial suction, and elastic modulus and Poisson's ratio controls the maximum tensile stress. Secondly, the depths to zero tensile stress do not change with the k value. In all of the curves in Figure 3.5, the depths to zero tensile stress are approximately 0.75m.

In fact, some of the maximum tensile stresses shown in Figure 3.5 are not realized because the cracks occur when the tensile stress reaches the tensile strength of the soil.

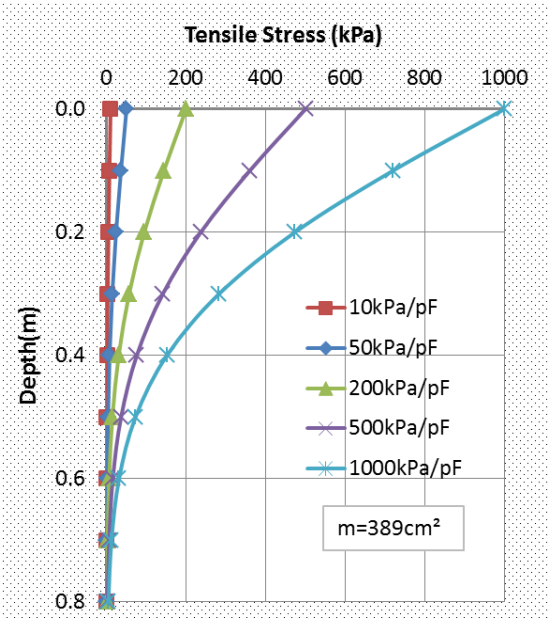

Figure 3.5 Sensitivity Analysis of the "k" Parameter

Figure 3.6 depicts the effect of various m values on the profile of tensile stress while the "k" value is fixed at 142kPa which is the product of 5000kPa elastic modulus, 0.3 Poisson's ratio, 0.04 suction compression index, 0.5pF difference between the final surface suction and initial suction. In this analysis, the "m" value varies from 1 cm^2 to 15000 cm^2. It can be seen in Figure 3.6 that the maximum tensile stress does not change with the m value. The maximum tensile stress is always equal to 142kPa when the m value increases from 1 cm^2 to 15000 cm^2. The reason behind this is that k value is constant. Also, the depth to zero tensile stress increases from less than 0.1m to greater than 2.0m when the m value increases from 1 cm^2 to 15000 cm^2. This means that the drying time and diffusion coefficient control the distribution of tensile stress with depth and the depth to zero tensile stress.

In summary, the "k" value decides the maximum tensile stress and does not have any effect on the depth to zero tensile stress, while the "m" value governs the depth to zero tensile stress and does not exert any influence on the maximum tensile stress.

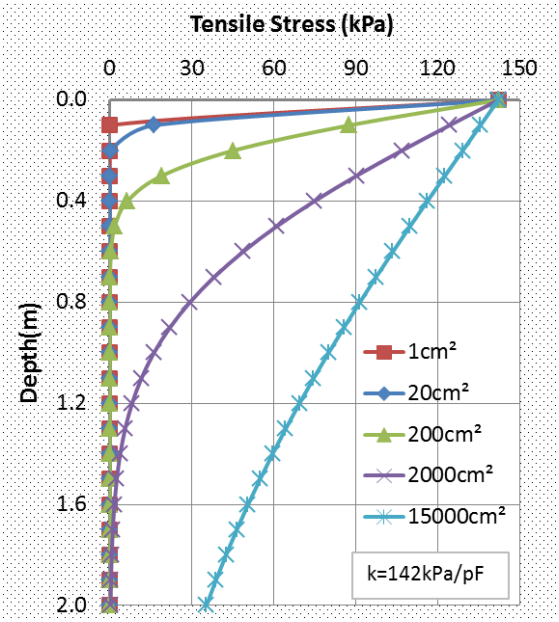

Figure 3.6 Sensitivity Analysis of the "m" Parameter

3.5 Application of the New Tensile Stress Model

The new model can be used to analyze geotechnical problems, and benefits the design and treatment of expansive soils. Some of applications are described in the following sections.

3.5.1 Prediction of Crack Initiation by SWCC

Tensile strength of the soil should be known before the tensile stress obtained from the new model can be used to predict the initiation of crack. The literature review presents many models for the tensile strength based on experiments and theoretical assumptions, and some of them are listed in Table 3.3. A close observation of the models in Table 3.3 indicates that those models can be divided into two types. The first type without containing the term of suction is for saturated soils, and the second type with the suction term is applicable for unsaturated soils. This analysis studies the change of tensile stress for unsaturated expansive soils. In table 3.3, the model of Zeh and Witt model (2005) is selected to determine the tensile strength of the soils analyzed in this study because this model only contains one parameter which is suction.

Table 3.3 Tensile Strength Models

Authors	Tensile strength equations	Definitions of variables	Type
Fang and Chen (1971)	$\sigma_t = 31.44 + 1.24\text{PI} - 0.01761\text{PI}^2 + 0.00011\text{PI}^3$	σ_t is tensile strength PI is plasticity index	Type 1
Barzegar et al. (1995)	$\sigma_t = 632.10 + 38.23\text{CL}$ $\sigma_t = -125.21 + 21.10\text{CEC}$	σ_t is tensile strength CL is clay content	Type 1
Zeh and Witt (2005)	$\sigma_t = 10.349 + 331.214 \times \exp\left\{-0.5[\ln\left(\frac{u}{15388.92}\right)/2.187]^2\right\}$	σ_t is tensile strength u is suction	Type 2
Venkataraman et al.(2009)	$\sigma_t = 0.01\text{CL}^{1.5}\text{CEC}^{0.5}u^{0.5}$	σ_t is tensile strength CL is clay content CEC is cation exchange capacity u is suction of the soil	Type 2

Figure 3.7 is a typical soil water characteristic curve (SWCC) where x-axis is suction and y-axis is water content. The parameters involved in calculating the tensile stress are the initial suction, final suction, elastic modulus, diffusion coefficient, drying time and depth. The elastic modulus is 5000kPa, suction compression index is 0.02 and initial suction is 2.5pF (pF=1+log kPa). In this analysis, the tensile stress is determined at the surface of the subgrade soils, so that diffusion coefficient and drying time can be neglected when the depth, z=0, is substituted into Equation [3.14].

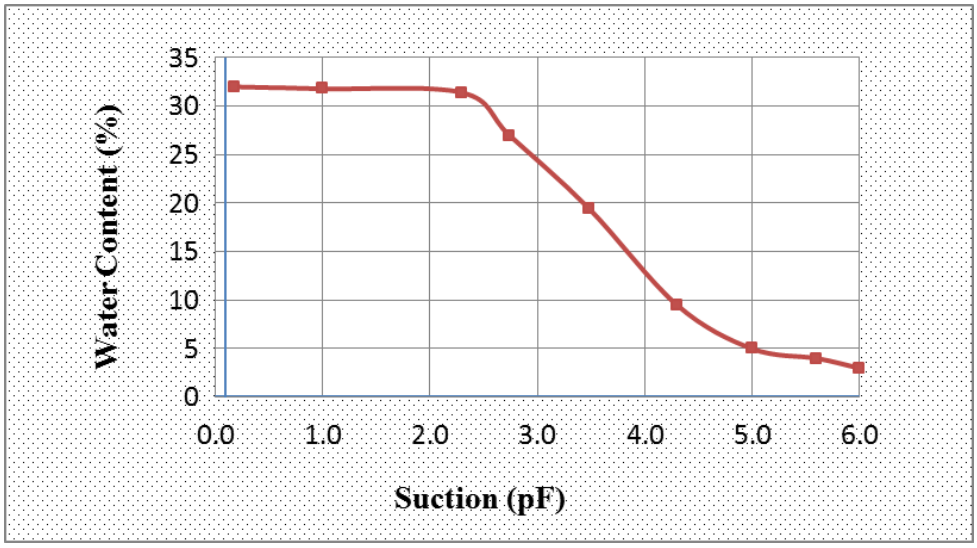

Figure 3.7 A Typical SWCC

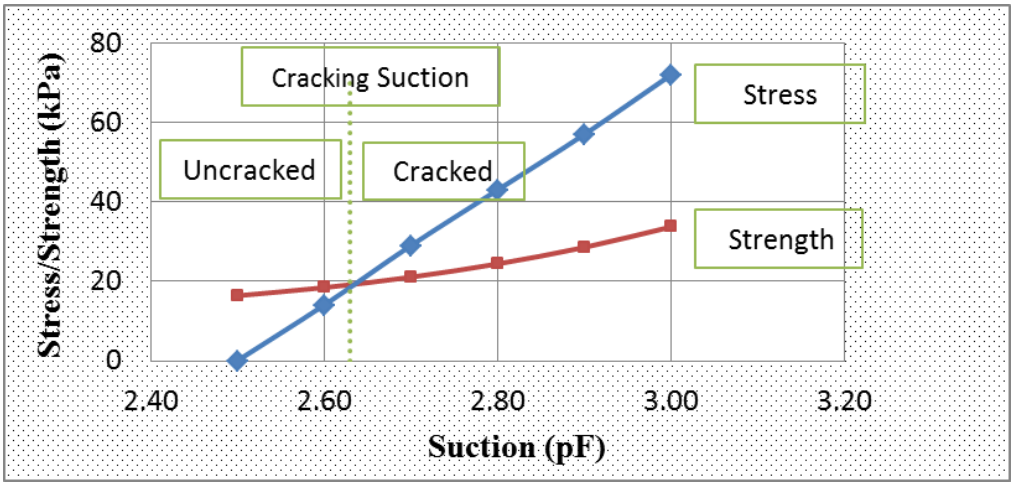

Figure 3.8 Cracking Initiation Predicted by the New Model

Using the suction values from Figure 3.7 and the parameters stated above, the tensile stress and tensile strength are obtained from Equation [3.14] and Zeh and Witt's model (2005), respectively, and the results are plotted in Figure 3.8. There is an intersection point between tensile stress and tensile strength in Figure 3.8. Tensile stress is lower than tensile strength before the intersection point, which means that the soil cracks do not occur at the beginning period of the drying time. This zone is marked "uncracked" in Figure 3.8. While tensile stress increases faster than tensile strength and quickly exceeds tensile strength as the drying time increases, and then cracks occur. This zone is marked "cracked" in Figure 3.8.

Another point is that the suction value where cracks occur (i.e., the intersection point) is very close to the initial suction. The intersection point is located at 2.63pF in Figure 3.8, and its difference with the initial suction is only 0.13pF. This conclusion is confirmed by the experiment conducted by Varsei et al. (2014) and the laboratory test results in Chapter 6.

3.5.2 Estimation of Crack Depth for a Specific Drying Time

Another application of Equation [3.14] is to predict the crack depth when the drying time is given. The average drying time for a specific area and climatic conditions can be estimated or obtained from different sources such as NCDC (National Climatic Data Center) and Oklahoma Mesonet. If the crack depth can be estimated for a specific drying time, it can greatly benefit the design of pavements on expansive soils.

The new model provides a convenient way to estimate the crack depth. As stated above, the new model depicts the profile of tensile stress with depth. The point where the tensile stress is equal to the tensile strength is the crack depth. For example, given that the drying time is 2 months, final surface suction is $4.5pF$, initial suction is $3.5pF$, suction compression index is 0.02, elastic modulus is $5000kPa$, Poisson's ratio is 0.3 and diffusion coefficient is $1 \times 10^{-4} cm^2/sec$. The profile of the tensile stress is generated using Equation [3.14] and the results are depicted in Figure 3.9. Assuming that the tensile strength of the soil is 30kPa, the depth of the intersection point becomes 0.4m which is the crack depth. As shown in Figure 3.9, the crack depth less than 0.4m is marked "cracked", and the depth greater than 0.4m is marked "uncracked".

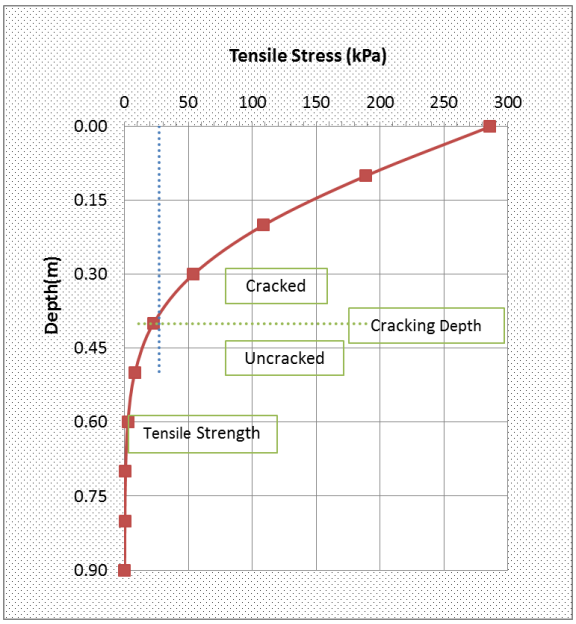

Figure 3.9 Estimation of Crack Depth for a Given Drying Time

Using the same approach, for various drying times, the corresponding crack depths are given in Table 3.4.

Table 3.4 Crack Depth and Drying Time

Crack depth	Drying time	Crack depth	Drying time
0.2m	0.5 month	0.6m	4 months
0.3m	1month	0.8m	8 months
0.4m	2 months	1.0m	12 months

3.5.3 Estimation of Drying Time for a Specific Crack Depth

Equation [3.14] can also be used to estimate the required drying time for a specific crack depth. For instance, the same parameters given in section 3.5.2 are employed except that 2 months drying time is replaced by 0.2m crack depth. Figure 3.10 depicts the profile of the tensile stress with the drying time at 0.2m crack depth. Given that the tensile strength is 30kPa, the intersection point between the tensile stress and tensile strength is the cracking time which is approximately

15 days. Figure 3.10 is divided into two zones by the cracking time. The left side is the uncracked zone for the drying time less than 15 days, and the right side is cracked zone for the drying time greater than 15 days, as shown in Figure 3.10.

Using the same approach as discussed in the previous section, for various crack depths, the corresponding drying times are given in Table 3.4.

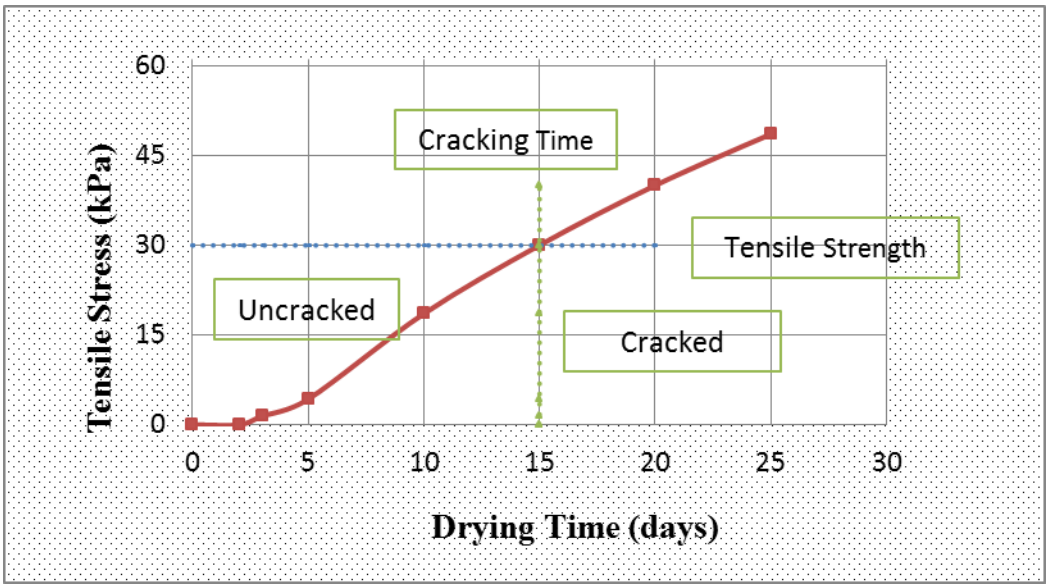

Figure 3.10 Estimation of Drying Time for a Specific Crack Depth

CHAPTER IV

VALIDATION OF THE NEW MODEL BY FINITE ELEMENT METHOD

4.1 Introduction

Chapter III presented a new model which can be used to predict the tensile stress from suction in unsaturated subgrade soils. The purpose of this chapter is to verify the model using finite element method, and the software used in the analysis is Abaqus. As introduced above, the model is developed using the suction profile proposed by Mitchell (1979) model. Hence, the first step in this chapter is to verify the suction obtained by Mitchell's model, and the second one is to verify the tensile stress obtained by the new model.

Abaqus software package has been widely used in engineering practice. For example, Luo (2007) employed Abaqus to analyze the location of crack initiation by means of stress intensity factor, and compared the effects of different reinforcements on pavement performance. Abaqus can be used in the analysis of suction variation in unsaturated soils because of the similarity the between heat diffusion in Abaqus and suction diffusion. Both heat transfer and moisture (suction) diffusion are governed by the same form of differential equation. The heat diffusion in solid materials is governed by Equation [4.1].

$$\frac{\partial T}{\partial t} - \phi \nabla^2 T = \frac{W}{c\rho} \qquad 4.1]$$

where T =temperature; w = interior heating source; c = specific heat capacity; ρ = mass density, and ϕ = thermal diffusivity which is defined by Equation [4.2] where λ is thermal conductivity.

$$\emptyset = \frac{\lambda}{c\rho} \quad [4.2]$$

Assuming that there is no interior heating source, and thermal diffusivity is replaced by moisture diffusion coefficient (i.e.,$\emptyset = \alpha$), then the model of heat diffusion is the same as the model of moisture diffusion as shown in Equation [4.3]. Therefore, the heat transfer model in Abaqus is capable of analyzing suction distribution in soils.

$$\frac{\partial u}{\partial t} = \alpha \frac{\partial^2 u}{\partial z^2} \quad [4.3]$$

Where u = suction; t = drying time or wetting time; α = moisture diffusion coefficient, and z = depth.

4.2 Model for Subgrade Soil

A 3-D model, shown in Figure 4.1, is developed in Abaqus program to analyze the suction and tensile stress during the process of desiccation, and its coordinate system is defined as follows: x-axis is longitudinal (traffic direction), y-axis is transverse and z-axis is vertical. The origin of the coordinate system is located at the center of the surface plane (ABCD).

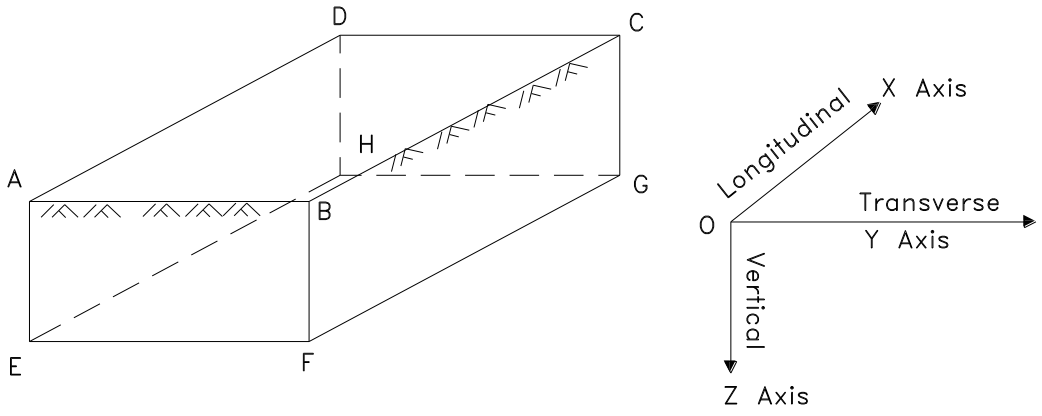

Figure 4.1 3-D Coordinate System for Finite Element Analysis

The model shown in Figure 4.1 is 6.0m deep, 12.0m wide and 20.0m long. The dimension of the model is determined based on the following criteria. In most cases, the depth of active moisture zones is less than 13 feet or 396 cm (Farrow and Roland 2006), so it is reasonable to assume that the suction, displacements and stresses for the soil below 6.0m are not influenced by cyclic seasonal climatic change in most cases. The 20m length can guarantee that the boundary conditions in longitudinal direction cannot affect the result of analysis, and 12m width is a typical width of a pavement.

There are six planes in Figure 4.1. The EFGH plane is the bottom of the subgrade and regarded as fixed for displacements, and has no suction change along this boundary. The FBCG plane and the EADH plane are the shoulders of the pavement subgrade. They can move freely in vertical direction and transverse direction while they are fixed in longitudinal direction, and the horizontal moisture flow is ignored. The ABEF plane and the CGDH plane are used to demonstrate a segment from the pavement subgrade. The ABCD plane is the surface which can move freely, and is exposed to the different values of constant suctions depending on the climatic conditions under investigation.

The finite element model is discretized using 8-node linear brick elements as shown in Figure 4.2. The element sizes are 0.2m in vertical direction and transverse direction while they are 0.4m in longitudinal direction.

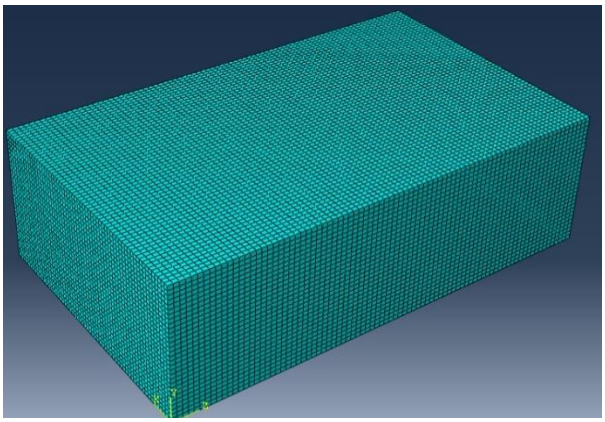

Figure 4.2 The Element Mesh of Model

The analysis of tensile stress is divided into two steps. At first, the model of heat transfer in Abaqus is employed to obtain suction, and then the output file containing the suction is used as an input file. Secondly, the 3-D stress model in Abaqus is applied to calculate the tensile stress in subgrade.

4.3 Suction Analysis

As shown in Equation [3.13], the parameters involved in Mitchell's suction model are drying time, diffusion coefficient, the difference between final surface suction and initial suction. In order to fully compare the suction from FEM with the suction from Mitchell's model, three cases are analyzed. Case 1 has different drying time than Case 2, and Case 2 has different diffusion coefficient than Case 3, while Case 3 has different final surface suction, drying time and diffusion coefficient than Case 1. The detailed information for each case is listed in Table 4.1.

Table 4.1 Parameters Involved in Suction Analysis

Case No.	Initial Suction	Final surface suction	Drying Time	Diffusion Coefficient
Case 1	3.0pF	4.0pF	3 months	$5.0 \times 10^{-5}\, cm^2/s$
Case 2	3.0pF	4.0pF	6 months	$5.0 \times 10^{-5}\, cm^2/s$
Case 3	3.0pF	4.5pF	6 months	$10.0 \times 10^{-5}\, cm^2/s$

Figure 4.3 shows the suction profile for Case 3 obtained from Abaqus. The red color in Figure 4.3 depicts the highest suction, and the blue color represents the lowest suction, and the other colors are for the transitional zone. It can be seen that the suction decreases with depth. Case 1 and Case 2 have the similar suction profiles with Case 3, so their suction profiles are not presented.

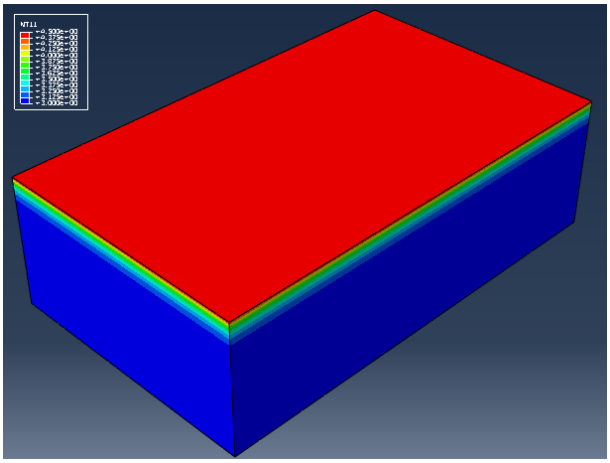

Figure 4.3 Suction Profile by FEM

For all the three cases, the suctions from Mitchell's model and the suctions from FEM are listed in Table 4.2. Figure 4.4, 4.5 and 4.6 are obtained using the data in Table 4.2. The close observation indicates that the curves in Figure 4.4, 4.5 and 4.6 can be divided into two phases. The first phase is for the shallow soil, and the second one is for the deep soil. The suctions from

Mitchell's model are larger than those from FEM in the first phase, while the situation is the opposite in the second phase. In other words, the suctions from Mitchell's model are lower than those from FEM. Generally, they share similar shape and the differences are small. Therefore, Mitchell's model can provide reasonable suction profile.

Table 4.2 Suction Comparison between Mitchell's Model and FEM

Depth (m)	Case 1 (pF)		Case 2 (pF)		Case 2 (pF)	
	Mitchell	**FEM**	**Mitchell**	**FEM**	**Mitchell**	**FEM**
0.0	4.00	4.00	4.00	4.00	4.50	4.50
0.2	3.47	3.37	3.61	3.50	4.08	3.91
0.4	3.15	3.14	3.31	3.25	3.71	3.55
0.6	3.03	3.05	3.13	3.12	3.42	3.33
0.8	3.00	3.02	3.04	3.06	3.23	3.20
1.0	3.00	3.01	3.01	3.03	3.11	3.12
1.2	3.00	3.00	3.00	3.01	3.05	3.04
1.4	3.00	3.00	3.00	3.01	3.02	3.03

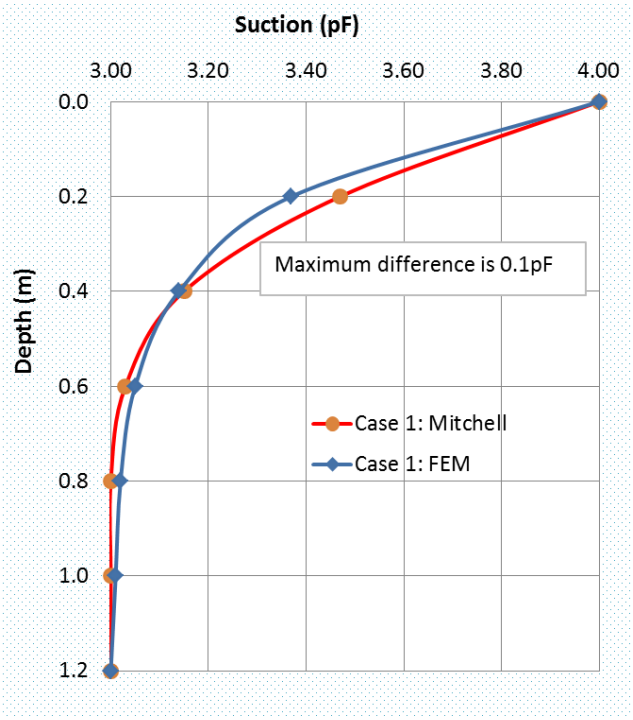

Figure 4.4 Suction Comparison for Case 1

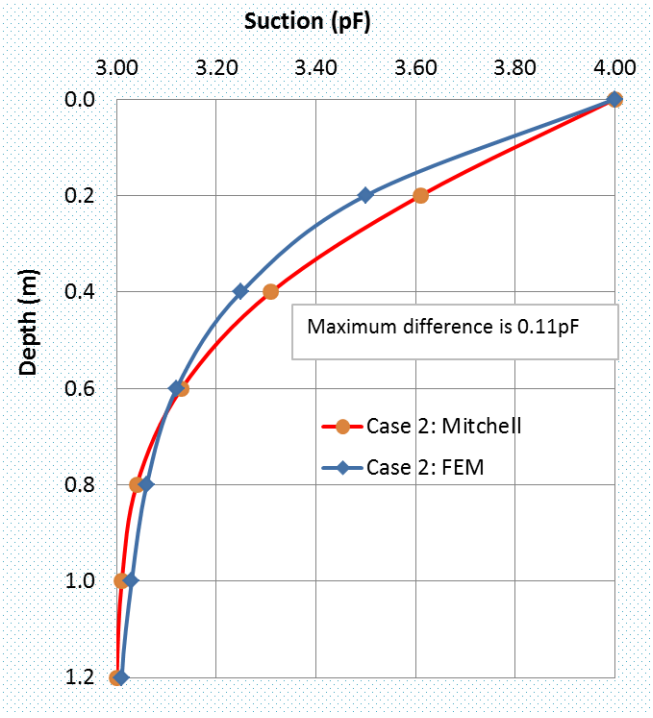

Figure 4.5 Suction Comparison for Case 2

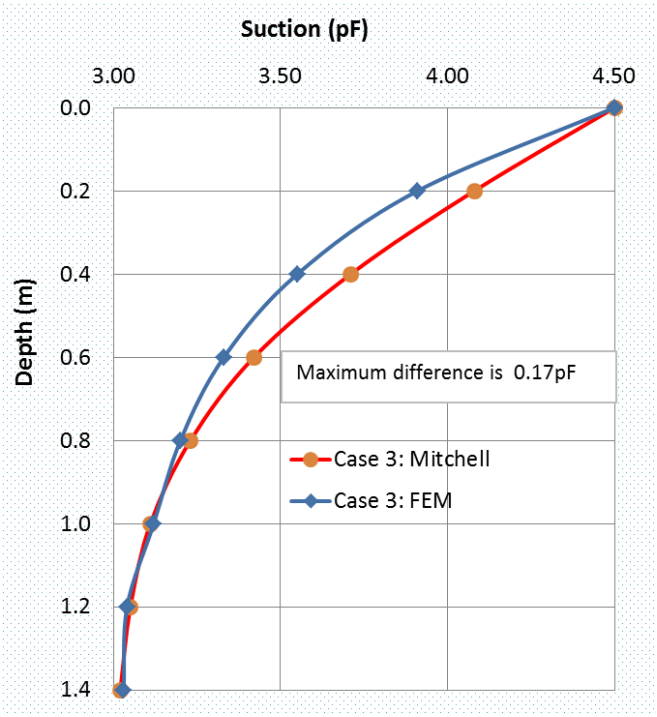

Figure 4.6 Suction Comparison for Case 3

4.4 Tensile Stress Analysis

The second step is to apply the 3-D stress model in Abaqus to analyze the profile of tensile stress in subgrade soil. The file containing the suctions obtained from the heat transfer model is used as an input file. The geometrical model used in this section is the same as the one used in the analysis of suction.

In order to be consistent with the analysis of suction, the three cases (i.e., Case 1, Case 2 and Case 3) used in the analysis of the suction are employed to analyze the tensile stress. Besides the parameters listed in Table 4.1, the other parameters involved in the analysis of the tensile stress are the unit weight of the expansive soil ($19\text{kN}/m^3$), Poisson's ratio (0.3), elastic modulus (5000kPa), and suction compression index (0.02). The tensile stresses obtained from the new model (i.e., Equation 3.14) and finite element method are listed in Table 4.3. Figure 4.7, 4.8 and 4.9 are generated using the data in Table 4.2.

The comparison study between the new model (i.e., Equation 3.14) and FEM indicates that the new model makes reasonable prediction for the depth greater than 0.2m as compared to the results from FEM. It is found in Figure 4.7, 4.8 and 4.9 that the curve from the new model and the curve from FEM are almost overlapping when the depth exceeds 0.2m. On the other hand, the tensile stress from the new model is a bit different from that obtained by FEM for shallow depths. In the case of 0.0m depth (i.e., surface of the subgrade), the tensile stress in Case 3 is 214kPa for the new model, while it is 172kPa for FEM, approximately 24% increase. It is believed that the difference close to the subgrade surface is due to the boundary conditions imposed in the analysis of FEM.

It is found that some of the tensile stress values listed in Table 4.2 are very large, such as 214kPa, 172kPa and 154kPa. In geotechnical practice, those large tensile stresses usually do not realize because of the development of cracks before the tensile stress reaches those values.

Table 4.3 Tensile Stress Comparison between New Model and FEM

Depth (m)	Case 1 (kPa)		Case 2 (kPa)		Case 3 (kPa)	
	New Model	FEM	New Model	FEM	New Model	FEM
0.0	143	98	143	107	214	172
0.2	67	68	87	80	154	138
0.4	21	26	44	40	101	84
0.6	4	10	19	20	60	51
0.8	0	4	6	10	33	31
1.0	0	2	1	5	16	18
1.2	0	1	0	2	7	11
1.4	0	0	0	1	3	7

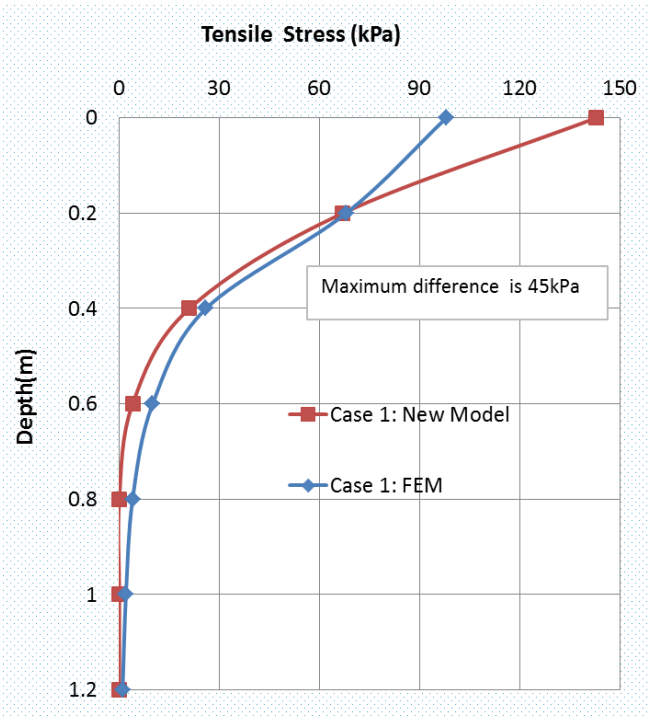

Figure 4.7 Tensile Stress Comparison for Case 1

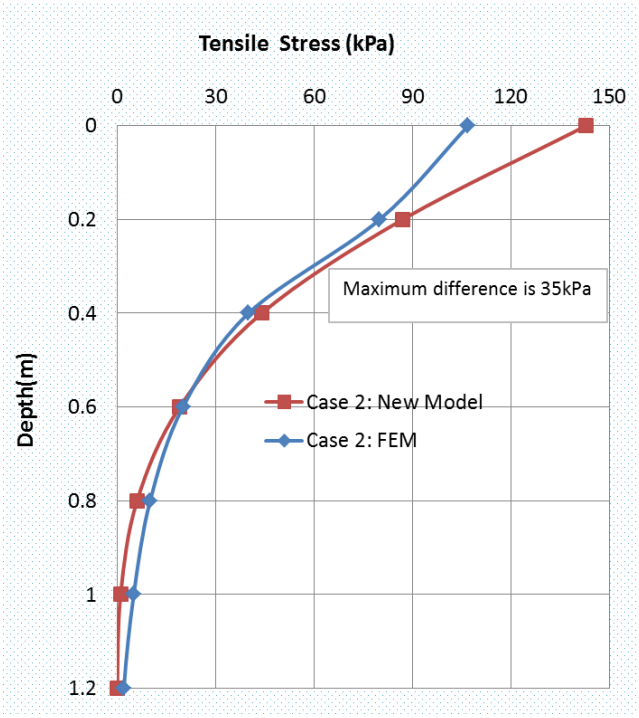

Figure 4.8 Tensile Stress Comparison for Case 2

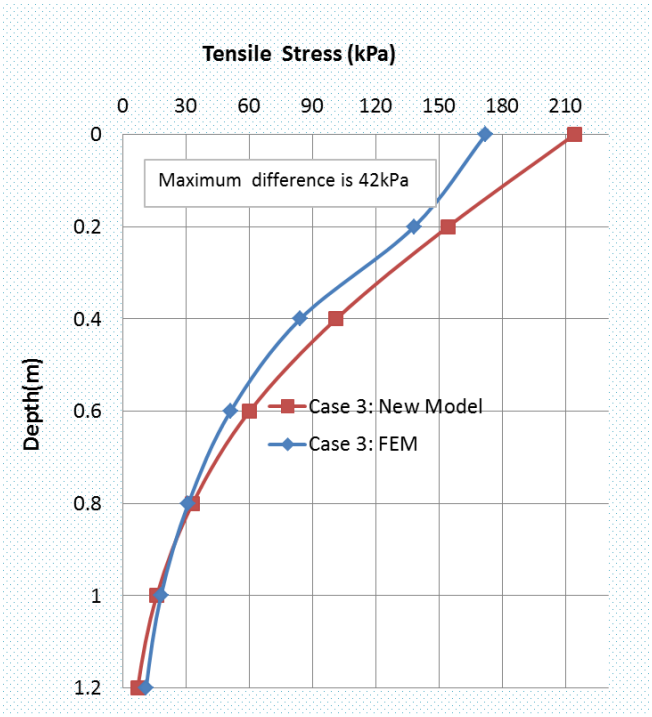

Figure 4.9 Tensile Stress Comparison for Case 3

CHAPTER V

LABORATORY EXPERIMENTAL PROGRAM

The experimental program is conducted using the modified restrained ring method, and it includes two parts. The first part is to measure the suction and tensile stress between the state close to saturation and the development of cracks. The purpose of the first part is to simulate the soil after a heavy rainfall. The second part is to measure the suction and tensile stress between the optimum water content and the development of cracks. The purpose of the second part is to simulate the soil after compaction.

5.1 Sample Properties

The soil samples are obtained from Lake Hefner site and Ardmore site which are typical expansive soils in Oklahoma. The sample is prepared by sieving the soils through No. 40 sieve to eliminate the bias caused by large particles. The distribution of grain size is obtained by hydrometer analysis based on the Stoke's law. The percentages of soil particles passing through No. 200 and 2 microns, liquid limit, plastic limit and index are listed in Table 5.1. According to USCS soil classification, the soils from Lake Hefner and Ardmore are CL and CH, respectively.

Proctor compaction is conducted in accordance with ASTM D698 (Standard Test Methods for Laboratory Compaction Characteristics of Soil Using Standard Effort), and maximum dry density and optimum water content are listed in Table 5.1.

Also, according to ASTM D4767-11 (Standard Test Method for Consolidated Undrained Triaxial Compression Test for Cohesive Soils), three specimens for every soil sample are used to measure elastic modulus at optimum water content, and their confining pressures are 0.0psi (unconfined), 10psi (6.895kPa) and 20 psi (13.790kPa), respectively. The average elastic modulus is 9.6MPa for Lake Hefner soil, and is 6.5MPa for Ardmore soil.

The measurement of elastic modulus close to saturation is different from the soil sample at optimum water content. Soil sample is soft after soaking in water for 48 hours, so it is easily broken when placing soil sample into triaxial membrane. In order to deal with the problem, the soil sample is installed into the membrane first, and then is soaked in water. Three samples for every soil sample are tested, and their confining pressures are 20psi (13.790), 40psi (27.580kPa) and 60 psi (41.370kPa), respectively. The average elastic modulus is 1.9MPa for Lake Hefner soil, and is 1.4MPa for Ardmore soil.

The last parameter measured is the suction compression index. In this research, the method proposed by Covar and Lytton (2001) is selected to obtain the suction compression index. The calculation of the suction compression index includes three steps. At first, the zone is determined by the liquid and plasticity index, and then the volume change guide number is obtained after checking the chart provided by Covar and Lytton (2001). In the end, the actual suction compression index is calculated from the guide number by Equation [2.9]. By substituting the variables involved in Equation [2.9], the suction compression index is 0.02 for the samples from Lake Hefner, and is 0.04 for the samples from Ardmore.

Table 5.1 Properties of Soil Samples

Items	Lake Hefner	Ardmore
% of soil finer than No. 200	63	52
% of soil finer than # 2 microns	20	21
Liquid Limit (%)	37.6	52.6
Plastic Limit (%)	23.4	27.0
Plasticity Index (%)	14.2	25.6
Maximum dry density (kN/m^3)	15.9	14.3
Optimum water content (%)	22.5	25.5
Elastic modulus at OWC (MPa)	9.6	6.5
Elastic modulus close to saturation(MPa)	1.9	1.4
Suction compression index	0.02	0.04

5.2 Sample Preparation and Installation

After the soil sample is sieved through No.40, it is thoroughly mixed with the water to bring the soil sample to the optimum water content. Then the soil is compacted in three layers with 25 blows per layer in accordance with ASTM D698. The soil sample after standard Proctor compaction is shown in Figure 5.1 (a).

Next, the soil sample is trimmed to fit in the restrained ring by the following steps. The first step is to cut the cylindrically shaped soil sample into the pieces with 4.1cm in height as shown in Figure 5.1 (b). Then using the sharp-edged steel ring, a hole of 5.3cm in diameter is made in the soil sample as shown in Figure 5.2. Thirdly, the inner ring made of Polyvinyl Chloride (PVC) is

pressed into the hole slowly and evenly as shown in Figure 5.3(a). Enough attention must be paid in this step. Otherwise, the soil sample will be damaged or small cracks will be initiated. The last step is to place the soil sample into the outer ring directly as shown in Figure 5.3 (b). The diameter of the outer ring is the same as the diameter of the standard Proctor test mold (10.16cm or 4.0in), which makes it easy to place the soil sample without any trimming.

Figure 5.1 (a) Cylindrical Soil Specimen (b) Soil Sample with 4.1cm Height

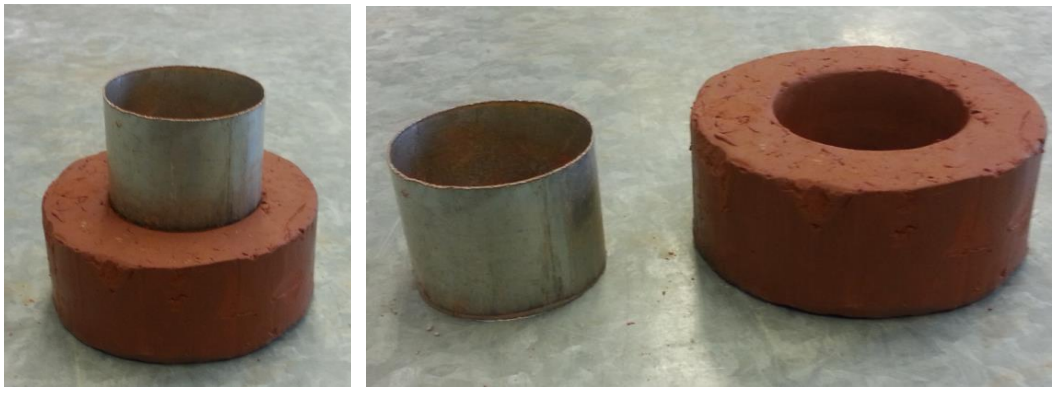

Figure 5.2 A Ring-shape Soil Sample cut by Sharp-edge Ring

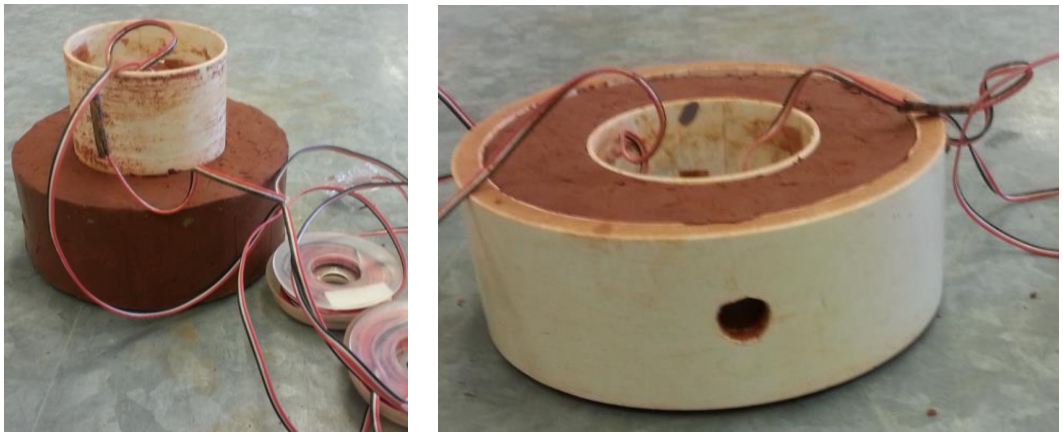

Figure 5.3 (a) Inner Ring Installation (b) Outer Ring Installation

After the soil sample is correctly installed as stated above, it is placed on a scale with 0.1g accuracy. The water content is back calculated from the difference between the initial weight and successive weights during the test. A high-resolution camera is fixed on a tripod to record the change of scale reading and suctions. The measurements are recorded with 10 minutes intervals. Figure 5.4 shows the experimental setup.

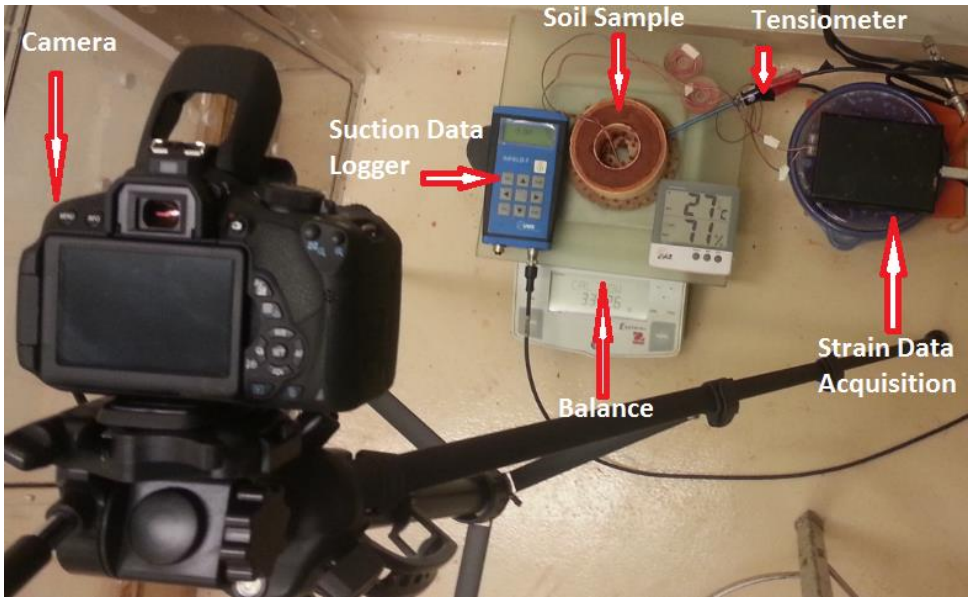

Figure 5.4 Experiment Setup

According to ASTM standard and AASHTO standard, the criteria used to stop the experiment for early-age concrete is the sudden decrease of compressive strain more than 30 micro strains. However, for expansive soils, the tensile stress produced is much lower as compared to the early-age concrete, which is not enough to produce sudden decrease in strains. Therefore, in this research, the experiment is stopped when the compressive strain starts decreasing continuously.

The devices used in this research are strain gauge, data acquisition for strain gauge, filter paper, tensiometer, data logger for tensiometer, inner ring, outer ring, and other apparatus. Detail information is listed in Table 5.2.

Table 5.2 Devices Involved in the Experiment

Items	**Description**	**Purpose**
Filter paper	No. 589^2-WH (Schleicher & Schuell)	Measure suction from optimum water content
Tensiometer	Infield 7 (UMS)	Measure suction from saturated state
Strain gauge	CEA-06-125UW-350/P2 (Micro-Measurements)	Measure strain.
Data acquisition	Model D4 acquisition (Micro-Measurements)	Record strains
Proctor Compaction	ASTM D-698	Prepare soil sample
Triaxial device	ASTM D-4767	Measure elastic modulus
Balance	0.1g accuracy	Measure the water content of the sample
Sensitive Balance	0.0001g accuracy	Measure the water content of filter paper
High resolution camera	EF-S 18-55mm (Canon)	Record the weight change of the soil sample and the development of crack
Outer ring	Inside diameter: 10.16cm Height: 4.1cm PVC material	Hold soil sample
Inner ring	Inside diameter: 5.08cm Thickness: 0.16cm Height: 4.1cm PVC material	Restrained ring

5.3 Suction Measurement

There are two techniques used for measuring soil suction. The first technique is the tensiometer which measures suction close to saturation, and the second one is the filter paper which measures suction at OWC.

5.3.1 Measurement of Suction at the State Close to Saturation

The main advantage of the tensiometer is the ability to measure low suction and reach equilibrium in a few minutes. The soil sample is very wet after soaking in water. In this case, tensiometer is the first choice to measure the suction. The type of the tensiometer used here is T5-10 manufactured by UMS (shown in Figure 5.5a). Compared to other tensiometers, it has a shorter tube (20cm) and a shorter ceramic cup (0.5cm), so the response time is faster and the accuracy is higher than others (UMS manual). Figure 5.5b shows the data logger.

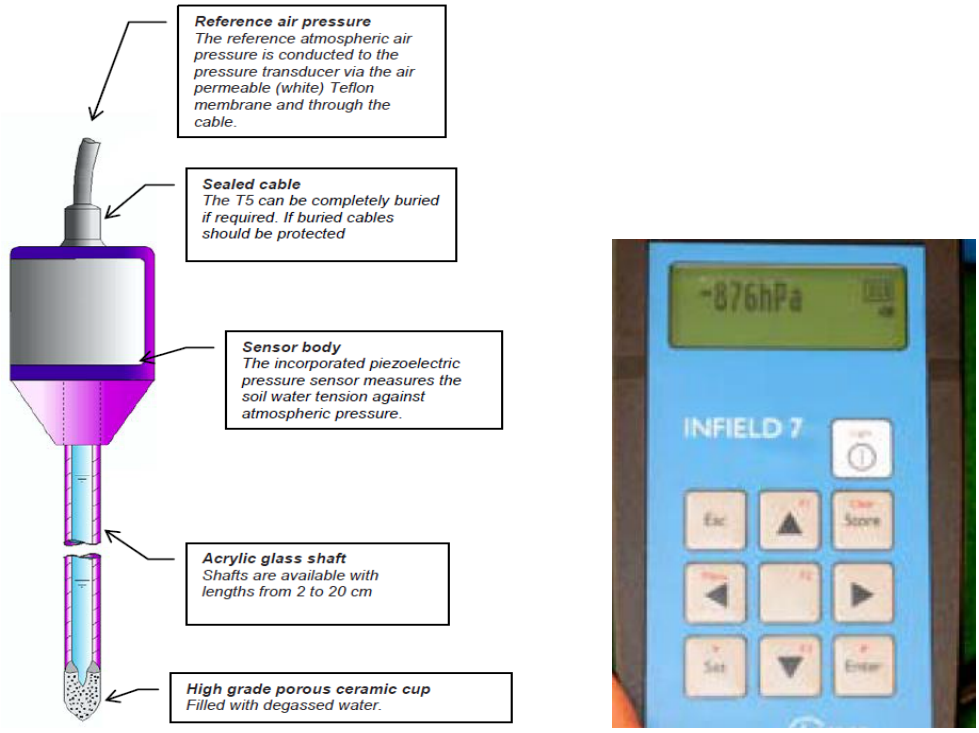

Figure 5. 5 (a) T5-10 Tensiometer (b) Infield 7 Data Logger (UMS Manual)

5.3.2 Measurement of Suction at Optimum Water Content (OWC)

The suction of the soil sample at optimum water content is greater than 3.2pF (158kPa) which exceeds the range of the T5-10 tensiometer, so it is necessary to find another method. The filter paper method is selected due to its low cost, high reliability and no damage to the soil sample (such as punching a hole or inserting a sensor). The experiment is conducted in accordance with Bulut et al (2001) and ASTM D5298-10 (Standard Test Method for Measurement of Soil Potential (Suction) Using Filter Paper). The type of filter paper is No. 589^2-WH manufactured by Schleicher & Schuell company.

Based on the preliminary test results, it is found that cracks often occur in 3-8 hours and the decreasing rate of water content is approximately 0.3-1.0% per hour. The purpose of this experiment is to study the relationship between the tensile stress and suction from the optimum water content to the development of a crack, so it is not necessary to measure the suction in the entire range. In this experiment, water content varies from OWC to the OWC-8%, and the five points during this range of water content are measured. The corresponding suctions are obtained checking the calibration curve developed by Bulut et al. (2001). See Figure 5.6.

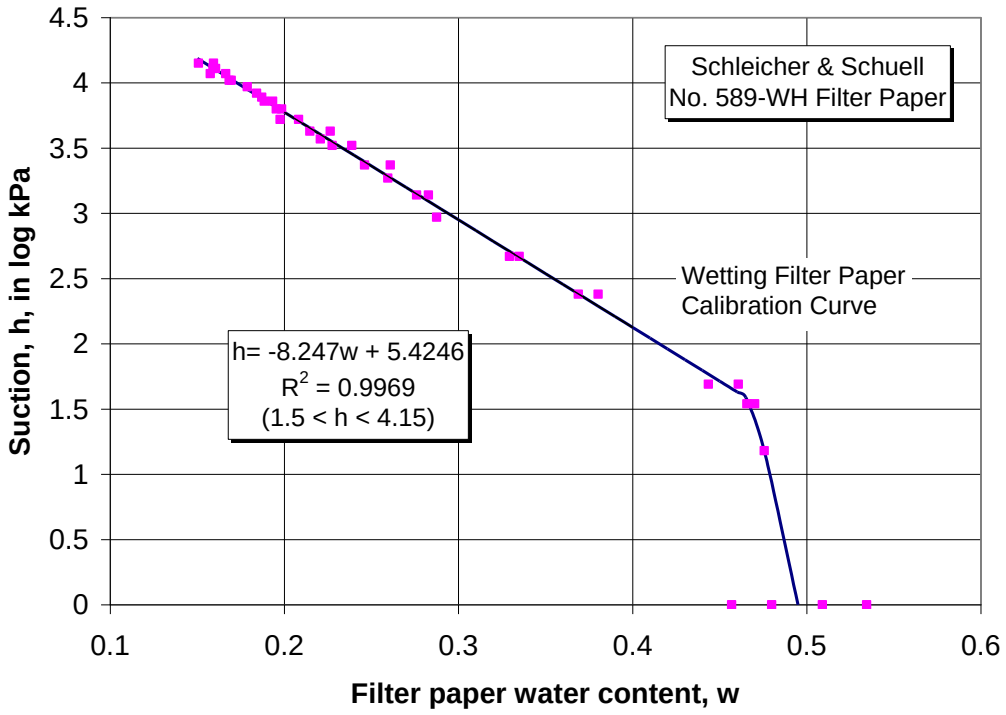

Figure 5.6 The Calibration Curve (Bulut et al. 2001)

There are many models available to establish SWCCs. The model proposed by Fredlund and Xing (1994) is one of the most widely accepted models in geotechnical engineering, so it is adopted in this research. As shown in Equation [5.1], there are three fitting parameters, $a_f, n_f \; and \; m_f$, which will be solved using the least square error method.

$$\theta(\psi, a_f, n_f, m_f) = \frac{\theta_s}{(\ln(e+\left(\psi/a_f\right)^{n_f})^{m_f}} \qquad [5.1]$$

The parameters involved in Equation [5.1] have been defined in the previous chapter.

5.4 Measurement of Tensile Stress

Two quarter-bridge strain gauges (Figure 5.7) installed in the inner ring are utilized to measure the strain due to the shrinkage of the soil sample, and the installation direction of the strain gauge is parallel to the circumference. The working principle of the strain gauge is that the resistance of

strain gauge changes with the length of the strain gauge when subjected to tensile stress or compressive stress, then strain can be obtained by the calibration equation between the resistance and length (Mayergoyz and Lawson 1996). In order to measure the change in resistance, a very low electric current is applied through the data acquisition device.

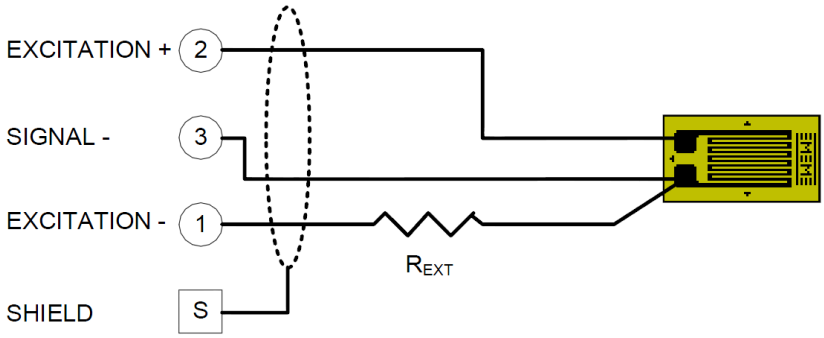

Figure 5.7 Quarter-bridge Strain Gauge (Data Acquisition Manual 2013)

Based on the principles mentioned above, the following two points are very important during the experiment. At first, the strain gauge must be completely prevented from moisture infiltration. Even if a small amount of water comes in contact with the strain gauge, the resistance will be greatly changed (Vishay Measurement Manual). This will lead to the failure of the experiment. Secondly, the heat generated by electric current is difficult to dissipate because the strain gauge is installed in the PVC material instead of metal material in this experiment. The accumulation of heat can reduce the accuracy of strain gauge. Hence, 350Ω strain gauge is chosen because the speed of heat dissipation of 350Ω strain gauge is 9 times faster than the speed of 120Ω strain gauge (Vishay Measurement Manual). Strains are recorded by the D4 data acquisition with four channels which can continuously record the change of strain with time. See Figure 5.8.

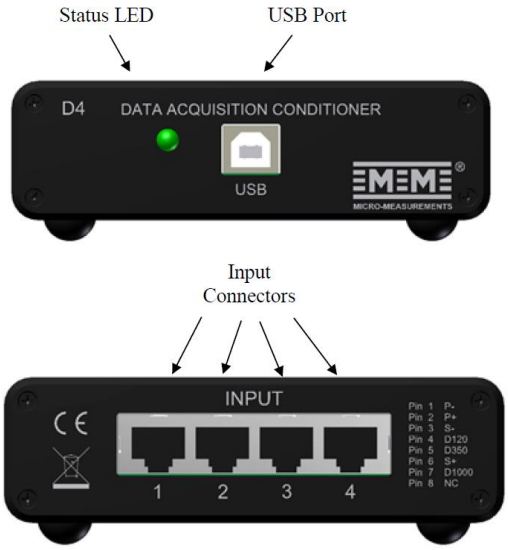

Figure 5.8 Front and Rear View of D4 Data Acquisition

After installing the software of D4 data acquisition in the computer, the strains of the soil sample can be displayed and recorded in real time. Figure 5.9 is a screen shot of a software. The "Ch1, Ch2, Ch3 and Ch4" in Figure 5.9 are the four channels of the data acquisition, and the "Max and Min" are the maximum and minimum strains occurring during the experiment.

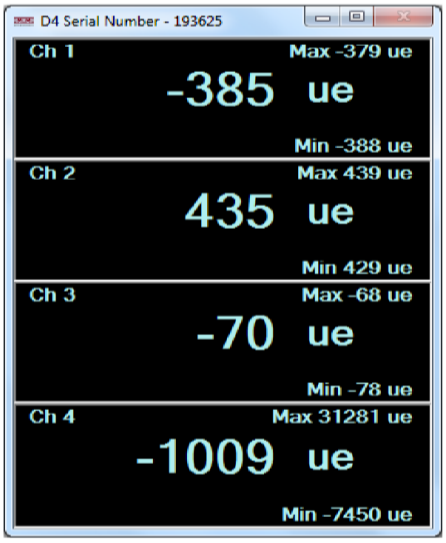

Figure 5.9 Monitor Displaying Strains

The tensile stress in the soil sample can be obtained by the method proposed by Weiss and Furgeson (2001). In the method, the soil sample is taken as an elastic and isotropic material before cracking, and the problem can be divided into two parts. As shown in Figure 5.10, in the first part, the inner ring is subjected to compressive pressure which is induced by the shrinkage of the soil sample, and in the second part, the cylindrical soil sample is subjected to tensile pressure. As shown in Figure 5.10, the compressive pressure in the inner ring and the tensile pressure in the cylindrical soil sample are a pair of action-reaction forces (Najm et al 2009).

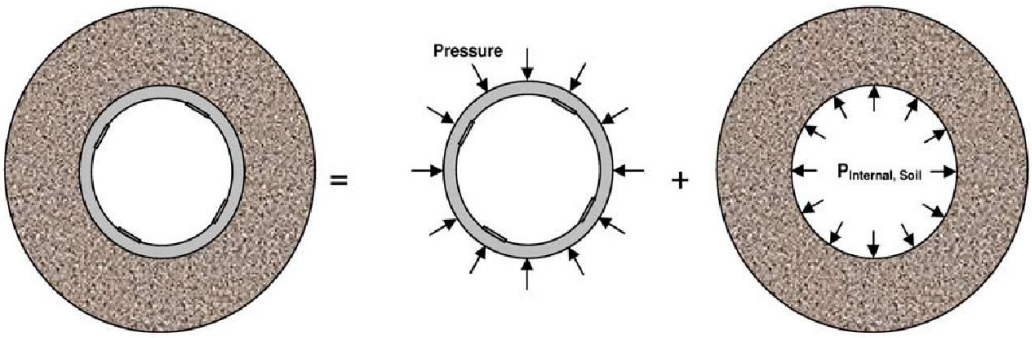

Figure 5.10 Ring Pressure and Soil Cylinder Pressure (Najm et al. 2009)

The tensile stress for an elastic cylinder pressured inside can be calculated by Equation [5.2] and Equation [5.3] (Timoshenko and Goodier, 1987; Weiss, 1997). Equation [5.2] shows that the maximum tensile stress occurs at the position where r is equal to R_{Oring} (i.e., the position of inner ring), so the maximum tensile stress can be calculated by Equation [5.4] where r is substituted by R_{Oring}.

$$P_{in}(t) = \varepsilon(t)_{ring}\, E_{ring} \frac{(R_{Oring}^2 - R_{Iring}^2)}{2R_{Oring}^2} \quad [5.2]$$

$$\sigma_\theta = P_{in}\left(\frac{R_{Oring}^2}{R_{Osoil}^2 - R_{Oring}^2}\right)\left(1 + \frac{R_{Osoil}^2}{r^2}\right) \quad [5.3]$$

$$\sigma_{\max tensile\ stress} = P_{in}\left(\frac{R_{Oring}^2}{R_{Osoil}^2 - R_{Oring}^2}\right)\left(1 + \frac{R_{Osoil}^2}{R_{Oring}^2}\right) \quad [5.4]$$

where $P_{in}(t)$ = the internal compressive pressure of the ring at time (t), $\varepsilon(t)_{ring}$ = the strain measured from the strain gauges at time (t), R_{Oring} and R_{Iring} = the outside and inside radius of the restrained ring, respectively, E_{ring} = the elastic modulus of the PVC ring, R_{Osoil} = the outside radius of the cylindrical soil sample, σ_θ = the tensile stress and r = the radius of any point in the soil sample. Figure 5.11 shows the R_{Oring}, R_{Iring}, R_{Osoil} and r in Equation [5.2], [5.3] and [5.4].

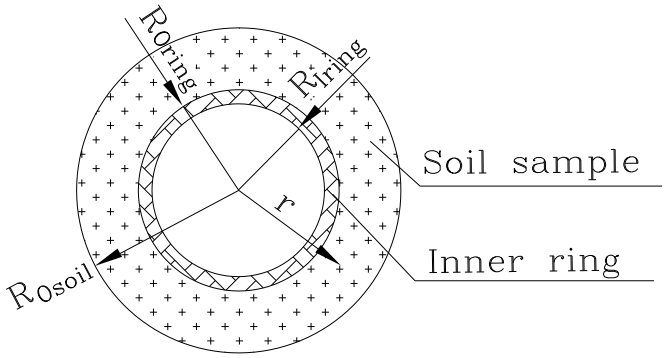

Figure 5.11 Radius of Inner Ring and Soil Sample

CHAPTER VI

TEST RESULTS AND THEIR ANALYSIS

The experimental program includes two parts. The first part is to measure the suction and tensile stress from the state close to saturation to the development of crack, and the second part is to measure the suction and tensile stress from optimum water content (OWC) to the development of crack. For each part, six soil specimens are tested. Three of soil specimens are from Lake Hefner which belongs to a low expansive soil, and the other three are from Ardmore which is a medium expansive soil.

6.1 Suction Analysis at OWC

As stated in Chapter 5, the filter paper method is utilized to measure the suction at optimum water content, and the model proposed by Fredlund and Xing (1994) is used to setup the soil water characteristic curve (SWCC).

6.1.1 SWCC for the Samples from Lake Hefner

In order to obtain the three unknown curve fitting parameters in the model proposed by Fredlund and Xing (1994), five data points are determined from laboratory experiment. The starting water content is equal to optimum water content which is 22.5% for the samples from Lake Hefner. The detailed information for each point is listed in Table 6.1.

Table 6.1 Suctions Measured by Filter Paper for the Sample from Lake Hefner

Water content	Moisture Tin No.	T_c (g)	M_1 (g)	M_2 (g)	T_h (g)	W_f (%)	h_1 (pF)
22.5%	D4 (Bottom)	36.35964	36.58903	36.51600	36.33550	27.1	3.19
	A7 (Top)	36.78376	37.01362	36.93350	36.75180	26.5	3.24
21.0%	D5 (Bottom)	36.38676	36.60533	36.52975	36.35527	25.3	3.34
	C3 (Top)	36.89259	37.10607	37.04591	36.87455	24.6	3.40
19.5%	E5 (Bottom)	37.05700	37.26808	37.21296	37.04154	23.1	3.52
	A9 (Top)	37.04450	37.26302	37.19430	37.01718	23.4	3.52
17.5%	D1 (Bottom)	36.87767	37.08703	37.03359	36.86056	21.0	3.69
	B1 (Top)	36.74885	36.96473	36.90577	36.72701	20.7	3.72
15.5%	D7 (Bottom)	36.64448	36.84706	36.79975	36.62808	18.0	3.94
	E7 (Top)	36.62635	36.84027	36.80176	36.61928	17.3	4.00

Note: T_c is the mass of cold tare, M_1 is the mass of wet filter paper and cold tare, M_2 is the mass of dry filter paper and hot tare, T_h is the mass of hot tare, W_f is the water content of filter paper, and h_1 is suction.

Substituting the water content and suction listed in Table 6.1 into the model proposed by Fredlund and Xing (1994), the three fitting parameters are obtained by means of the least square error method, and they are $a_f = 233, n_f = 0.92\ and\ m_f = 1.02$. The saturated water content is 28%. The residual suction is assumed as 1500kPa (Fredlund et al.1994). Equation [6.1] is obtained by substituting the fitting parameters, saturated water content and residual suction into Equation [5.1]. Figure 6.1, generated using Equation [6.1], is the SWCC for the soil samples from Lake Hefner.

$$\theta = \left(1 - \frac{\ln\left(1+{}^{\psi}/_{1500}\right)}{\ln\left[1+\left({}^{10^6}/_{1500}\right)\right]}\right) \times \frac{0.28}{\left(\ln\left(e+\left({}^{\psi}/_{233}\right)^{0.92}\right)\right)^{1.02}} \qquad [6.1]$$

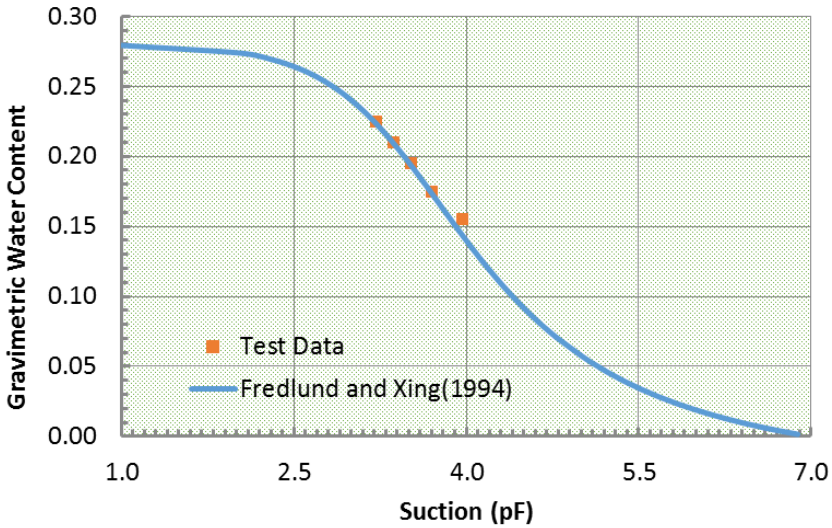

Figure 6.1 SWCC for the Soil Sample from Lake Hefner

6.1.2 SWCC for the Samples from Ardmore

For the soil samples obtained from Ardmore, the suctions corresponding to water content at 24.5%, 22.5%, 21.0%, 19.0% and 17.0% are measured by the filter paper method, and the results are listed in Table 6.2. The starting point of water content in Table 6.2 is 24.5% which is optimum water content for the samples from Ardmore.

Table 6.2 Suctions Measured by Filter Paper for the Sample from Ardmore

Water content	Moisture Tin No.	T_c (g)	M_1 (g)	M_2 (g)	T_h (g)	W_f (%)	h_1 (pF)
24.5%	A4 (Bottom)	36.98677	37.20004	37.13118	36.95979	24.4	3.41
	A7 (Top)	36.78472	36.99862	36.92584	36.75326	23.9	3.45
22.5%	C3 (Bottom)	36.89417	37.10532	37.04470	36.87277	22.3	3.59
	A6 (Top)	36.69188	36.90211	36.84533	36.67221	21.4	3.66
21.0%	A5 (Bottom)	36.78070	36.98710	36.92138	36.75049	20.8	3.71
	E1 (Top)	36.72450	36.92885	36.86532	36.69507	20.0	3.77
19.0%	D2 (Bottom)	36.89962	37.10405	37.04669	36.87495	18.8	3.87
	D5 (Top)	36.38900	36.59967	36.37894	36.20258	17.8	3.96
17.0%	A5 (Bottom)	36.78634	36.98721	36.93462	36.76170	16.2	4.09
	C9 (Top)	36.80206	37.00751	36.67018	36.49181	15.2	4.17

The three unknown fitting parameters in the model proposed by Fredlund and Xing (1994) are solved using the suctions and water contents in Table 6.2 and they are $a_f = 382, n_f = 0.94$ and $m_f = 1.01$. The saturated water content is 31%. The residual suction is assumed as 1500kPa (Fredlund et al. 1994). As shown in Equation [6.2], the suction is expressed as a function of the water content. Figure 6.2 is produced using Equation [6.2], and is the SWCC for the soil samples from Ardmore.

$$\theta = \left(1 - \frac{\ln\left(1+{}^{\psi}/_{1500}\right)}{\ln\left[1+\left({}^{10^6}/_{1500}\right)\right]}\right) \frac{0.31}{\left(\ln\left(e+\left({}^{\psi}/_{382}\right)^{0.94}\right)\right)^{1.01}} \qquad [6.2]$$

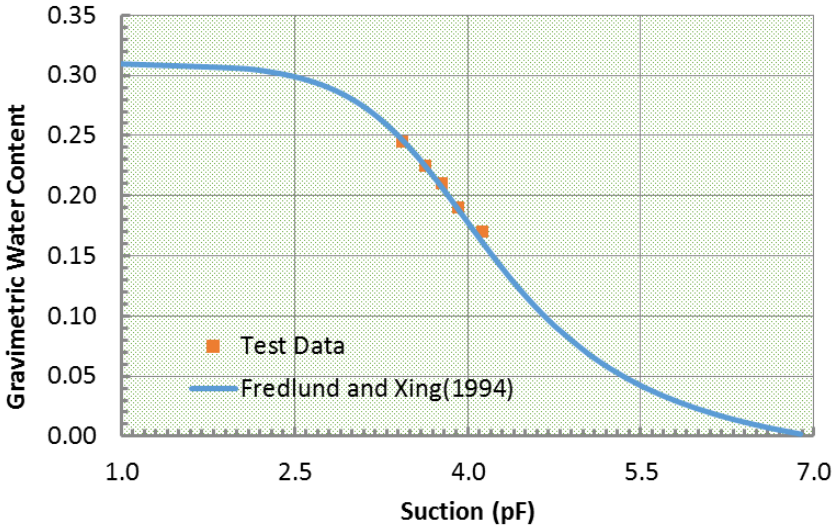

Figure 6.2 SWCC for the Soil Sample from Ardmore

6.1.3 Predicted Suction by SWCC

The suction corresponding to any water content can be obtained after SWCCs are established. In this analysis, the suction from the SWCC is the predicted suction. Six soil samples are used to measure the changes in suction with the drying time. Sample A, B and C are from Lake Hefner, and Sample D, E and F are from Ardmore. The difference between the two successive reading recorded by the camera is equal to the reduction of water weight in the soil sample, and then the water content at any time can be back calculated when the initial water content is given. In these experiments, the initial water content for all the samples is equal to optimum water content (OWC), which is 22.5% for the soil sample obtained from Lake Hefner, and is 24.5% for the soil sample obtained from Ardmore.

The suction at any water content can be calculated using Equation [6.1] and [6.2]. The changes of suction with the drying time for Sample A, B, C, D, E, and F are listed in Appendix A. See Table A.1, Table A.2, Table A.3, Table A.4, Tble A.5 and Table A.6 in Appendix A.

6.1.4 Theoretical Suction by Mitchell's Model

As shown in Equation [6.3], the variables involved in the Mitchell's model are final surface suction, initial suction, diffusion coefficient and soil depth. All of which are determined as follows.

$$u = u_0 + (u_f - u_0)\left(1 - \mathrm{erf}\frac{x}{2\sqrt{\alpha t}}\right) \quad [6.3]$$

where, u is the suction, t is the time, x is the depth, and α is the diffusion coefficient, u_0 is the initial equilibrium suction, u_f is the final surface suction, and the term "erf" is the error function.

The initial suction at OWC is measured from the filter paper method, and the final surface suction is assumed 6.0pF which is equal to the air-dry suction. The diffusion coefficient is determined in the laboratory, and is $4.0 \times 10^{-5} cm^2/s$ for the samples from Lake Hefner and $2.0 \times 10^{-5} cm^2/s$ for the samples from Ardmore. As far as the soil depth is concerned, the height of the soil sample is 4.1cm, the strain gauge is installed in the mid-height of the soil sample (i.e., 2.05cm) and the width of strain gauge is 0.7cm. Therefore, the theoretical suction is taken as the average of suctions at 1.5cm and 2.5cm in this experiment. Table A.7 and Table A.8 list the theoretical suctions for the samples from Lake Hefner and Ardmore obtained by Mitchell's model, respectively.

6.1.5 Comparison between Measured Suction and Theoretical Suction at OWC

Figure 6.3 is produced using the measured suctions in Table A.1, Table A.2 and Table A.3 and the theoretical suctions in Table A.7. Figure 6.3 depicts the changes in suction with the drying time for the samples from Lake Hefner. The curves in the figure can be divided into two phase. In the first phase from the start of experiment to approximately 200 minutes, the measured suctions from Sample A, B and C are larger than the suctions from Mitchell's model. In the second phases when the time is greater than 200 minutes, the measured suctions are smaller than the suctions

from Mitchell's model. However, the difference between the measured suction and Mitchell's suction is not significant. For the case of Sample B, when the measured suction is 3.35pF, the suction from Mitchell's model is 3.24pF, only 0.11pF difference. Generally speaking, the measured suction is close to the suction from Mitchell's model.

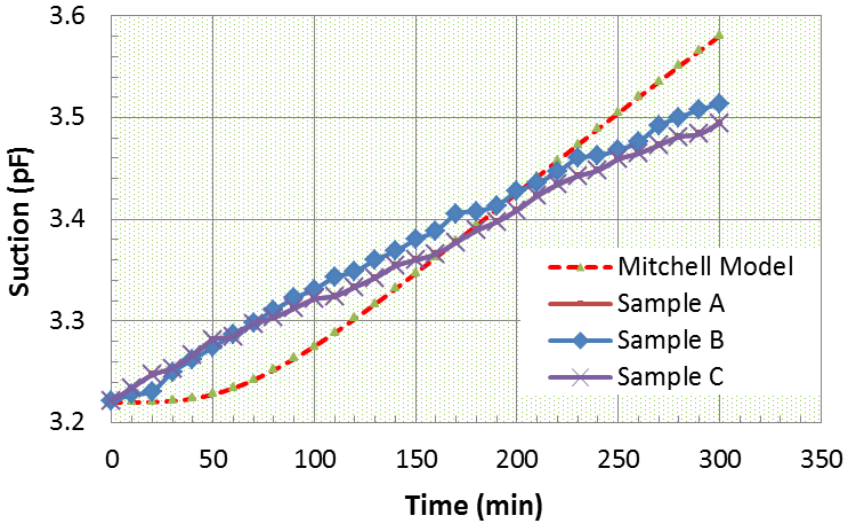

Figure 6.3 Changes in Suction with the Drying Time (Lake Hefner)

Likewise, Figure 6.4 is plotted using the measured suctions in Table A.4, Table A.5 and Table A.6 and the theoretical suctions in Table A.8. Figure 6.4 describes how suction changes with the drying time for the samples from Ardmore. It can be found from Figure 6.4 that the measured suctions from Sample D, E and F are larger than the suctions from Mitchell's model from the start to the end of the experiment, but their difference is small. For the case of Sample E, the maximum suction difference between the measured suction and the suction from Mitchell's model is 0.12pF. Thus, the measured suction is in close agreement with the suction from Mitchell's model.

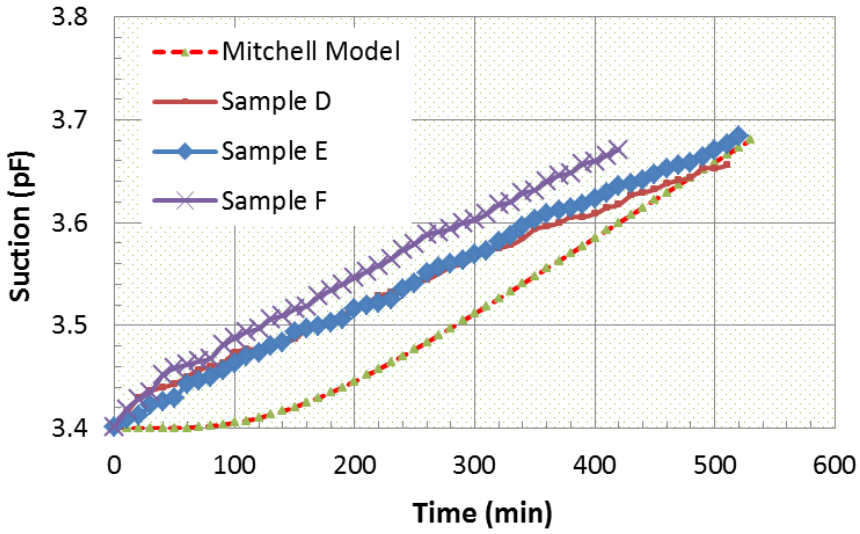

Figure 6.4 Changes in Suction with the Drying time (Ardmore)

6.2 Suction Analysis at the Moisture State Close to Saturation

Tensiometer is used to measure the suctions at the moisture state close to saturation. Six soil samples are tested. Sample G, H and I are obtained from Lake Hefner, and Sample J, K and L are obtained from Ardmore. The unit of suction displayed in the data logger of the tensiometer is kPa, whereas the unit of suction in the new model is pF, so it is necessary to transfer the unit of suction from kPa to pF in the following analysis. The change of suction with the drying time is listed in Appendix A. See Table A.9, A.10, A.11, A.12, A.13 and A.14 in Appendix A.

Similar to the soil samples tested at OWC, the theoretical suction at the moisture state close to saturation is predicted by Mitchell's model. The initial theoretical suction is equal to the initially measured suction. It is found that the initial measured suction varies slightly from one sample to another sample due to the non-uniformity of soil samples. For example, the initial measured suction is 1.57pF for Sample G, while it is 1.51pF for Sample I. Another point is that the initial measured suctions for the samples obtained from Lake Hefner are lower than those from Ardmore due to the difference of diffusion coefficient. The initial measured suctions are approximately

1.5-1.6pF for the samples from Lake Hefner, while they are approximately 1.7-1.8pF for the samples from Ardmore.

The final surface suction is assumed as 6.0pF which is equal to the air-dry suction. The diffusion coefficient is $8.0 \times 10^{-5} cm^2/s$ for the samples from Lake Hefner, and is $4.0 \times 10^{-5} cm^2/s$ for the samples from Ardmore. Similar to the analysis of suction at OWC, the theoretical suction is the average of suctions at 1.5cm and 2.5cm. For Sample G, H, I, J, K and L, their theoretical suctions are listed in Table A.9, A.10, A.11, A.12, A.13 and A.14 in Appendix A.

Figure 5 and Figure 6 are generated using the data in Table A.9, A.10, A.11, A.12, A.13 and A.14 in Appendix A. The relationship between the measured suction and the suction from Mitchell's model at the state close to saturation is similar to that at OWC. At the beginning period, the measured suction is larger than the suction from Mitchell's model, while the measured suction is smaller than the suction from Mitchell's model in the second period. The reason behind this is that the suction from Mitchell's model increases faster than the measured suction as the drying time increases.

Figure 5 and Figure 6 demonstrate that the measured suction from the tensiometer is close to the suction from Mitchell model. The maximum suction differences for Sample G, H, I, J, K and L are 0.20pF, 0.18pF, 0.11pF, 0.15pF, 0.23pF and 0.14pF, respectively. If the measured suction is 2.3pF, then the differences are less than 10% of the measured suction.

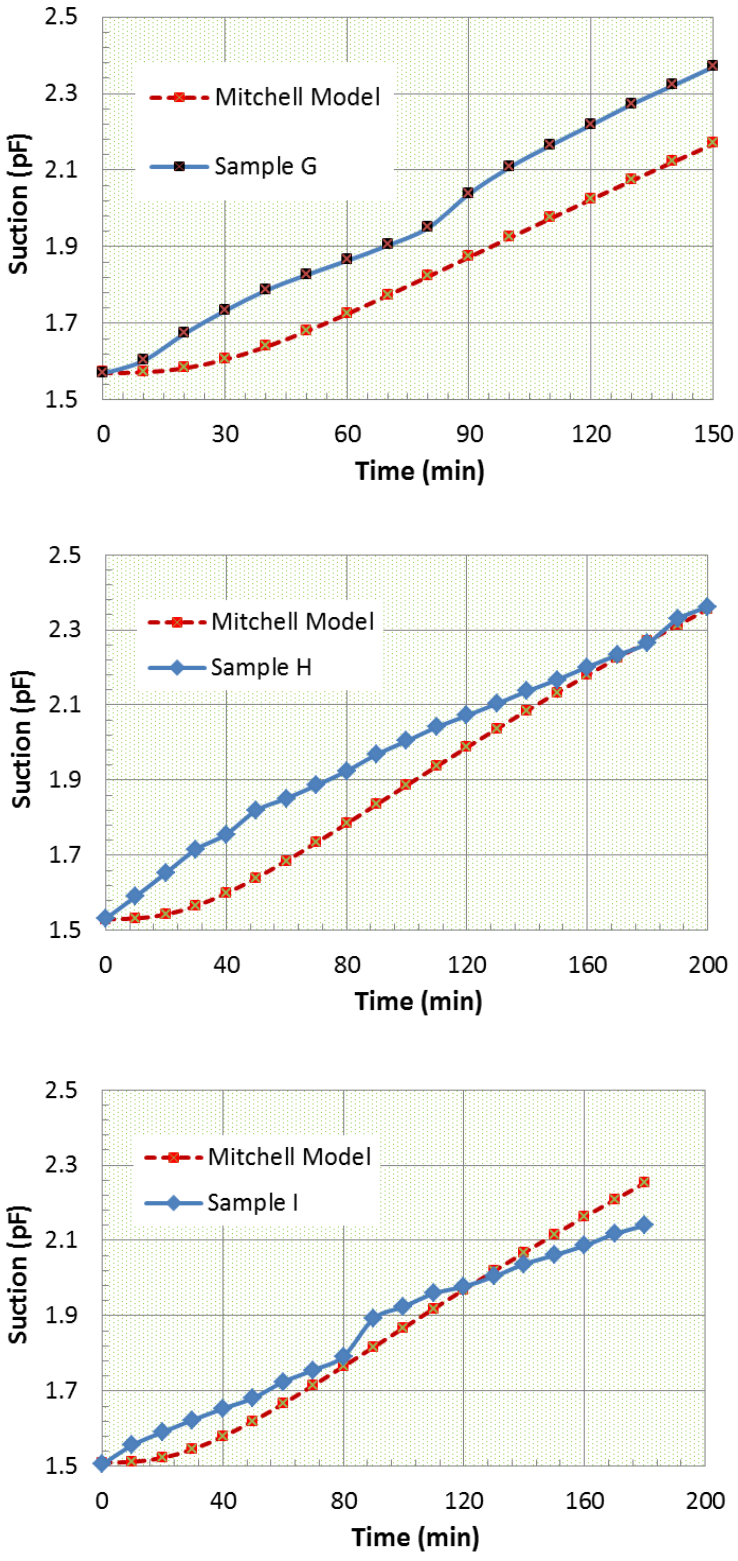

Figure 6.5 Suction Comparison at the State Close to Saturation (Lake Hefner)

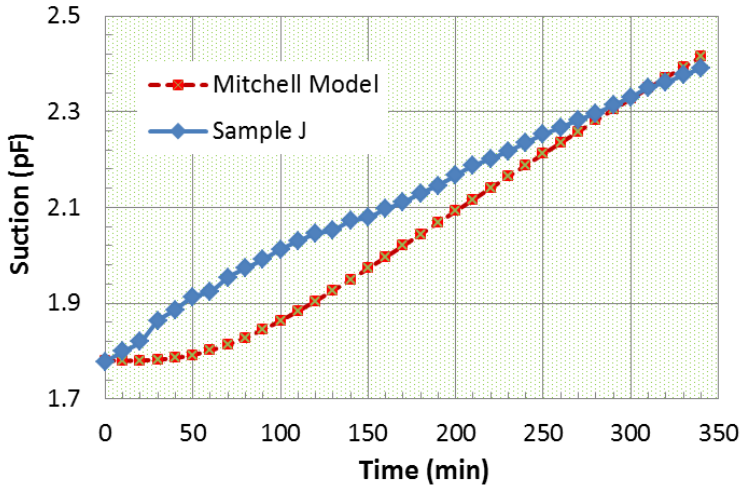

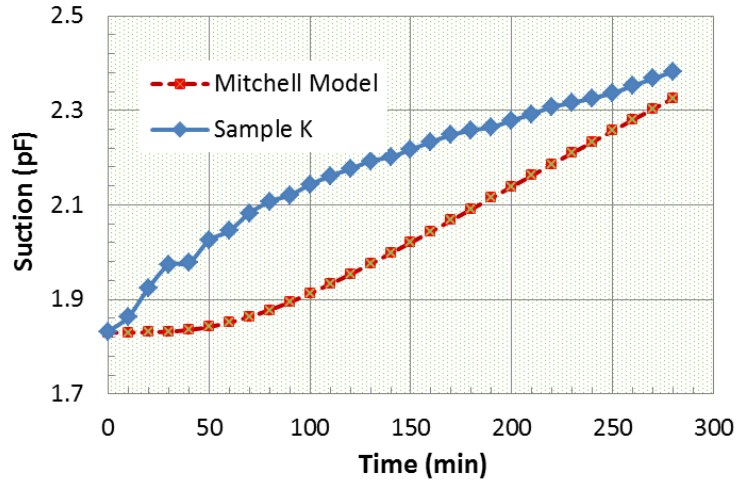

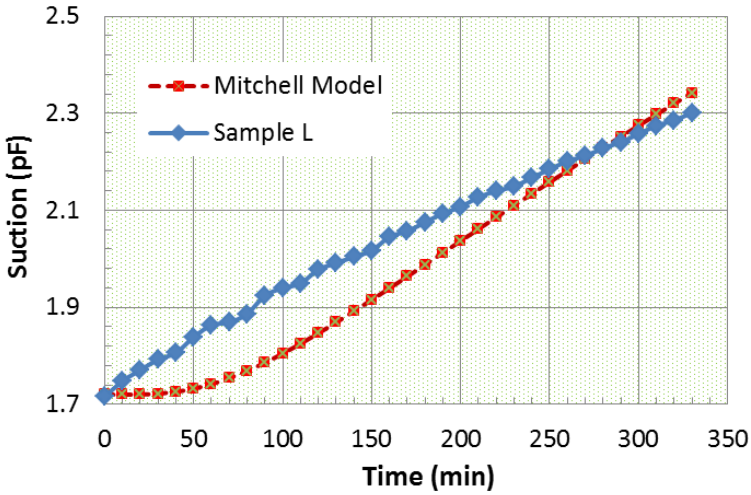

Figure 6.6 Suction Comparison at the State Close to Saturation (Ardmore)

6.3 Tensile Stress Analysis

Sections 6.1 and 6.2 illustrate that the theoretical suction from Mitchell's model are in close agreement with the measured suction by the filter paper method and tensiometer device. The next step is to compare the tensile stress from the new model with the tensile stress from experiments.

6.3.1 Theoretical Tensile Stress by the New Model

The tensile stress from the new model has two parts. As shown in Equation [3.14], the first part is the tensile stress caused by mechanical pressure (i.e., overburden pressure), and the second part is the tensile stress due to suction. In the experiments, the depth of soil sample is 4.1cm, the unit weight is $19.5kN/m^3$, and Poisson's ratio is taken as 0.3. The tensile stress caused by the overburden pressure becomes 0.34kPa by substituting the values given above into the new model as follows

$$\sigma_t = \frac{\nu\sigma_z}{1-\nu} = \frac{0.3\times19.5\times0.041}{1-0.3} = 0.34kPa$$

Compared to the tensile stress due to suction discussed below, 0.34kPa is so small that it is reasonable to ignore.

The parameters involved in the second part include the elastic modulus, Poisson's ratio and suction compression index, which are listed in Table 5.1. The term "$(u_f - u_0) \times \left(1 - \mathrm{erf}\frac{x}{2\sqrt{\alpha t}}\right)$" in the new model is the suction change Δu which is obtained from the Mitchell models. Substituting those values into Equation [3.14], the corresponding relationships for different soil samples are described and given in Table 6.3.

Table 6.3 Equations for Calculating Theoretical Tensile Stress

Soil Sample	Moisture State	Parameters	Equation
Lake Hefner	OWC	$E = 9600\text{kPa}$, $\upsilon = 0.3$, $\Upsilon_h = 0.02$ $\alpha = 4.0 \times 10^{-5} cm^2/s$ $x = 2.05cm$	$\sigma_t = \frac{E}{1-\upsilon}\gamma_h(u_f - u_0) \times (1 - \text{erf}\frac{x}{2\sqrt{\alpha t}})$ $= \frac{9600}{1-0.3}0.02\Delta u = 274.3\Delta u$ ……..Equation [6.4]
	Close to Saturation	$E = 1900\text{kPa}$, $\upsilon = 0.3$, $\Upsilon_h = 0.02$ $\alpha = 8.0 \times 10^{-5} cm^2/s$ $x = 2.05cm$	$\sigma_t = \frac{E}{1-\upsilon}\gamma_h(u_f - u_0) \times (1 - \text{erf}\frac{x}{2\sqrt{\alpha t}})$ $= \frac{1900}{1-0.3}0.02\Delta u = 54.3\Delta u$ ……..Equation [6.5]
Ardmore	OWC	$E = 6500\text{kPa}$, $\upsilon = 0.3$, $\Upsilon_h = 0.04$ $\alpha = 2.0 \times 10^{-5} cm^2/s$ $x = 2.05cm$	$\sigma_t = \frac{E}{1-\upsilon}\gamma_h(u_f - u_0) \times (1 - \text{erf}\frac{x}{2\sqrt{\alpha t}})$ $= \frac{6500}{1-0.3}0.04\Delta u = 371.4\Delta u$ ……..Equation [6.6]
	Close to Saturation	$E = 1400\text{kPa}$, $\upsilon = 0.3$, $\Upsilon_h = 0.04$ $\alpha = 4.0 \times 10^{-5} cm^2/s$ $x = 2.05cm$	$\sigma_t = \frac{E}{1-\upsilon}\gamma_h(u_f - u_0) \times (1 - \text{erf}\frac{x}{2\sqrt{\alpha t}})$ $= \frac{1400}{1-0.3}0.04\Delta u = 80.0\Delta u$ ……..Equation [6.7]

Using the equations listed in Table 6.3, the tensile stresses for all the soil samples are obtained, and the results are shown in Table A.15 and Table A.16. When the tensile stress exceeds the tensile strength, the crack initiates and the tensile stress begins to drop. Thus, the maximum tensile stresses listed in Table A.15 and Table A.16 are the stresses corresponding to the development of cracks.

6.3.2 Measured Tensile Stress by Strain Gauge

The measured tensile stress is calculated using the solution of a pressured elastic cylinder. In this experiment, the elastic modulus of the PVC is 2.9GPa, the inside radius and outside radius of the inner ring are 2.54cm and 2.70cm respectively, and the outside radius of the cylindrical soil sample cylinder is 5.08cm. The testing setup is shown in Figure 5.4. Using the model proposed by Weiss et al. (2009), the measured tensile stress is obtained by Equation [6.8].

$$P_{in}(t) = \varepsilon(t)_{ring}\, E_{ring} \frac{\left(R_{Oring}^2 - R_{Iring}^2\right)}{2R_{Oring}^2} = \varepsilon \times 2.9 \times \frac{(2.70^2 - 2.54^2)}{2\times 2.70^2} = 0.17\varepsilon$$

$$\sigma_t = P_{in}\left(\frac{R_{Oring}^2}{R_{Osoil}^2 - R_{Oring}^2}\right)\left(1 + \frac{R_{Osoil}^2}{R_{Oring}^2}\right) = 0.17\varepsilon \times 0.39 \times 4.5 = 0.30\varepsilon \ \ (kPa) \qquad [6.8]$$

Two strain gauges are installed in the inside of the inner ring as shown in Figure 5.3, and the average of the tensile stresses from the two strain gauges is taken as the measured tensile stress.

For Sample A, the changes in the strain and stress from Gauge 1 and Gauge 2 with the drying time are listed in Table A.17. Figure 6.7 is generated using the data in Table A.17. As shown in Figure 6.7, the stresses from Gauge 1 and Gauge 2 increase with the drying time. The stress at Gauge 1 reaches its maximum value 92kPa at 280 minutes drying time, and then begins to decrease, while the stress at Gauge 2 reaches its maximum value 77kPa at 270 minutes drying time. It is noted that the strains in both gauges do not reduce to zero after the initiation of cracks. This is attributed to the testing setup that the inner ring is still subjected to the tensile stress because the development of crack only releases part of tensile stress.

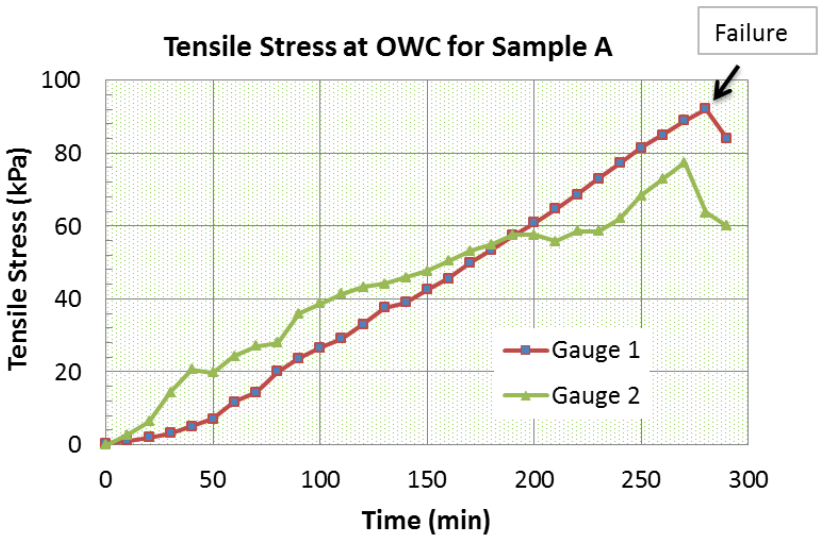

Figure 6.7 Measured Tensile Stress with Time for Sample A

The measured tensile stresses for Samples A, B, C, D, E, F, G, H, I, J,K and L are listed in Table A.18 and Table A.19. Figures 6.8, 6.9, 6.10 and 6.11 are generated using the data listed in Table A.18 and Table A.19. Those figures and tables indicate that the decrease of tensile stress is faster at OWC than at the state close to saturation after the maximum tensile stress. For example, the tensile stress drops from 70kPa to 45kPa for Sample B at OWC, approximately 56% decrease, while the tensile stress drops from 39kPa to 37kPa for Sample K at the moisture state close to saturation, only 6% drop. This is attributed that the soil samples at OWC are more brittle than the samples at the state close to saturation.

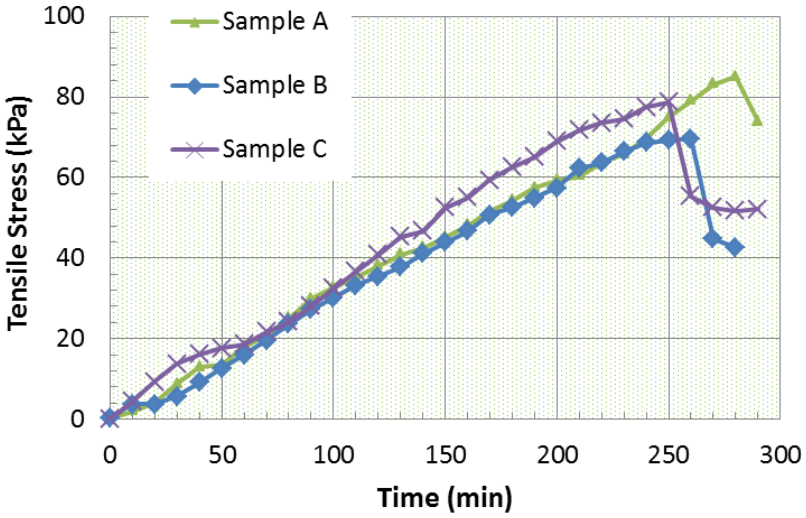

Figure 6.8 Measured Tensile Stress at OWC (Lake Hefner)

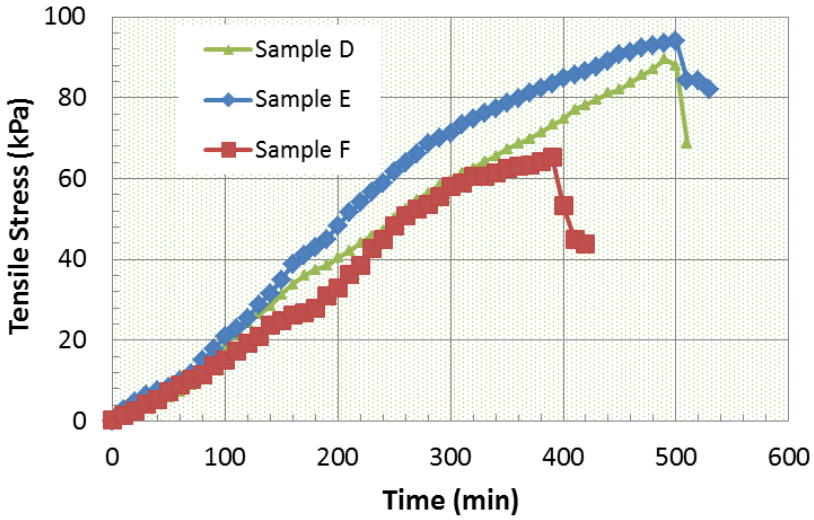

Figure 6.9 Measured Tensile Stress at OWC (Ardmore)

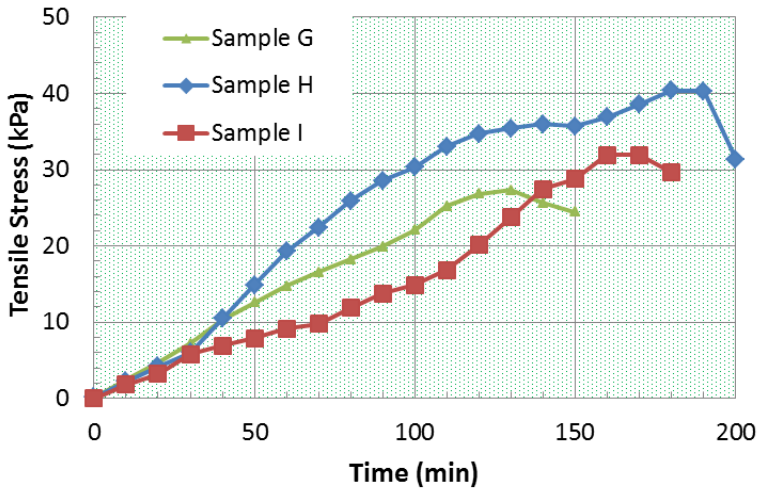

Figure 6.10 Measured Tensile Stress at the State Close to Saturation (Lake Hefner)

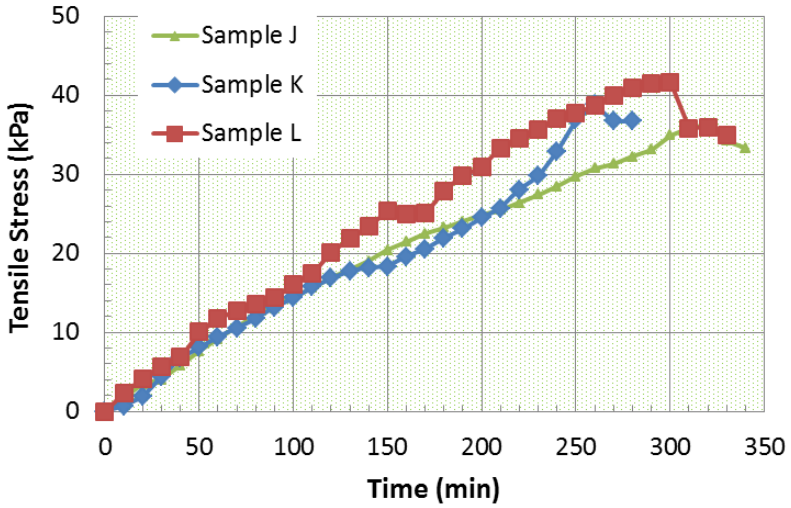

Figure 6.11 Measured Tensile Stress at the State Close to Saturation (Ardmore)

In order to better analyze the difference between the stress from the new model and the measured stress, Figure 6.12, 6.13, 6.14 and 6.15 are generated using the stress from the new model (Table A.16 and Table A.17) as x-axis and the measures stress (Table A.18 and Table A.19) as y-axis. Also, a 1:1 (45 degree) line is generated in those figures. If the measured tensile stress is greater

than the stress from the new model, then the data point of the measured tensile stress is above the 1:1 line. Otherwise, the data point is under the 1:1line.

As shown in Figure 12, 13, 14 and 15, the relationship between the measured tensile stress and the tensile stress from the new model can be divided into two phases. In the first phase, the measured tensile stress is greater than the tensile stress from the new model. In the second phases, the measured tensile stress is smaller than that from the new model. This result coincides with the result made from the analysis of suction.

For Sample A, B, C, D, E and F which are at the state of OWC, the maximum differences between the measured tensile stress and the tensile stress from the new model are 18kPa, 15kPa, 19kPa, 25kPa, 33kPa and 20kPa respectively. The ratios of those differences over their maximum tensile stresses are 21%, 21%, 24%, 28%, 35% and 31%, respectively. For Sample G, H, I, J, K and L at the state close to saturation, the maximum differences between the measured tensile stress and the tensile stress from the new model are 7kPa, 12kPa, 4kPa, 8kPa, 8kPa and 10kPa respectively. The ratio of those differences over their maximum tensile stress are 26%, 30%, 12.5%, 22%, 21% and 24%, respectively. Because the measurement of tensile stress is a complex process which is involved many factors presented in the following section, it can be said that the measured tensile stress are in good agreement with the tensile stress from the new model.

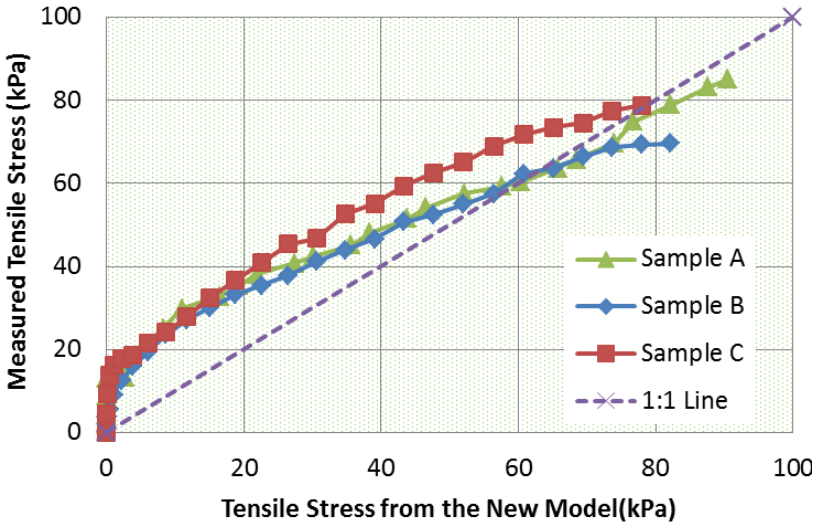

Figure 6.12 Tensile Stress Comparison at OWC (Lake Hefner)

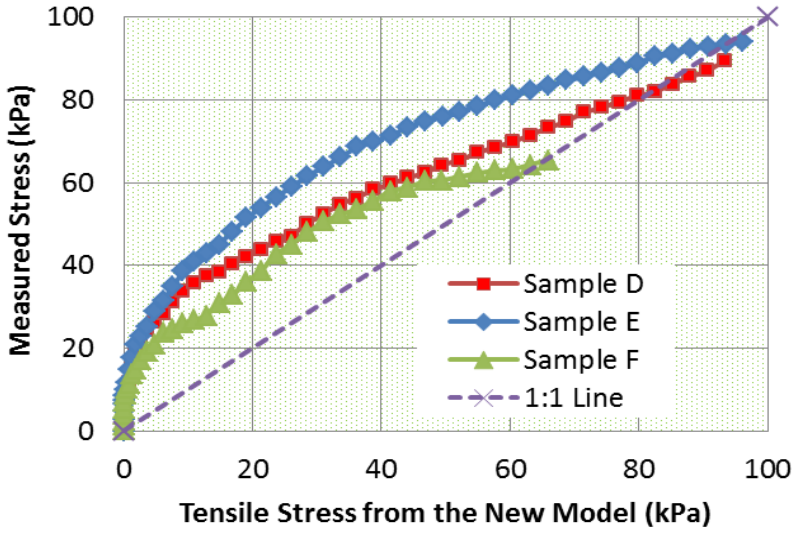

Figure 6.13 Tensile Stress Comparison at OWC (Ardmore)

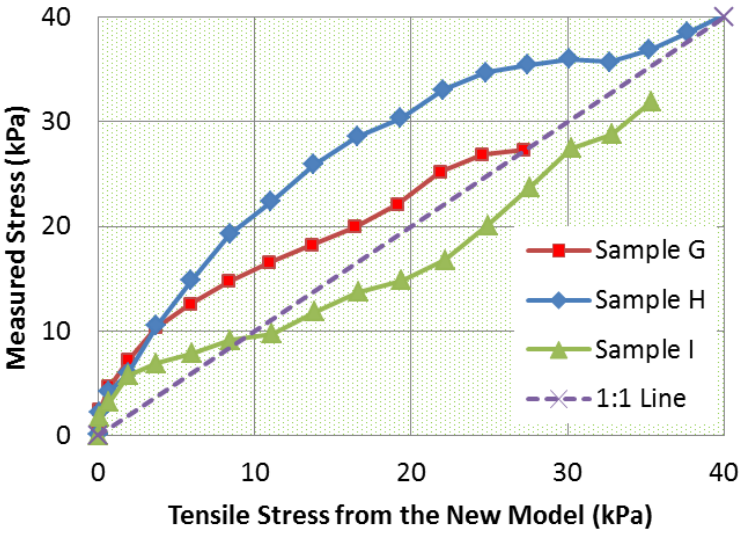

Figure 6.14 Tensile Stress Comparison Close to Saturation (Lake Hefner)

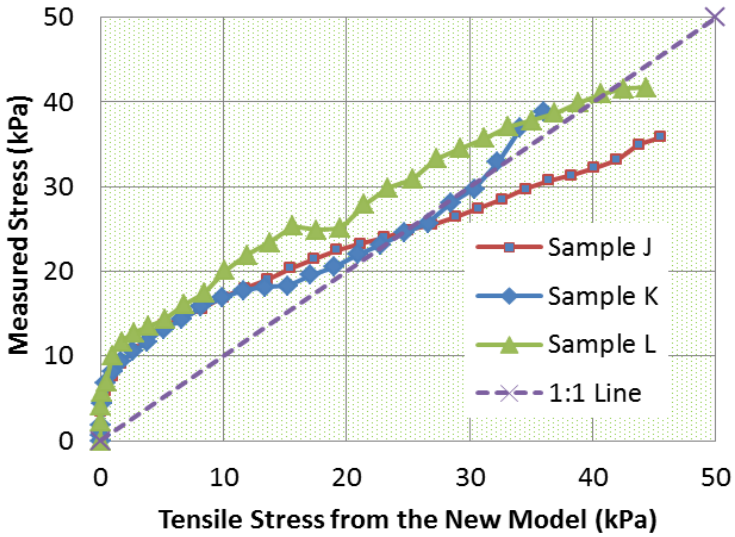

Figure 6.15 Tensile Stress Comparison Close to Saturation (Ardmore)

As state above, there is approximately 25% difference between the measured tensile stress and the tensile stress from the new model. The reasons causing the theoretical stress to deviate from the measured stress are listed as follows.

a) The first reason lies in the suction. As stated in Section 6.1 and Section 6.2, the measured suctions are not exactly the same as the suction from Mitchell's model. Because the suction in the new tensile stress model is calculated by Mitchell's model, it is unavoidably that the accuracy of Mitchell's model affects the tensile stress calculated by the new model.

b) The second reason is that the measured tensile stress is the average of the two strain gauges. Due to the complexity of soil sample and soil drying mechanism, the distribution of tensile stress along the inner ring is not uniform. As shown in Figure 6.9, the tensile stress @220 minutes is 69kPa for Gauge 1, while it is 59kPa for Gauge 2. Therefore, the accuracy of tensile stress is reduced when the average of the two strain gauges is taken as the measured tensile stress.

c) The third reason is from suction compression index. Suction compression index is estimated based on the chart provided by Covar and Lytton (2001). For the same input parameters, someone may estimate that suction diffusion coefficient is 0.02, while others possibly estimate that it is 0.022. There is 10% error between 0.02 and 0.022.

d) The fourth reason comes from elastic modulus and Poisson's ratio. They are affected by many factors. For the soil sample prepared by standard proctor compaction, its elastic modulus changes with position, Generally speaking, the elastic modulus is highest at the bottom, and lowest at the top. For different soil samples, their elastic moduli are not exactly the same due to the complexity of soil structure and non-uniformity of compaction. Also, the Poisson's ratio is obtained by estimation.

e) The last reason is due to diffusion coefficient. The measured diffusion coefficient is not exactly the same as its real diffusion coefficient.

6.4 Cracking time, Water Content and Diffusion Coefficient

Table 6.4 lists the cracking time, the reduction of water content and tensile strength which is equal to the maximum tensile stress. Also, the diffusion coefficients are included in Table 6.4.

Table 6.4 Cracking time, Water Content Reduction and Tensile Strength

State	Soil Sample		Cracking time (min)	Water content Reduction (%)	Tensile Strength (kPa)	Diffusion Coefficient (cm^2/s)
OWC	Lake Hefner	Sample A	270	2.4	85	4.0×10^{-5}
		Sample B	260	2.4	70	
		Sample C	250	2.2	79	
		Average	260	2.4	78	
	Ardmore	Sample D	480	2.4	89	2.0×10^{-5}
		Sample E	500	2.6	94	
		Sample F	390	2.5	65	
		Average	457	2.5	83	
Close to saturation	Lake Hefner	Sample G	120	1.6	27	8.0×10^{-5}
		Sample H	180	2.2	40	
		Sample I	160	2.0	32	
		Average	153	1.9	33	
	Ardmore	Sample J	310	2.8	36	4.0×10^{-5}
		Sample K	260	2.2	36	
		Sample L	300	2.4	44	
		Average	290	2.5	39	

6.4.1 The Relationship between Cracking Time and Diffusion Coefficient

Figure 6.16 is generated using the average cracking time and diffusion coefficient listed in Table 6.4. The dashed line is for the samples at OWC, and the solid line is for the samples at the state close to saturation.

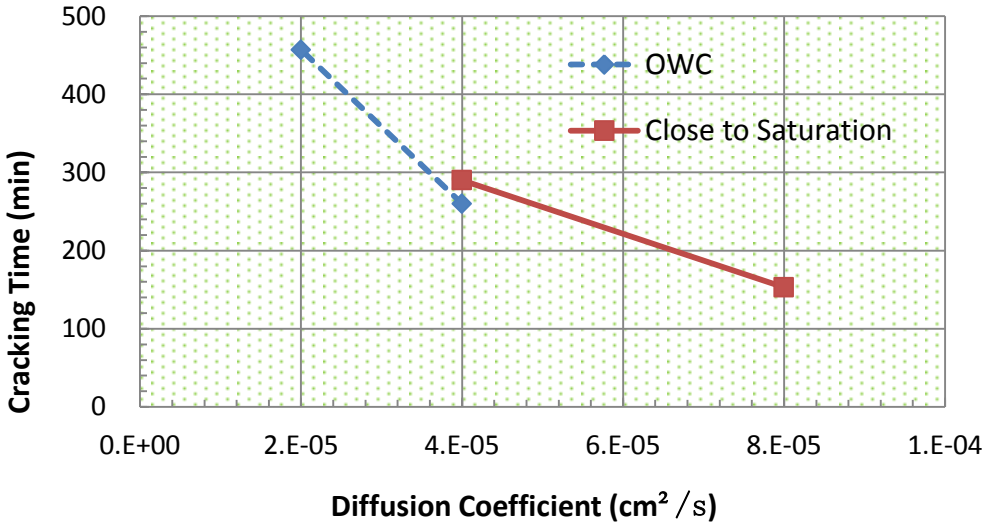

Figure 6.16 Diffusion Coefficients with Cracking Time

It is found that the cracking time increases as diffusion coefficient decreases. Figure 6.16 shows the average cracking time at OWC is 260 minutes for the sample from Lake Hefner, while it is 457 minutes for the samples from Ardmore. This is attributed to the decrease of diffusion coefficient. The diffusion coefficient at OWC is $4.0 \times 10^{-5} cm^2/s$ for the samples from Lake Hefner, while it is $2.0 \times 10^{-5} cm^2/s$ for the samples from Ardmore. The same conclusion can be made when comparing the average cracking time for the sample at the moisture state close to saturation as shown in the solid line in Figure 6.16.

Another point is that the cracking time at OWC is larger than the cracking time at the state close to saturation. For the sample obtained from Lake Hefner, the average cracking time is 260 minutes at OWC, while it is 153 minutes at the moisture state close to saturation. This means that

the soil at OWC has higher capacity to resist the development of cracking. This conclusion is confirmed when analyzing the sample from Ardmore. The average cracking time is 457 minutes at OWC, while it is 290 minutes at the state close to saturation.

6.4.2 Tensile Strength

The maximum tensile stress measured by the strain gauges is equal to the tensile strength of the soil. As stated in Chapter 3, many models for predicting the tensile strength of the soils have been proposed based on various experiments of setups and theoretical assumptions. Those models can be divided into two groups. The first one is for saturated soils, and the second one is for unsaturated soils.

As shown in Equation [6.9], Fang and Chen's (1971) model for saturated soils is selected to verify the tensile strength close to saturation. Zeh and Witt's (2005) model (Equation [6.10]) for unsaturated soils is used to verify the tensile strength at OWC. The calculating results are listed in Table 6.5.

$$\sigma_t = 31.44 + 1.24PI - 0.0176PI^2 \quad [6.9]$$

$$\sigma_t = 10.349 + 331.214 \times \exp\{-0.5[\frac{\ln\left(\frac{u}{15388.92}\right)}{2.187]^2}\} \quad [6.10]$$

Where PI =plasticity index (%), u = suction (kPa), σ_t= tensile strength (kPa)

Table 6.5 Tensile Strength Validation

State	Soil Sample		Tensile Strength (measured) (kPa)	Zeh and Witt (2005) (kPa)	Fang and Chen (1971) (kPa)
OWC	Lake Hefner	Sample A	85	74	N/A
		Sample B	70	76	N/A
		Sample C	79	74	N/A
		Average	78	75	N/A
	Ardmore	Sample D	89	100	N/A
		Sample E	94	103	N/A
		Sample F	65	89	N/A
		Average	83	97	N/A
Close to saturation	Lake Hefner	Sample G	27	N/A	45
		Sample H	40	N/A	
		Sample I	32	N/A	
		Average	33	N/A	
	Ardmore	Sample J	36	N/A	52
		Sample K	36	N/A	
		Sample L	44	N/A	
		Average	39	N/A	

N/A :Not available

It can be seen in Table 6.5 that the predicted tensile strength by Zeh and Witt model (2005) is close to the measured tensile strength. The average measured tensile strengths at OWC for the samples from Lake Hefner and Ardmore are 78kPa and 83kPa respectively, while the predicted tensile strengths, based on the Zeh and Witt (2005) model, are 75kPa and 97kPa respectively. .

For the samples close to saturation, the predicted tensile strength by Fang and Chen (1971) model is larger than the measured tensile strength. For example, the predicted strength for the samples obtained from Ardmore is 52kPa, while the measured tensile strength is 39kPa, but the difference is not large. It can be said that the restrained ring method can provide reasonable tensile strength.

Another point worth to point out is the change of tensile strength with water content. As shown in Table 6.5, the tensile strengths from Lake Hefner and Ardmore soils are 78kpa and 83kPa at OWC, while they decrease to 33kPa and 39kPa close to saturation, more than 50% decrease. This indicates that the tensile strength of the soil may depend on the initial moisture content.

6.4.3 Diffusion Coefficient

The laboratory experiments also demonstrate that the diffusion coefficient changes with water content or suction. For the samples obtained from Ardmore, the diffusion coefficient is $2.0 \times 10^{-5} cm^2/s$ at OWC, while it is $4.0 \times 10^{-5} cm^2/s$ at the moisture state close to saturation. For the samples obtained from Lake Hefner, the diffusion coefficient is $4.0 \times 10^{-5} cm^2/s$ at OWC, while it is $8.0 \times 10^{-5} cm^2/s$ at the moisture state close to saturation. Thus, it can be concluded that the diffusion coefficient decreases with the increase of water content. The conclusion confirms the results presented by Yi (2014).

CHAPTER VII

THE EFFECT OF CRACKS ON PAVEMENT PERFORMANCE IN PRESENCE OF MOISTURE BARRIER

7.1 Introduction

The last task of this research is to apply the new model described in Chapter III to estimate the depths of the cracks developing outside the pavement slab. Then, analyze the effect of these cracks on the performance of the pavement in presence of vertical and horizontal moisture barriers using the finite element method. Another purpose of this chapter is to compare the performance of vertical moisture barrier and horizontal moisture barrier with each other.

In order to deal with the volume change behavior of expansive soils, many methods have been proposed, and can be divided into three categories (Rojas et al. 2006). The first category is to replace expansive soils with inert materials such as gravel and sand. The second one is to use chemical stabilization using lime, cement, fly ash and so on. The last one is to employ vertical or horizontal moisture barriers to reduce moisture fluctuations under the pavement slab.

The method of moisture barrier (i.e., the third category) has many advantages over the first category and second category, such as low cost and fast construction. However, moisture barriers have not performed as well as expected in some cases. For example, based on the analysis of 8.0 feet vertical moisture barrier installed at IH-30 in Texas, Gay (1994) presented

that the reduction of serviceability index (SI) during the 1984-1990 period was 0.2567 SI/year, while the average SI reduction for the control section was 0.2527 SI/year, which is not a significant difference. Another example is from Canada where a 3.0m vertical moisture barrier was installed at the runway of an airport. The results of monitoring indicated that the test sections performed better than control section in the first 3 years, and then had no difference after 5 years (Diyaljee and Wiens 1995).

Up to date, many researchers have studied the working principles of moisture barriers. Rojas et al. (2006) proposed a new model for analyzing water flow under moisture barrier. Gay (1994) developed a computer program to simulate the moisture variation in presence of vertical moisture barriers. Also, Gay (1994) analyzed the influence of the length of vertical barrier on SI, IRI and expected bump height of the pavement. Marco et al. (1998) studied the effects of different barrier materials including lime, fly ash and geo-membrane on the performance of pavement.

However, literature review shows that little attention is given to the cracks developed outside the pavement slab. As we know, the working principle of moisture barriers is to keep the water content stable by increasing the diffusing length of the moisture movement. In fact, the area protected by the moisture barrier is limited to the zones between the vertical barriers or under the horizontal barriers, while the outside area is vulnerable to the initiation and propagation of cracks, which then become the pathways of moisture movement. Figure 7.1 is the pavement section with an outside crack in presence of vertical moisture barriers (Chen and Bulut 2015). Water can infiltrate or evaporate through the bottom and sides of the outside crack, so the length of moisture movement in the right side (right dashed arrow line) is significantly shorter than the left side (left dashed arrow line). Therefore, the benefit of the vertical moisture barrier is significantly counteracted in presence of the outside crack.

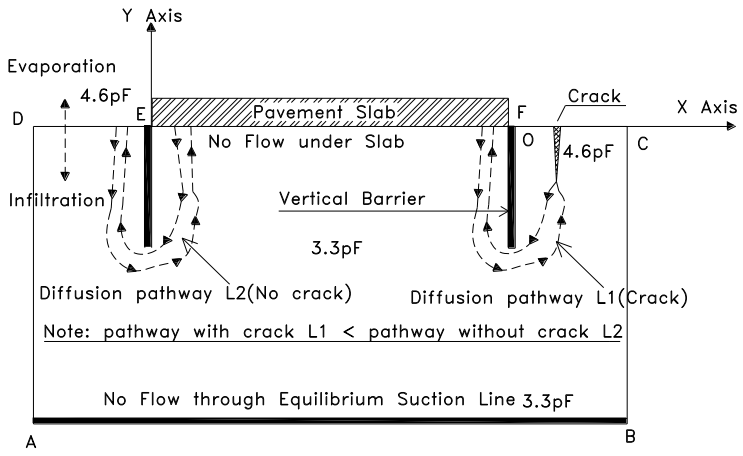

Figure 7.1 Diffusion Pathway Changed by Outside Crack (Chen and Bulut 2015)

Compared to vertical moisture barriers, horizontal moisture barriers have caught more attention due to their relatively easy installation. This study includes not only vertical moisture barrier, but also horizontal moisture barrier. The performance of vertical moisture barrier will be compared to the performance of horizontal moisture barrier, and some useful conclusions will be drawn based on finite element analysis.

The method adopted in this chapter includes two steps. The first step is to predict the depth of crack using the new model (i.e., Equation 3.14). The second step is to study the changes in suction, settlement and stress caused by the outside crack using the finite element method. There are two sub-steps in the second step. The first sub-step is to analyze the distribution of suction using the heat transfer model in Abaqus software, and the second sub-step is to predict the profiles of settlement and stress using the plain strain model in Abaqus. Loads and displacements change in the vertical direction and transverse direction, while they are constant in the longitudinal direction, so the plain strain model is selected in this analysis.

7.2 Prediction of Cracking Depth

A pavement section analyzed here includes three parts: pavement slab, subgrade and moisture barriers, whose parameters are listed in Table 7.1. It is noted that the length of moisture barrier is assumed as 2.0m in Table 7.1. The purpose of this assumption is to simplify the problem and better analyze the effect of cracks. How the length of vertical moisture barrier affects the performance of pavement has been studied by Chen and Bulut (2015).

Table 7.1 Parameters of Slab, Subgrade and Moisture Barrier in FEM

Slab: Elastic modulus = 2500MPa, Poisson's ratio = 0.3, Thickness = 0.3 m, Length = 7.2 m, Diffusion coefficient = 0.00cm^2/sec (impermeable layer).
Subgrade: Poisson's ratio = 0.3, Length = 12 m, Depth = 6 m, Suction compression index = 0.04, Elastic modulus = 5 MPa, Diffusion coefficient =$1.0 \times 10^{-4}\text{cm}^2/\text{sec}$, Final surface suction = 4.6 pF, Initial suction = 3.3pF, and unit density$18kN/m^3$.
Moisture barrier: Length = 2.0 m (vertical barrier or horizontal barrier), Diffusion coefficient = 0.00cm^2/sec (impermeable layer).

In the analysis, the crack is represented by a finite element where the diffusion coefficient and elastic modulus for the crack area are assumed to be zero. the crack is directly connected to the atmosphere, so it is reasonable to assume that the crack is an extension of the subgrade surface, and then the suction of the crack is equal to the final surface suction. The thickness of the moisture barrier is very thin, so the effect of moisture barrier on the elastic modulus and Poisson's ratio of the subgrade is ignored. The FEM model is meshed using 4-node quadrilateral elements whose dimensions are 0.1 m by 0.1 m.

The drying times analyzed here are 3 months and 9 months, which can cover wide range of climate regions. The distribution of tensile stress with depth is obtained when substituting the values in Table 7.1 into the new model (Equation 3.14). See Figure 7.2.

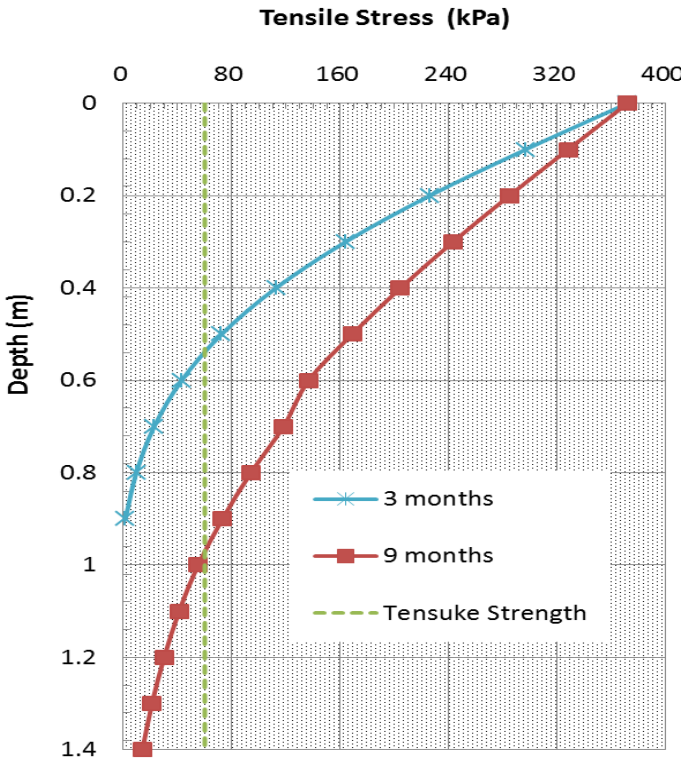

Figure 7.2 The Profiles of Tensile Stress for 3 and 9 Months of Drying Time

If the soil strength is assumed as 60kPa which is close to the tensile strength measured by the restrained ring method as described in Chapter V, then the intersection points between the soil tensile strength line and the tensile stress curves are the crack depths. Figure 7.2 shows that the crack depth is approximately 0.5m for 3 months drying time and 1.0m for 9 months.

7.3 Effect of Outside Crack in Presence of Vertical Moisture Barrier

Four cases are used to analyze the effect of an outside crack on the performance of pavement in presence of a vertical moisture barrier. Case 1 is a control section without a crack and without vertical moisture barrier. Case 2 is another control section with a vertical moisture barrier and

without a crack. Case 3 and Case 4 are the other two sections with 0.5m and 1.0m crack depths, respectively. The details for each case are listed in Table 7.2, and the geometrical models are shown in Figure 7.3. The distance between the outside crack and the vertical moisture barrier is assumed as 0.5m.

Table 7.2 Parameters Involved in Vertical Barrier

Case Number	Vertical Barrier (m)	Horizontal Barrier (m)	Crack Depth (m)
1	0.0	0.0	0.0
2	2.0	0.0	0.0
3	2.0	0.0	0.5
4	2.0	0.0	1.0

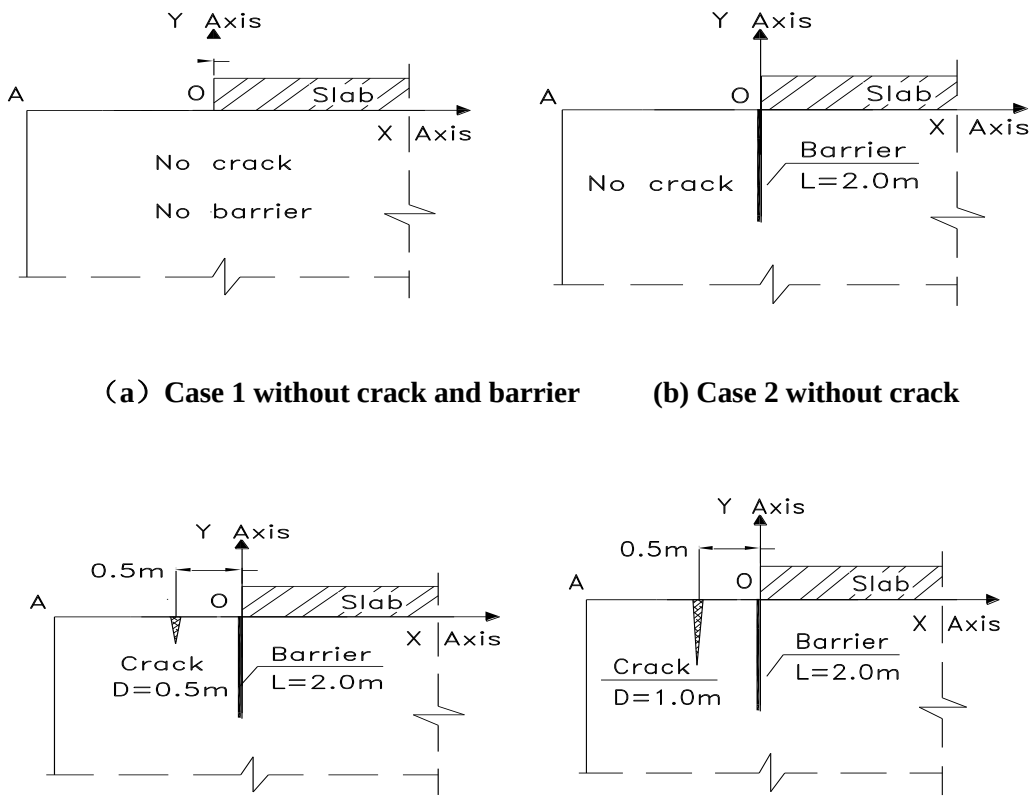

（a）Case 1 without crack and barrier **(b) Case 2 without crack**

（c） Case 3 with 0.5m crack **(d) Case 4 with 1.0m crack**

Figure 7.3 Four Cases in the Analysis of Vertical Moisture Barriers

7.3.1 Suction Analysis

Using the heat transfer model in Abaqus, the suction profiles for Case 1, 2, 3 and 4 are obtained and shown in Figure 7.4, where the zone with red color exhibits the highest suction of 4.6pF, and the zone with blue color shows the lowest suction of 3.3pF, and the zone with other transition colors shows the suction ranging from 3.3pF to 4.6pF.

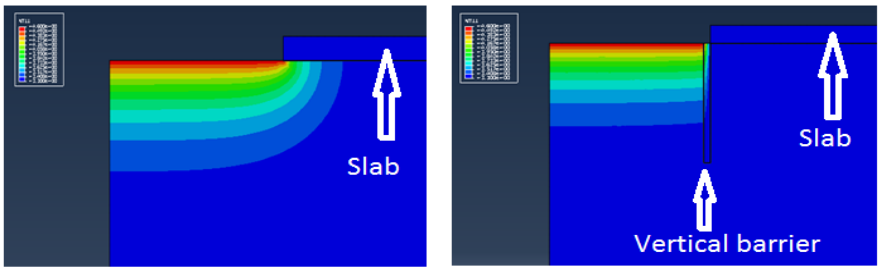

(a) Case 1 without crack and barrier (b) Case 2 without crack and with barrier

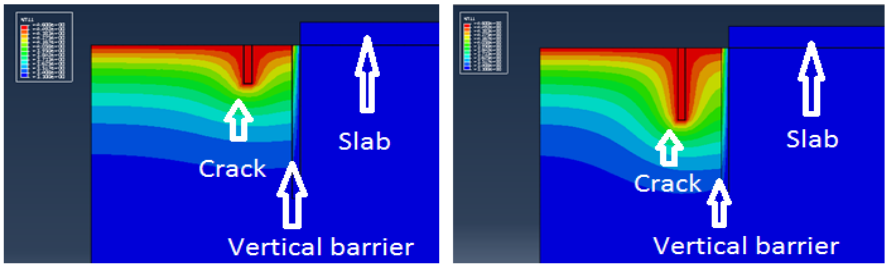

(c) Case 3 with barrier and 0.5m crack (d) Case 4 with barrier and 1.0m crack

Figure 7.4 Suction Profiles in Presence of Vertical Moisture Barrier

The presence of a vertical moisture barrier greatly alters the distribution of suction in the subgrade. As shown in Figure 7.4, the suction in the zone under the pavement slab in Case 1 (no barrier) is much higher than the suction in the same zone in Case 2 (2.0m barrier). Figure 7.5, generated using the suctions obtained from Abaqus, depicts the changes in suction in Case 1 and Case 2. The x-axis in Figure 7.5 is the horizontal distance from the pavement slab edge point "O" as shown in Figure 7.3, and the y-axis is the suction. For example, the suction at the slab edge is 4.6pF for Case 1, while it is only 3.32pF for Case 2. Thus, it is clear that the installation of a vertical moisture barrier can successfully prevent the change in suction for the zone under the pavement slab.

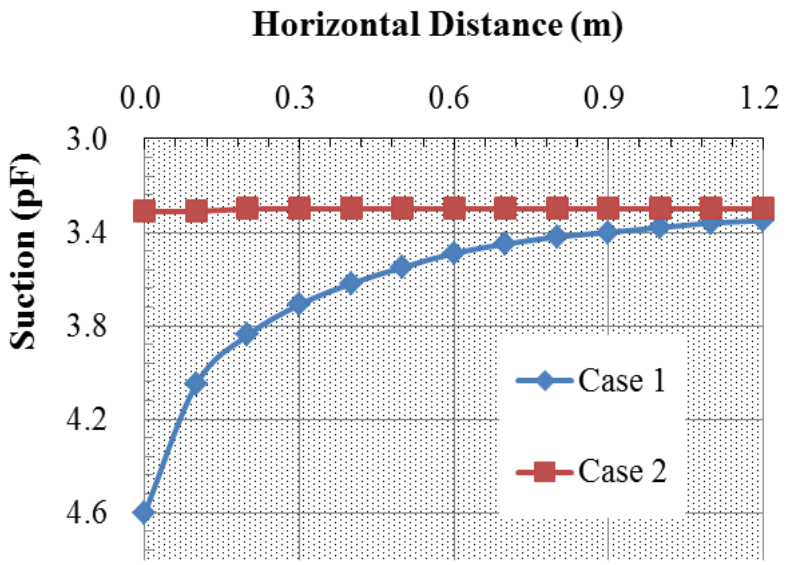

Figure 7.5 Suction Change in Horizontal Direction for Case 1 and 2

Another conclusion is that the distribution of suction with depth is greatly influenced by the outside crack when analyzing Figure 7.4 (b), (c) and (d). Figure 7.6, generated using the suctions obtained from Abaqus, describes the changes in suction with depth for Case 2, 3 and 4. The y-axis in Figure 7.6 is the vertical distance from the slab edge point "O" as shown in Figure 7.3, and the x-axis is suction. It can be seen that the suction in vertical direction increases with the depth of outside crack. For instance, the suction at 0.5m depth is 3.80pF in Case 2 (no crack), while it is 4.02pF in Case 3 (0.5m crack) and is 4.18pF in Case 4 (1.0m crack). The increase of suction results in the increase of shrinkage settlement in subgrade and tensile stress in slab, which will be analyzed next.

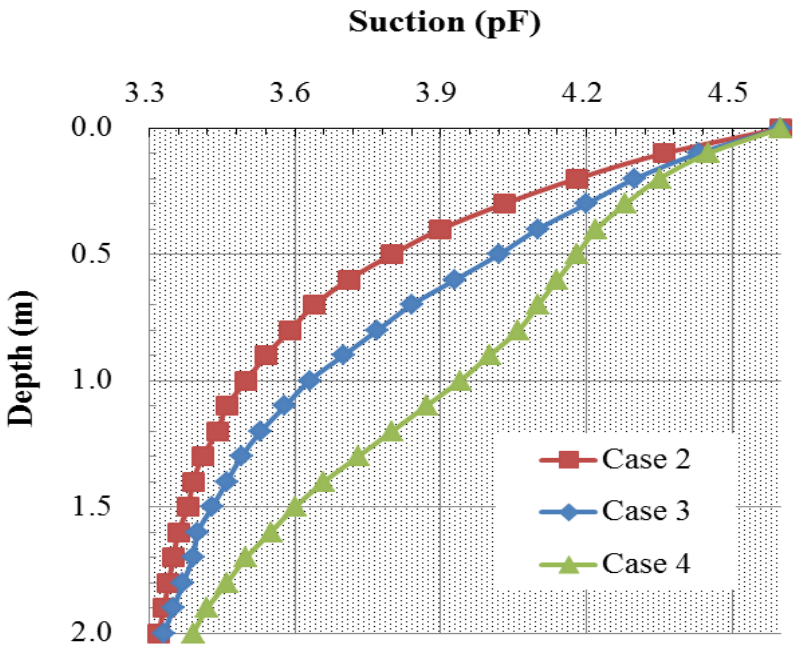

Figure 7.6 Suction Changes in Vertical Direction for Case 2, 3 and 4

7.3.2 Settlement Analysis

This section analyzes the effect of the outside crack on the distributions of settlement in the subgrade. In this analysis, the output file containing the suctions obtained above is used as the input file, and the plain strain model is applied to analyze the settlement of the subgrade. Given that the pavement slab is not bounded to the subgrade, the profiles of the settlements for Case 1, 2, 3 and 4 are shown in Figure 7.7.

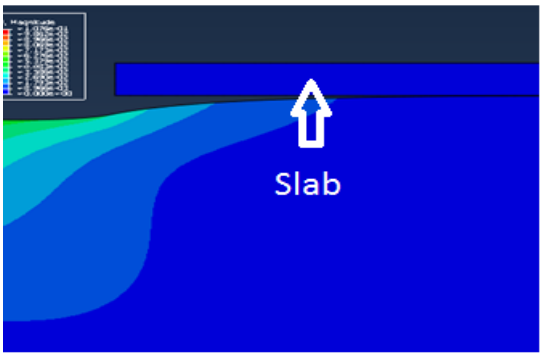

(a) Settlement profile for Case 1

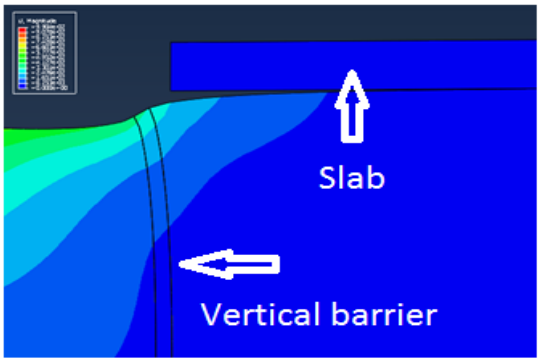

(b) Settlement profile for Case 2

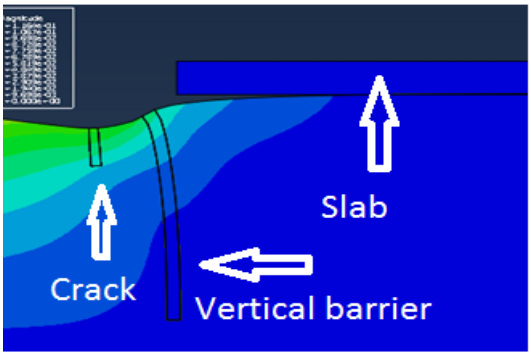

(c) Settlement profile for Case 3

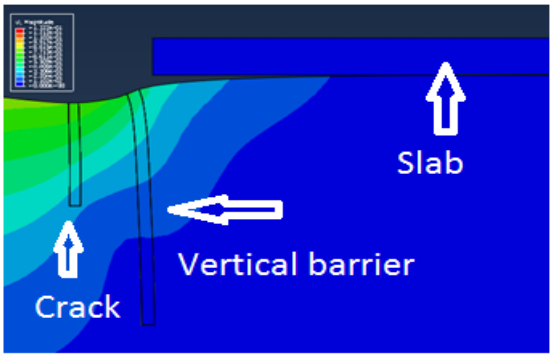

(b) Settlement profile for Case 4

Figure 7.7 Settlement Profiles in Presence of Vertical Barrier

It is seen in Figure 7.7 that the gap between the pavement slab and the subgrade is the maximum at the pavement slab edge, and then decreases with the increase of horizontal distance from the pavement edge. The settlements obtained from Abaqus are utilized to plot Figure 7.8 where x-axis is the horizontal distance from the pavement slab edge, and y-axis is the settlement.

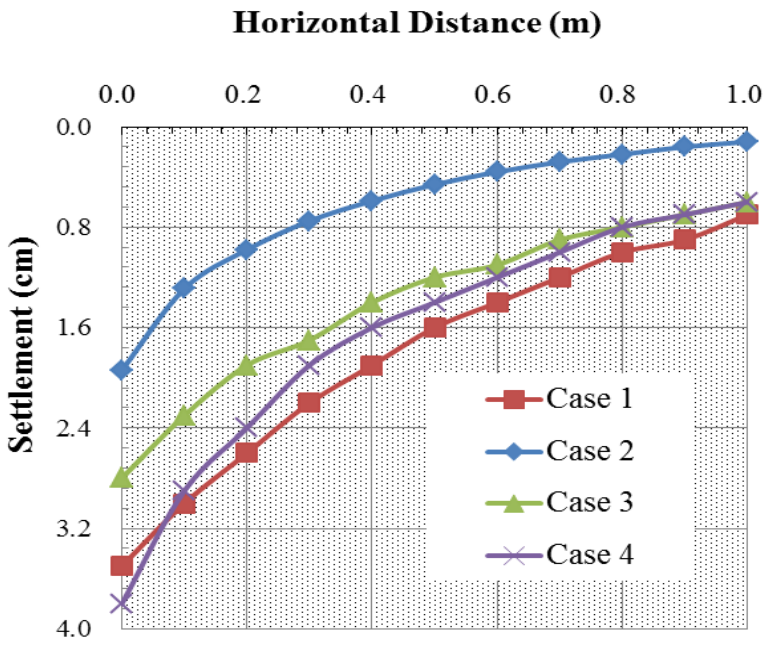

Figure 7.8 Changes in Settlement under Pavement Slab

Two points can be drawn from Figure 7.8. Firstly, the maximum settlements at the pavement edge is 3.5cm for Case 1 (no barrier and no crack), while it is 1.9cm for Case 2 (2.0m barrier and no crack), approximately 46% reduction compared to Case 1. This means that the installation of vertical moisture barrier greatly reduces the settlement, but it cannot completely eliminate the settlement of the pavement slab due to drying shrinkage.

Secondly, the presence of an outside crack greatly increases the amount of settlement. The maximum settlement at pavement slab edge is 1.9cm for Case 2 (no crack), while it is 2.8cm for Case 3 (0.5m crack), about 42% increase, and is 3.8cm for Case 4 (1.0m crack), about 100% increase. It is worth to point out that the settlement for Case 4 is even larger than the settlement for Case 1 (no crack and no barrier). In this case, the effect of 2.0m vertical moisture barrier is completely counteracted by the 1.0m crack. Hence, the development of an outside crack might cause great damage to pavement.

7.3.3 Analysis of Tensile Stress in Pavement Slab

The two extremely boundary conditions are considered for the pavement slab and subgrade soil interaction. The first extreme condition is that the pavement slab is completely free from the subgrade. In other words, there is no bonding between the pavement slab and subgrade soil. The second one is that the pavement slab is completely bonded to subgrade. For the first condition, as shown in Figure 7.7, there are no deformations in the pavement slab, and thus no stresses are developed in the slab. For the second condition, the pavement slab shares the same settlement values with the subgrade at the interface. Tensile stresses are unavoidably induced in the pavement slab. Figure 7.9 shows the profile of tensile stress for Case 4. In Figure 7.9, the red color in the pavement slab means tensile stress and the blue color in the pavement slab means compressive stress.

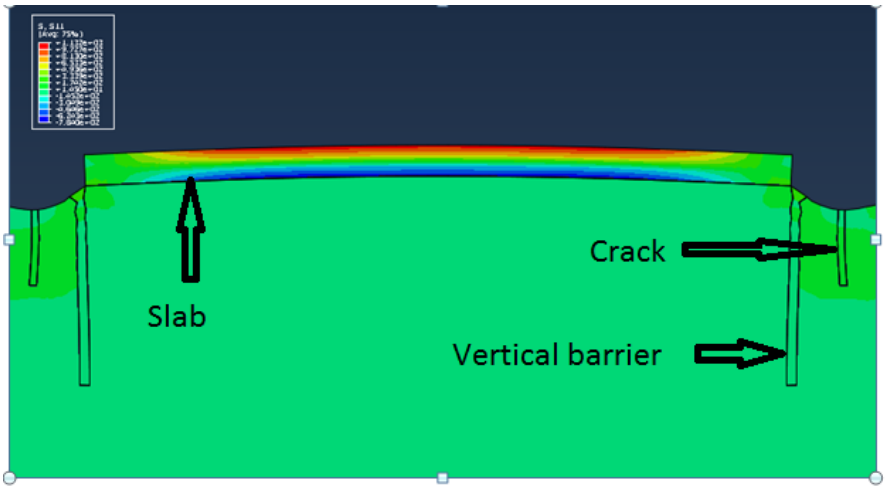

Figure 7.9 Tensile Stress Profile in Abaqus

It is the tensile stress that leads to the development of cracks in pavement slabs, so only tensile stress is analyzed in this section. It can be seen that the location of the maximum tensile stress is close to the center of the pavement slab. The behavior of the pavement slab is like a cantilever beam when the settlement is large. Also, it is noted that the maximum tensile stress occurs at the

top surface of pavement slab. The two points given above indicate that the potential location for a crack to occur is at the center of the pavement and belongs to top-down crack type.

Figure 7.10 is generated using the tensile stresses obtained from Abaqus. In Figure 7.10, x-axis is the horizontal distance from the pavement slab edge, and y-axis is the tensile stress in the pavement slab. It can be seen in Figure 7.10 that the distribution of tensile stress in pavement slab for Case 1 (without crack and without barrier) is very similar to that for Case 4 (with 1.0m crack and 2.0m vertical barrier). Therefore, the point that the benefit of a 2.0m vertical moisture barrier is completely counteracted by a 1.0m outside crack is proven again. Another point is that the maximum tensile stress for Case 2 (2.0m vertical barrier and no crack) is 550kPa, approximately 50% of the maximum tensile stress compared to Case 1 (1100kPa). The maximum tensile stress for Case 3 (2.0m vertical barrier and 0.5m crack) is 800kPa which is 72% of the maximum tensile stress compared to Case 1. Therefore, the maximum tensile stress in the pavement slab increases with the depth of crack.

Carrasquillo et al. (1981) proposed a model to predict splitting tensile strength from compressive strength as shown in Equation [7.1] where f_{sp} is the splitting tensile strength and f_c' is the compressive strength. Given that the compressive strength of concrete pavement slab is 20MPa, the tensile strength is approximately 2500kPa. The values of tensile stress for Case 1 (without crack and without barrier) and Case 4 (with 1.0m crack and 2.0m vertical barrier) are more than 1000kPa. Meanwhile, there is a gap between the concrete slab and subgrade soil, so the load from vehicle definitely induces extra tensile stress in the concrete slab. If the combined tensile stress in the concrete slab exceeds the tensile strength, then cracks unavoidably initiate and propagate.

$$f_{sp} = 0.59\sqrt{f_c'} \qquad [7.1]$$

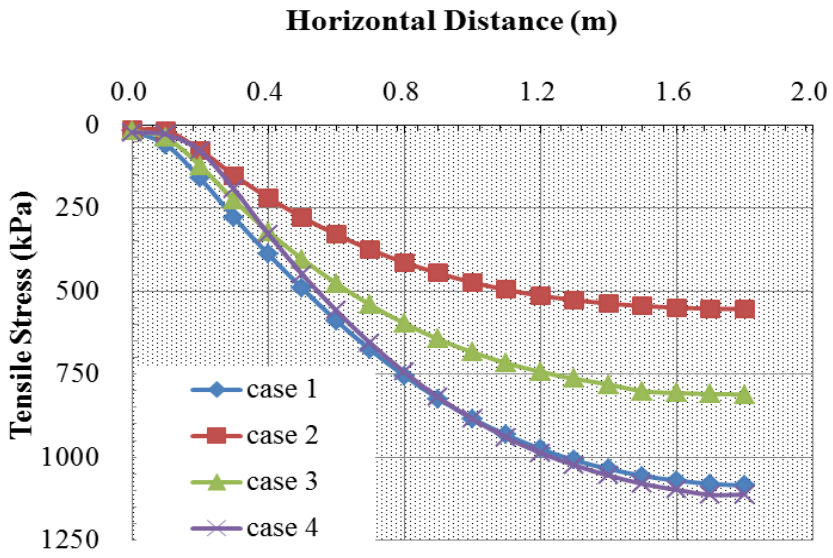

Figure 7.10 Tensile Stress Changes in Pavement Slab

7.4 Effect of Outside Crack in Presence of Horizontal Moisture Barrier

In this section, the pavement is constructed with a 2.0m horizontal moisture barrier. The change in the moisture content in the zone under the horizontal moisture barrier is smaller than that of the zone outside the barrier, so it is reasonable to assume that the location of the outside crack is the edge of the horizontal moisture barrier (i.e., 2.0m away from pavement edge), as shown in Figure 7.11.

Similar to the analysis of the vertical moisture barriers, four cases analyzed here are listed in Table 7.3. Case 1 is a control section without a crack and without a horizontal moisture barrier. Case 2 is the second control section with a horizontal moisture barrier and without a crack. Case 3 and Case 4 are the other two sections with 0.5m and 1.0m crack depths, respectively. The geometrical model of the each case is shown in Figure 7.11.

Table 7.3 Parameters Involved in Horizontal Barrier

Case Number	Vertical Barrier (m)	Horizontal Barrier (m)	Crack Depth (m)
1	0.0	0.0	0.0
2	0.0	2.0	0..0
3	0.0	2.0	0.5
4	0.0	2.0	1.0

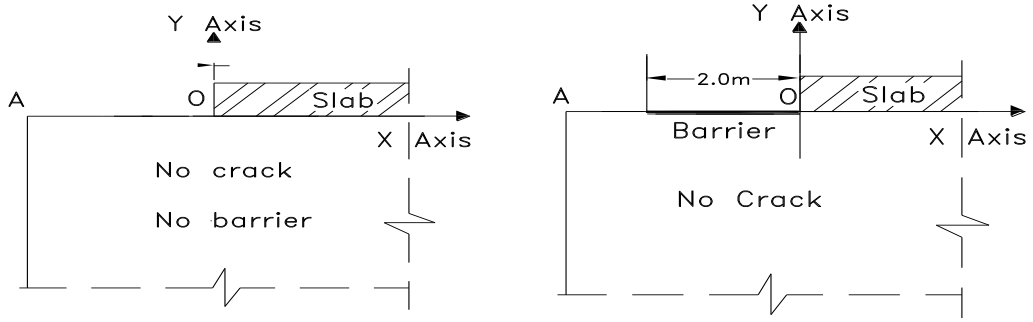

(a) Case 1 without crack and barrier (b) Case 2 with barrier and no crack

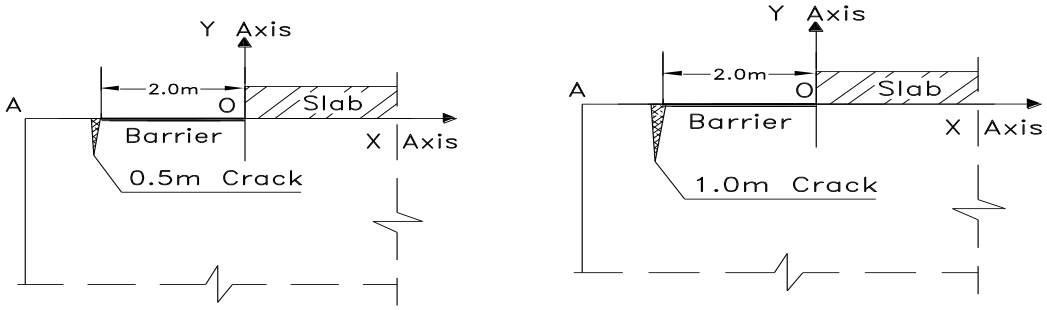

(c) Case 3 with 0.5m crack and barrier (d) Case 4 with 1.0m crack and barrier

Figure 7.11 Four Cases in the Analysis of Horizontal Moisture Barrier

7.4.1 Suction Analysis

The suction profiles for all the four cases are shown in Figure 7.12, where the red color means the highest suction 4.6pF, the blue color shows the lowest suction, and the other colors represents the transitional suctions between 4.6pF and 3.3pF.

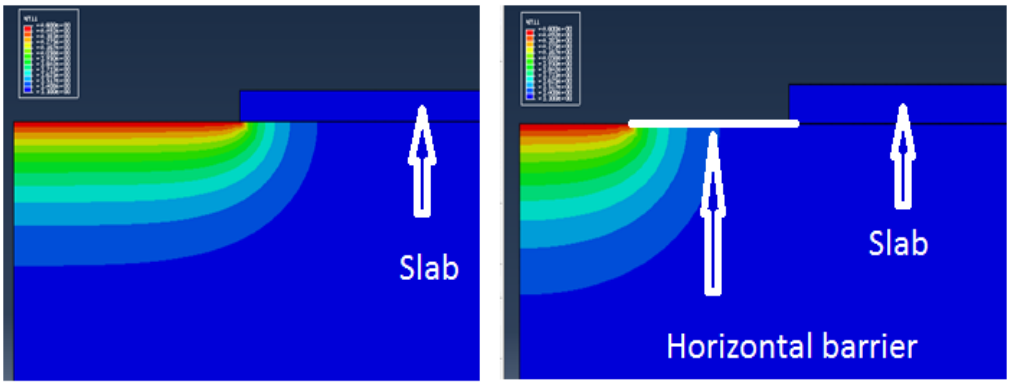

(a) Case 1 without crack and barrier (b) Case 2 without crack and with barrier

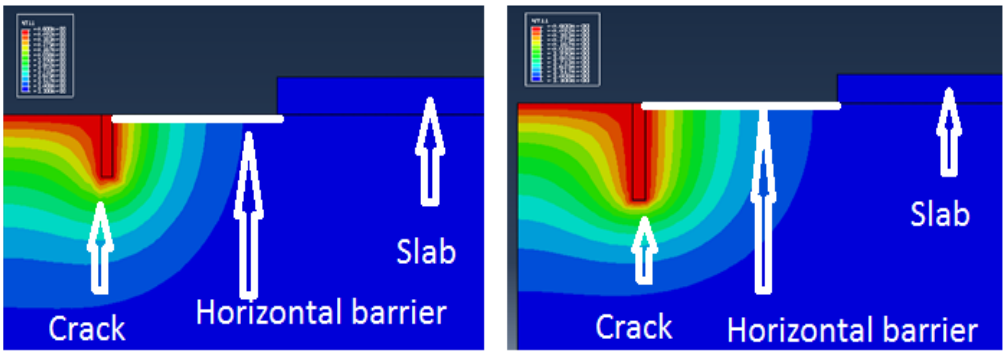

(c) Case 3 with 0.5m crack and barrier (d) Case 4 with 0.5m crack and barrier

Figure 7.12 Suctions profile in the analysis of horizontal barriers

It is found that the influence of the horizontal moisture barrier on the suction profile is significant when comparing Figure 7.12 (a) and Figure 7.12 (b). The installation of the horizontal barrier successfully pushes the suction contour away from the slab edge (Figure 7.12 a) towards the edge

of the moisture barrier edge (Figure 7.12 b). The maximum suction at the slab edge is 4.60pF in Case 1 (without a horizontal barrier), while it is only 3.31pF in Case 2 (with 2.0m horizontal barrier).

Also, the existence of an outside crack changes the distribution of suction with depth. It is seen that the suction contour is pushed deeper when comparing Figure 7.12 (c) and (d). For example, the suction at the point 1.5m vertically away from the slab edge is 3.32pF for Case 3 (0.5m crack), while it is 3.39pF for Case 4 (1.0m crack).

7.4.2 Settlement Analysis Due to Drying Shrinkage

The profiles of settlement for all the four cases are depicted in Figure 7.13. Figure 7.14 is generated using the data collected from Abaqus. In Figure 7.14, x-axis is the horizontal distance from the slab edge, and y-axis is the settlement.

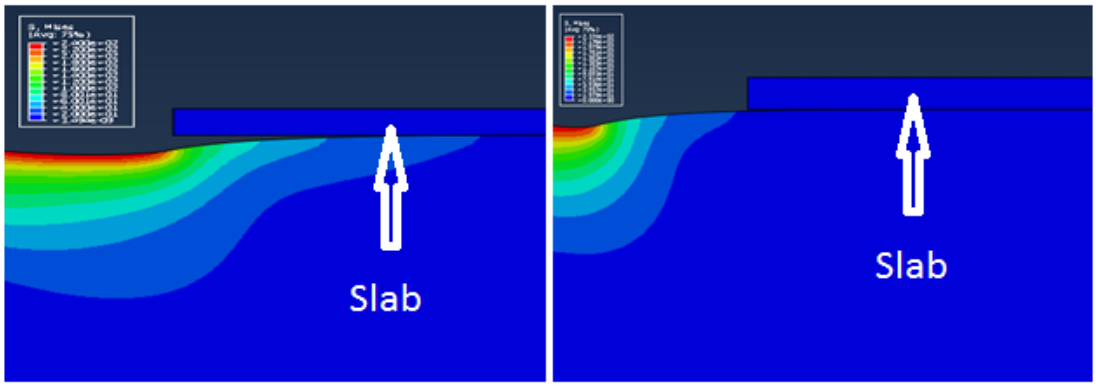

(a) Settlement profile for Case 1 (b) Settlement profile for Case 2

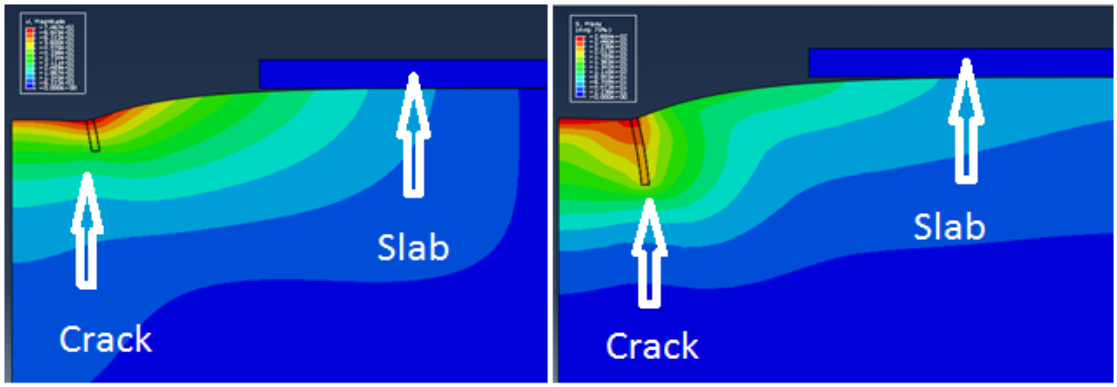

(c) Settlement profile for Case 3 (d) Settlement profile for Case 4

Figure 7.13 Settlement Profiles in the Analysis of Horizontal Moisture Barrier

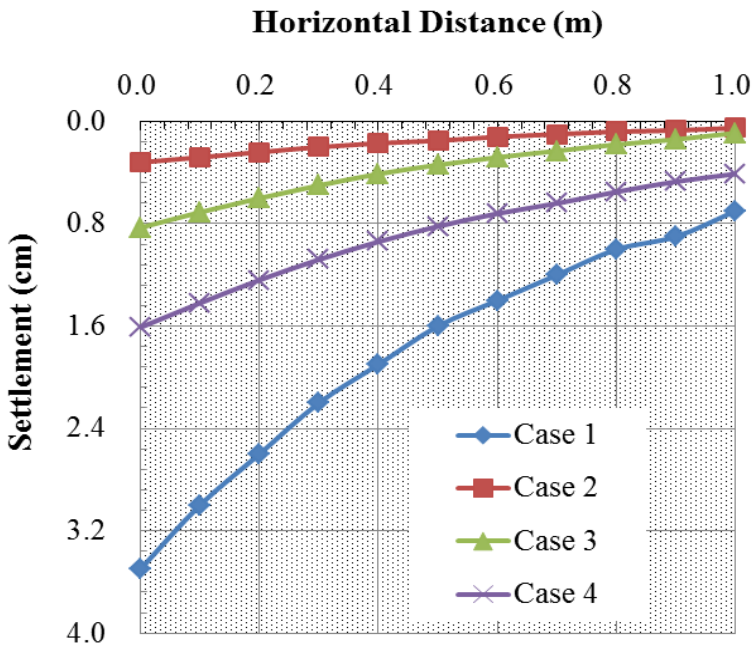

Figure 7.14 Settlement Change in Horizontal Direction

The first point drawn from Figure 7.13 and 7.14 is that the installation of a horizontal moisture barrier greatly reduces the settlement under the pavement slab. The settlement under the slab edge is 3.51cm for Case 1 (without a crack and horizontal barrier), while it is 0.32cm for Case 2 (with a horizontal barrier and no crack), approximately 90% reduction.

The second point is that the presence of an outside crack increases the settlement of the subgrade soil. The settlement under the slab edge is 0.83cm for Case 3 (with the horizontal barrier and 0.5m crack), about 150% increase compared to Case 2 (without crack and with barrier). The settlement under the slab edge is 1.61cm for Case 4 (with the horizontal barrier and 1.0m crack), approximately 400% increase compared to Case 2.

On the other hand, the settlements for Case 3 and Case 4 are 23% and 46% compared to that for Case 1, respectively. Therefore, unlike the vertical moisture barrier, the benefit of a 2.0m horizontal moisture barrier is not completely counteracted by the outside cracks.

7.4.3 Analysis of Tensile Stress in Pavement Slab

The settlement profiles given in Section 7.4.2 are for the condition that the pavement slab is not bounded to the subgrade soil. In other words, complete slippage is allowed at the interface the pavement slab and subgrade soil. Similar to the analysis of the vertical moisture barrier, the other extreme condition is that pavement slab is completely bounded to the subgrade soil, and the induced tensile stresses in the slab are analyzed in this section.

Figure 7.15 exhibits the profile of the tensile stresses in the pavement slab for Case 4. In Figure 7.15, the red color depicts the maximum tensile stress. The profiles of the tensile stresses for Case 2 and Case 3 are similar to that for Case 4, so they are shown in Appendix. It can be observed in Figure 7.15 that the location of the maximum tensile stress is at the bottom of the slab, and is close to the edge of the slab.

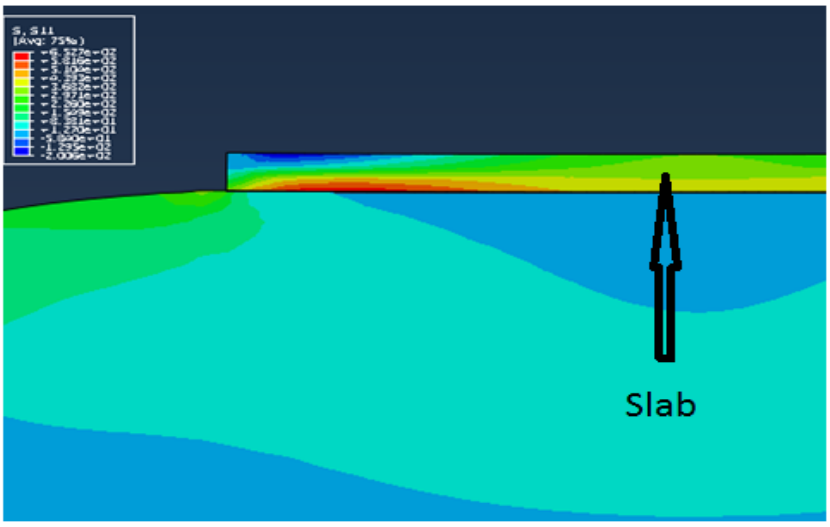

Figure 7.15 The Profile of Tensile Stress in the Pavement Slab for Case 4

Figure 7.16 is generated using the tensile stresses obtained from Abaqus for all the four cases. X-axis is the horizontal distance from the pavement slab edge, and y-axis is the tensile stress in the pavement slab. It can be seen that the curves for Case 2, 3 and 4 are significantly different from

the curve for Case 1. The position of the maximum tensile stress for Case 2, 3 and 4 is approximately 0.7m~0.9m from the pavement edge, while it is 1.8m from the pavement edge for Case 1. Therefore, the horizontal moisture barriers greatly change the profile of tensile stresses in pavements.

Also, the maximum tensile stresses for Case 2, 3 and 4 are 324kPa, 492kPa and 651kPa, while the maximum tensile stress for Case 1 reaches 1100kPa. This demonstrates that the presence of the horizontal moisture barrier significantly reduces the maximum tensile stress, and effectively reduces the potential for the development of cracks.

On the other hand, the development of outside cracks leads to the increases of tensile stresses. For Case 3 with the 0.5m crack depth, the maximum tensile stress is 492kPa, approximately 52% increase compared to Case 2. For Case 4 with the 1.0m crack depth, the maximum tensile stress is 651kPa, approximately 101% increase compared to Case 2. Again, it is shown that the outside cracks have significant influence on the performance of pavement.

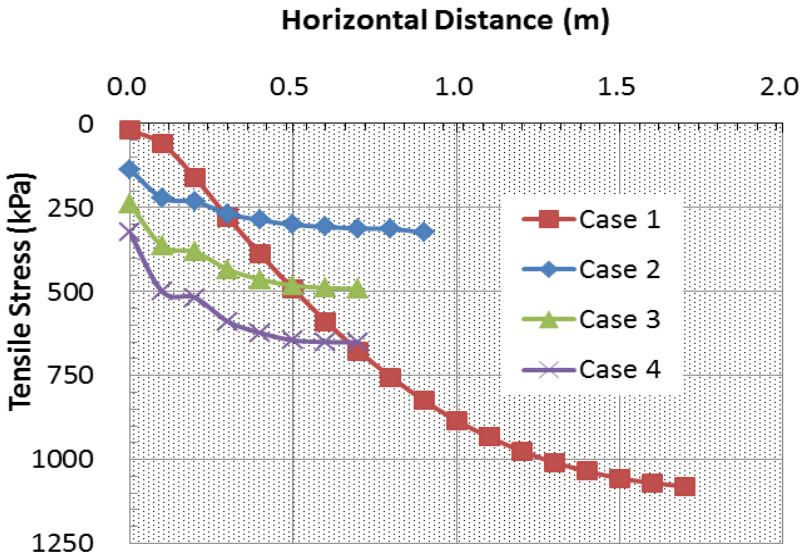

Figure 7.16 Tensile Stress Changes in Pavement Slab

7.5 Comparison between the performance of Horizontal Barrier and Vertical Barrier

The suction and settlement in the subgrade soil, and the tensile stress in the pavement slab in presence of vertical moisture barrier and horizontal moisture barrier are analyzed in section 7.3 and section 7.4, respectively. In this section, the performance of the horizontal moisture barrier will be compared to the performance of the vertical moisture barrier in two ways: the settlement in the subgrade and the tensile stress in the pavement slab. Suction is not included because suction is a middle variable whose final purpose is to calculate the settlement and tensile stress.

7.5.1 Settlement Comparison

Table 7.4 lists the maximum settlements for different crack depths and for the same length of horizontal moisture barrier and vertical moisture barrier.

Table 7.4 Maximum Settlement Comparison

Crack depth (m)	Moisture barrier length (m)	Settlement in Horizontal Barrier (cm)	Settlement in Vertical barrier (cm)
0.0	2.0	0.32	1.94
0.5	2.0	0.83	2.81
1.0	2.0	1.61	3.83

As shown in Table 7.4, for the case of the same crack depth, the settlement of the horizontal moisture barrier is much smaller than that of the vertical moisture barrier. For example, if the length of the horizontal moisture barrier is equal to the length of the vertical moisture barrier, and the crack depth is 1.0m, then the settlement at the slab edge is 1.61cm for the horizontal barrier, while it is 3.83 cm for the vertical barrier, more than 100% increase. The reason behind the big difference is that the location of the outside crack for the horizontal barrier is further away from the slab edge than that for the vertical barrier.

7.5.2 Tensile Stress Comparison

The maximum tensile stresses and their locations for different crack depths are listed in Table 7.5. The "location" in the 2nd column of Table 7.5 is the horizontal distance to the pavement slab edge, and the "bottom or top" in Table 7.5 means that the maximum tensile stress occurs at the bottom area or top area of the slab, respectively. Figure 7.17 is plotted using the data in Table 7.5. As shown in figure 7-17, the original point is the edge of pavement slab, y-axis is vertical direction and x-axis is horizontal direction.

Table 7.5 Location and Maximum Tensile stress Comparison

Crack depth (m)	Location (m)		Maximum tensile stress(kPa)	
	Horizontal	Vertical	Horizontal	Vertical
0.0	0.9 (bottom)	1.8m(top)	324	554
0.5	0.7(bottom)	1.8m(top)	492	811
1.0	0.7(bottom)	1.8m(top)	651	1113

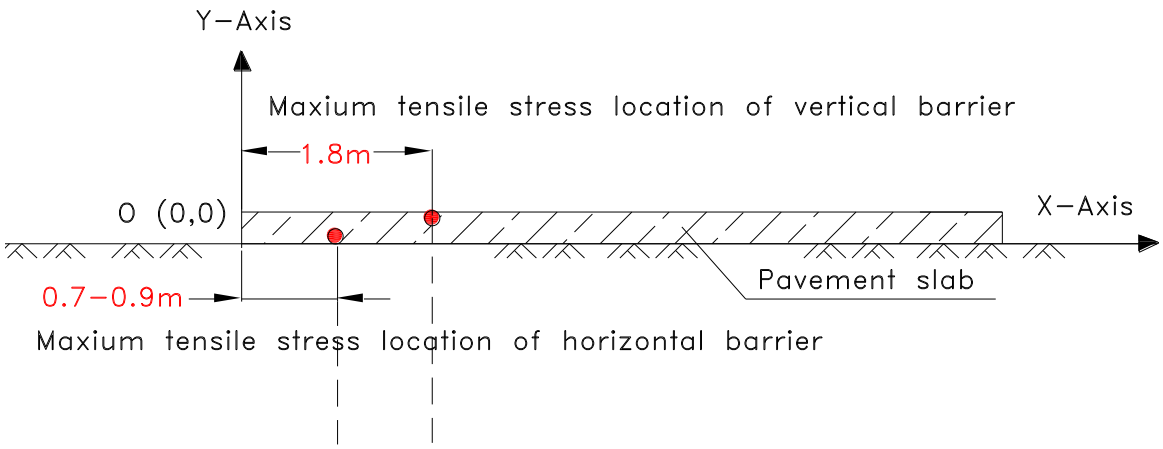

Maximum tensile stree (kPa)		
No crack	324	554
0.5m crack	492	811
1.0m crack	651	1113

Figure 7.17 Maximum Tensile Stresses and their locations

The first point obtained from Table 7.5 and Figure 7.17 is the difference in the maximum tensile stress locations. The locations of the maximum tensile stress are at 1.8m away from the slab edge and at the top area of the pavement slab for the vertical moisture barrier, while they are at around 0.7m-0.9m away from the slab edge and at the bottom of the pavement slab for the horizontal moisture barrier. This is attributed to the settlement of the pavement subgrade soil. For the case of the vertical moisture barrier, the settlement is larger, and the behavior of the pavement slab is similar to a cantilever beam. This leads to the conclusion that the maximum tensile stress lies in the top of pavement slab and close to the center of pavement. For the case of the horizontal moisture barrier, the settlement is smaller. If the pavement slab is assumed to have the same deformation as the subgrade soil, then the horizontal displacement of the bottom area is larger than that of the top area, so the maximum tensile stress occurs at the bottom of the pavement slab and close to the edge.

The second point drawn from Table 7.5 and Figure 7.17 is that the maximum tensile stress for the vertical moisture barrier is significantly higher than that for the horizontal moisture barrier. For the case of the 0.5m crack depth, the maximum tensile stress is 492kPa for the horizontal moisture barrier, while it is 811kPa for the vertical moisture barrier, approximately 65% increase compared to the horizontal barrier. For the case of the 1.0m crack depth, the maximum tensile stress is 651kPa for the horizontal moisture barrier, while it is 1113kPa for the vertical moisture barrier, approximately 71% increase.

Based on the comparisons of settlement and tensile stresses stated above, it is safe to make the conclusion that the horizontal moisture barrier performs better than the vertical moisture barrier for the same crack depth and barrier length.

CHAPTER VIII

CONCLUSIONS AND RECOMMENDATIONS

8.1 Conclusions

In this thesis research study, a new analytical model is developed for predicting tensile stress in unsaturated soils from suction measurement. The model is verified using finite element method and utilizing a laboratory experiment setup developed for this study. The new model is then applied to estimate the depth of cracks developing outside pavement slabs, and the performances of vertical moisture barriers are compared to the performances of horizontal moisture barriers in presence of outside cracks.

The major conclusions and observations from this research are summarized as follows:

- The new model is the first model in the literature which establishes a relationship between tensile stress and suction in expansive soils, in terms of simple material properties and moisture (suction) boundary conditions. The three fundamental variables (i.e., water content, suction and tensile stress) in unsaturated soil mechanics are integrated together, and it can greatly benefit our understanding of the mechanism of crack development.

- The new model can be utilized to estimate the development of cracks using the soil water characteristic curve (SWCC). The change of tensile stress with suction can be obtained from SWCC by the new model. Given the tensile strength of soil, the intersection point between tensile stress and tensile strength is the location where crack occurs.

- The new model can be used to predict the depth of potential cracks for a specific drying time. The key factor in controlling volume change of expansive soils is the determination of the crack depth. For a specific region, the typical drying times can be determined from local or national weather stations or databases. Using the new model, the depth of the potential crack can be estimated. Also, given the specific crack depth, the required drying time can be obtained too. Thus, the new model can provide a theoretical basis for design.

- Laboratory testing setup and protocol is developed to measure tensile stress in drying expansive soils. The new analytical model is verified using the new testing equipment and method. This experiment includes two parts. The first part is to verify the tensile stress at the moisture state close to saturation, and the second one is to verify the tensile stress at optimum water content. Laboratory test results demonstrate that the tensile stresses obtained from the new analytical model are close to the measured tensile stresses.

- The laboratory test results indicate that cracking time increases with the decrease of the diffusion coefficient. There are two soil types used in the experiment. The Lake Hefner soils are low expansive soils with higher diffusion coefficients and the Ardmore soils are medium expansive soils with lower diffusion coefficients. The test results show that the Ardmore soils have higher cracking times than the Lake Hefner soils at both the moisture state close to saturation and optimum water content.

- Another conclusion obtained from the experiments is that the cracking time at the optimum water content is larger than the cracking time at the moisture state close to

saturation. This can probably be attributed to the compaction. In the experiments, the soil sample at OWC is prepared by the standard Proctor compaction. It can be postulated that energy absorbed into soil sample during the compaction is higher for the soil samples at OWC than for the samples tested at the moisture state close to saturation. Therefore, the samples at OWC have stronger resistance against the development of cracks.

- Another conclusion drawn from the experiments is that the diffusion coefficient decreases with the reduction of water content or the increase of suction. For both the Lake Hefner soils and the Ardmore soils, the diffusion coefficients at OWC are approximately 50% of the diffusion coefficient at the moisture state close to saturation.

- The performances of moisture barriers in presence of outside cracks are analyzed using the finite element method. Based on the comparison of the suction, drying shrinkage settlement and tensile stress in the pavement. it is found that the horizontal moisture barrier performs better than vertical moisture barrier for the same crack depth and the same moisture dimension.

8.2 Recommendations for Future Research

As much as this research has setup a bridge between tensile stress and suction for dealing with cracks in expansive soils, it has also raised the need for further study on new research topics. Those problems must be solved if the new model proposed in this research is to become a practical analysis and design tool in dealing with expansive soils. The most significant problems include:

- The new analytical model describes the relationship between suction and tensile stress, and it is verified using the modified restrained ring testing method. However, due to the complexity of the boundary conditions and soil properties in the field, the tensile stress measured by the modified restrained ring method may be different from the tensile stress

measured in the field. Therefore, it is highly desirable that a new method, which can measure the suction and tensile stress in the field, is developed. Then the new analytical model can be verified by the actual field soil suction and tensile stress. This may also create an opportunity to calibrate the new analytical model against field measurement.

- The new model can be used to estimate the suction where the crack occurs, the depth of the potential crack for a given drying time, and the required drying time for a given crack depth. This study only conducts a theoretical analysis, and there is no field data to verify and use in the new model it. In the future research, if typical crack depths for different climatic zones can be obtained, then they can be compared to those predicted by the new model.

- The analysis based on the comparison of suction, settlement and tensile stress shows that horizontal moisture barriers perform better than vertical moisture barriers. This conclusion needs to be further verified in the field.

REFERENCES

AASHTO 334-08 (2008). "Standard Practice for Estimating the Crack Tendency of Concrete," *AASHTO Provisional Standards*, Washington D. C..

Amarisiri, A., Shannon, B., and Kodikara, J. (2013). "Numerical modelling of desiccation cracking in a restrained ring test". *Canadian Geotechnical Journal*, Vol. 51, No. 1, pp. 67–76.

ASTM C1581 (2007). "Standard Test Method for Determining Age at Cracking and Induced Tensile Stress Characteristics of Mortar and Concrete under Restrained Shrinkage1". *American Society for Testing and Materials*.

ASTM D5298-10 (2010). "Standard Test Method for Measurement of Soil Potential (Suction) Using Filter Paper". *American Society for Testing and Materials*.

ASTM D698 (2012). "Standard Test Methods for Laboratory Compaction Characteristics of Soil Using Standard Effort". *American Society for Testing and Materials*.

ASTM D4767-11 (1996). "Standard Test Method for Consolidated Undrained Triaxial Compression Test for Cohesive Soils". *American Society for Testing and Materials*.

Aubeny, C., Lytton, R.L., and Tang, D. (2003). 'Simplified analysis of Moisture Flow through Unsaturated Soil". *Transportation Research Record; Journal of the Transportation Research Board, No. 1821*, pp. 75-82.

Barzegar, A. R., Oades, J. M., Rengasamy, P. and Murray, R. S. (1995). "Tensile Strength of Dry, Remoulded Soils as Affected by Properties of the Clay Fraction". *Geoderma,* Vol. 65, pp.93–108.

Bishop, A. W., and Garga, V. K. (1969). "Drained tests on London clay." *Geotechnique*, Vol. 19(2), pp. 309–312.

Brooks, R.H. and Corey, A.T. (1964). "Hydraulic Properties of Porous Media". *Hydrology Paper* No. 3.

Brutsaert, W. (1967). "Some methods of calculating unsaturated permeability". *Transactions of ASABE*, Vol. 10, pp. 400-404.

Buckingham, E. (1907). "Studies on the movement of soil moisture. influence and connections". *USDA Bureau of Soils, Washington, DC. Rev. Geophys*. Vol. 37, pp.151–172.

Bulut, R., Wray, W.K., and Lytton, R.L. (2001). "Soil suction measurements by filter paper". *Geotechnical Special Publication* No. 115: 243-261.

Bulut, R. and Wray, W.K. (2005). "Free Energy of Water-Suction-in Filter Papers." *ASTM Geotechnical Testing Journal,* Vol. 28, pp. 355-264.

Bulut, R., Chen, L.Z., Mantri, S., Amer, O., Tian, Y. and Zaman, M.(2014). "Drying shrinkage problems in high PI subgrade soils". *ODOT SP&R Item Number 2236*. Oklahoma.

Carneiro, F.L.L.B. and Bracellos, A. (1953). "Concrete tensile strength". *International Association of Testing and Research Laboratories for Materials and Structures*. Bull. No.13.

Carslaw, H.S. and Jaeger, J.G. (1959). *Conduction of Heat in Solids*, Oxford at the Calderon Press.

Carrasquillo, R. L., Nilson, A. H., and Slate, F. O. (1981). "Properties of high-strength concrete subject to short-term loads." Journal of the American Concrete Institute, 78(3), 171-178.

Chen, L. and Bulut, R. (2015). "Numerical Analysis of Vertical Moisture Barriers in Controlling Expansive Soils in Presence of Soil Cracks". *IFCEE 2015*: pp. 2102-2111.

Chen, F. H. (1988). *Foundations on Expansive Soils.* Elsevier Science Publishing Company Inc., New York.

Chertkov, V.Y. (2002). "Modelling cracking stages of saturated soils as they dry and shrink". *Europe Journal of Soil Science*, Vol. 53, March, pp. 105-118.

Costa, S. and Kodikara, J. (2012). "Evaluation of J-integral for clay soils using a new ring test," *Geotechnical Testing Journal*, Vol. 35, No. 6, pp. 1–9.

Covar, A.P. and Lytton, R.L. (2001). "Estimating soil swelling behavior using Soil classification properties". *ASCE Geotechnical Special Technical Publication.* No. 115.

Diyaljee, V.A. and Wiens, B. (1995). "The use of edge membranes in airport pavement rehabilitation." *Proceedings 2nd International Congress on Unsaturated Soils*, Paris, pp. 959–966.

Donaldson, G.W.(1973). "The prediction of differential movement on expansive soils". *Proceedings. 3rd International Conference Expansive Soils*. Haifa, Isarael, pp. 289-293.

El-Garhy, B.M. and Wray, W.K. (2004). "Method for Calculating the Edge Moisture Variation Distance". *Journal of Geotechnical and Geoenvironmental Engineering*. Vol. 130. pp. 945-955.

Fang, H. Y., andChen, W. F. (1971). "New Method for Determination of Tensile Strength of Soils". *Highway Soil Engineering*, 375, pp.62–68.

Farrow, M. and Roland, M. (2006). "Deep Seated Swell in the Eagle Ford Shale Caused by Water Line Leakage". *Proceedings from the Fall Meeting of the American Society of Civil Engineers – Texas.* Section. (2006): 29.

Fredlund, D.G and Rahardjo. (1993). *Soil Mechanics for Unsaturated Soils*. John Wiley and Sons, Inc.

Fredlund, D.G. and Xing, A. (1994). "Equations for the soil-water characteristic curve". *Canadian Geotechnical Journal,* Vol. 31(3), pp. 521-532.

Fredlund, D.G. and Xing, A. and Huang, S. (1994). "Predicting the permeability function for unsaturated soils using the soil-water characteristic curve". *Canadian Geotechnical Journal*, Vol. 31: 533-546.

Fredlund, D.G, Sheng, D. C. and Zhao, J.D. (2011). "Estimation of soil suction from the soil-water characteristic curve". *Canadian Geotechnical Journal,* Vol. 48, pp. 186-198.

Gardner, W.R. (1958). "Mathematics of isothermal water conduction in unsaturated soils". *Highway Research Board Special Report 40, presented at the International Symposium on Physico-Chemical Phenomenon in Soils,* Washington, DC, pp. 78-87.

Gay, D.A. (1994). "Development of a predictive model for pavement roughness on expansive soils." *Dissertation in Texas A&M University*. Texas.

Harry, G.P. and Edward, H.D. (1974). "Elastic Solutions for Soil and Rock Mechanics". *John Wiley & Sons Inc.* ISBN-10: 0471695653

Hegney, M., Hoffman H. (2005). "Using tensiometers for scheduling irrigation for potatoes". *Department of Agriculture and Food*. Retrieved from http://archive.agric.wa.gov.au/PC_92500.html.

Hu, P., Yang, Q. and Li, P.Y. (2010). "Direct and indirect measurement of soil suction in the laboratory". *Electronic Journal of Geotechnical Engineering.* Vol. 15, Bund. A.

Jayatilaka, R., Gay , D.A, Lytton, R.L., and Wray, W.K. (1993). "Effectiveness of Controlling Pavement Roughness due to Expansive Clays with Vertical Moisture Barriers". FHWA/TX-92/1165-2F Research Report, *Texas Transportation Institute*, College Station, Texas.

Kodikara, J, Barbour, S. L. and Fredlund, D. G. (1999). "Changes in clay structure and behaviour due to wetting and drying". *Proceedings 8th Australia New Zealand Conference on Geomechanics*, Hobart, Australian Geomechanics Society, ACT 179-185.

Konrad, J. M., and Ayad, R. (1997) "Desiccation of A Sensitive Clay: Field Experimental Observations." *Canadian Geotechnical Journal*, Vol. 34, pp. 929-942.

Krohn, J.P., and Slosson, J.E. (1980). "Assessment of expansive soils in the United States". *Proceedings, 4th International Conference on Expansive Soils*. Denver, CO, pp.596-608.

Lai, W.M., Rubin, D. and Krempl E. (2009). "Introduction to Continuum Mechanics". Fourth Edition. *Elsevier,* ISBN-10**:** 0750685603.

Luo, R. (2007). *Minimizing Longitudinal Pavement Cracking due to Subgrade Shrinkage*. Ph.D. Dissertation. University of Texas-Austin, Texas.

Luo, R. and Prozzi, J.A. (2009). "Combining Geogrid Reinforcement and Lime Treatment to Control Dry Land Longitudinal Cracking". *Transportation Research Record: Journal of the Transportation Research Board,* pp. 88-96.

Lytton, R.L, Aubeny, C.P and Bulut, R. (2005). "Design procedure for pavements on expensive soils". *TxDOT Report No. 0-4518-1,* Texas Transportation Institute, College Station, Texas.

Mabirizi, D. and Bulut, R. (2010). "Unified testing method for measuring diffusion coefficients for unsaturated soil drying and wetting in laboratory". *Transportation Research Record: Journal of the Transportation Research Board,* No. 2170: pp. 109-118.

Marco, S.D. (1998). "Application of moisture barriers for expansive soils." *Swinburne University of Technology,* Melbourne, Australia.

Mayergoyz, I.D. and Lawson, W.(1996). "Basic Electric Circuit Theory: A One-Semester Text". *Academic Press*. ISBN-13: 978-0124808652

McKeen, R.G. (1981). *Design of Airport Pavements on Expansive Soils*. Report No. DOT/FAA-RD-81-25, Federal Aviation Administration, Washington, D.C.

Mitchell, P.W. (1979). "The structural analysis of footings on expansive soil". *Research Report No.1,* Kenneth W.G Smith and Associates Pty. Ltd,. Newton, South Australia.

Najm, M. A., Mohtar, R. H., Weiss, J. and Braudeau, E. (2009). "Assessing internal stress evolution in unsaturated soils". *Water Resources Research*, VOL. 45, W00C11, pp. 1-18.

Nuhfer, E.B., Proctor, R.J. and Moser, N. (1993). *The Citizen's Guide to Geologic Hazards. AIPG Press:* Arvada, CO; pp. 134.

Olive, W.W., Chleborad, A.F., Frahme, C.W., Schlocker, J., Schneider, R.R., and Schuster, R.L. (1989). "Swelling clays map of the conterminous United States." *U.S. Geological Survey Miscellaneous Investigations Series Map ID-1940*.

Peron, H., Hueckel, T., Laloui, L. and Hu, L.B. (2009). "Fundamentals of desiccation cracking of fined-grained soils: experimental characterization and mechanisms identification". *Canadian Geotechnical Journal*, Vol. 46, pp. 1177-1201.

Pham, H.Q. and Fredlun, D.G. (2005). "A volume-mass constitutive model for unsaturated soils". *Proceedings of the Fifty-Eighth Canadian Geotechnical Conference*, Saskatoon, SK, Vol. 2, pp. 173-181.

Puppala, A.J., Hoyos, L.R., and Saride, S. (2010). "Design of Short, Laterally Loaded Drilled Shafts in High-plastcity Clay". TxDOT 0-6146 Research Report. *The University of Texas-Arlington*.

Rahardjo, H. and Leong, E.C.(2006) "Suction measurements". *Proceedings of the Fourth International Conference on Unsaturated Soils. Geotechnical Special Publication No. 147*. Carefree, AZ, Vol. 1, pp. 81-104.

Rojas E., Romo, M.O., Garnicas, P. and Cervantes, R. (2006). "Analysis of deep moisture barriers in expansive soils. II: Water flow formulation and implementation". *International Journal of Geomechanics*. Vol. 6, No.5, pp. 319-327.

Shannkn, S., Kodikara, J. and Rajeev, P. (2015). "The use of restrained ring test method for soil desiccation studied". *Geotechnical Testing Journal*, Vol. 38, No. 1, pp. 98-112.

Shinde, S.B., Kala, V.U., Kadali, S., Tirumkudulu, M.S. and Singh, D.N. (2012). "A novel methodology for measuring the tensile strength of expansive clays". *Geomechanics and Geoengineering: An International Journal* Vol. 7, pp. 15–25.

Sih, G.C., Michopoulos, J.G. and Chow, S.C. (1968). *Hygro-thermo-Elasticity*, Nartinus Njihoff Publishers.

Springenschmid, R., Breitenbucher, R., and Mangold, M. (1994). "Development of cracking frame and the Temperature Stress Testing Machine", *Thermal Cracking in Concrete at Early Age*, Edited by Springenschmid, R., E&FN Spon, London, pp. 137-144.

Sumarac, D. (2004). "Moisture Diffusion Induced Soil Cracking". *The First International Conference on Computational Mechanics (CM'04)*, Belgrade, Serbia and Montenegro, pp. 1-13.

Tang, G. X. and Graham, J. (2000), "A method for testing tensile strength in unsaturated soils". *Geotechnical Testing Journal*, Vol. 23, No. 3, pp. 377–381.

Timoshenko, S., and Goodier, J. (1987). *Theory of Elasticity*, McGraw-Hill, New York, pp. 608.

Tindall, J. A. and Kunkel, J. R. (1999). *Unsaturated Zone Hydrology*, New Jersey, Prentice Hall.

UMS (2009). "T5/T5x Pressure Transducer Tensiometer User Manual". Version 12/2009.

Van Genuchten, M.Th. (1980). "A Closed-form Equation for Predicting the Hydraulic Conductivity of Unsaturated Soils" *Soil Science Society of America Journal*, Vol. 44, pp. 892-898.

Vanapalli S.K., Fredlund, D.G., Pufahl, D.E., and Clifton, A.W. (1996). "Model for the prediction of shear strength with respect to soil suction". *Canadian Geotechnical Journal*, Vol. 33, pp. 379-392.

Varsei, M., Bourasset, C. M. and Miller, G. A. (2014). "Laboratory Investigation of Desiccation Cracking". *Geo-Congress 2014 Technical Papers*, GSP 234 ASCE.

Venkataramana, K., Rao, B. H., and Singh, D. N. (2009). "A Critical Review of the Methodologies Employed for Determination of Tensile Strength of the Fine-Grained Soils". *Journal Testing Evaluation*, Vo. 37, pp.115–121.

Vishay Precision Group (2013). "Model D4 Data Acquisition Conditioner Instruction Manual". Version 1.34.

Vishay Measurement Group. "Introduction to Strain Gauge Technology". Vishay Measurements Group Educational Program.

Weiss, W., and Furgeson, S. (2001). "Restrained shrinkage testing: The impact of specimen geometry on quality control testing for material performance assessment". *Concreep 6: Creep, Shrinkage, and Curability Mechanic of Concrete and Other Quasi-Brittle Materials*, Elsevier, New York, pp. 645–651.

Weiss, W. J. (1997). "Shrinkage cracking in restrained concrete slabs: Test method, material compositions, shrinkage reducing admixtures, and theoretical modeling". Master thesis, *Northwest University*.

Williams, P.J. (1982). *The Surface of the Earth, an Introduction to Geotechnical Science*. Longman Inc., New York.

Wray, W.K. and Meyer, K.T. (2004). "Expansive Clay Soil-A Widespread and Costly GeoHazard". *GeoStrata, ASCE Geo-Institute*. Vol. 5, No. 4, pp. 24-28.

Wyoming Office of Homeland Security (2011), *Wyoming Multi-Hazard Mitigation Plan*. Boulevard , Cheyenne, WY 82002.

Tian, Yi (2014). "Predicting Unsaturated Soil Moisture Diffusivity Coefficient Using Slope of SWCC and Saturated Permeability Coefficient". *Master thesis, Oklahoma State University.*

Zeh, R. M., and Witt, K. J. (2005). "Suction-Controlled Tensile Strength of Compacted Clays". *16th International Conference Soil Mechanics Geotechnial Engineering*, Vol. 4, Osaka, Japan, pp.2347–2352.

APPENDICES

APPENDIX A

Table A.1 Measured Suctions at OWC for Sample A

Drying Time (min)	Water content (%)	Suction (pF) (Predicted from SWCC)
0	22.5	3.22
10	22.4	3.23
20	22.3	3.24
30	22.2	3.26
40	22.1	3.27
50	22.0	3.28
60	21.9	3.29
70	21.9	3.29
80	21.8	3.30
90	21.7	3.31
100	21.6	3.33
110	21.5	3.34
120	21.4	3.35
130	21.3	3.35
140	21.2	3.36
150	21.2	3.37
160	21.0	3.38
170	21.0	3.39
180	20.9	3.40
190	20.8	3.41
200	20.7	3.42

Drying Time (min)	Water content (%)	Suction (pF) (Predicted from SWCC)
210	20.7	3.42
220	20.6	3.43
230	20.4	3.45
240	20.3	3.46
250	20.2	3.47
260	20.2	3.48
270	20.1	3.48
280	20.0	3.49
290	19.9	3.50
300	19.8	3.51

Table A.2 Measured Suctions at OWC for Sample B

Drying Time (min)	Water content (%)	Suction (pF) (Predicted from SWCC)
0	22.5	3.22
10	22.4	3.23
20	22.4	3.23
30	22.3	3.25
40	22.2	3.26
50	22.0	3.27
60	21.9	3.29
70	21.8	3.30
80	21.7	3.31
90	21.6	3.32
100	21.5	3.33
110	21.4	3.34
120	21.4	3.35
130	21.3	3.36
140	21.2	3.37
150	21.1	3.38
160	21.0	3.39
170	20.8	3.41
180	20.8	3.41
190	20.8	3.41
200	20.6	3.43
210	20.5	3.44
220	20.4	3.45
230	20.3	3.46
240	20.3	3.46
250	20.2	3.47
260	20.1	3.48
270	20.0	3.49
280	19.9	3.50
290	19.8	3.51
300	19.8	3.51

Table A.3 Measured Suctions at OWC for Sample C

Drying Time (min)	Water content (%)	Suction (pF) (Predicted from SWCC)
0	22.5	3.22
10	22.4	3.23
20	22.3	3.25
30	22.2	3.25
40	22.1	3.27
50	22.0	3.28
60	22.0	3.28
70	21.8	3.30
80	21.8	3.30
90	21.7	3.31
100	21.6	3.32
110	21.6	3.32
120	21.5	3.33
130	21.4	3.34
140	21.3	3.35
150	21.3	3.36
160	21.2	3.37
170	21.1	3.38
180	21.0	3.39
190	20.9	3.40
200	20.8	3.41
210	20.7	3.42
220	20.6	3.43
230	20.5	3.44
240	20.4	3.45
250	20.3	3.46
260	20.3	3.46
270	20.2	3.47
280	20.1	3.48
290	20.1	3.48
300	20.0	3.49

Table A.4 Measured Suctions at OWC for Sample D

Drying Time (min)	Water content (%)	Suction (pF) (Predicted from SWCC)
0	24.5	3.40
10	24.4	3.42
20	24.3	3.43
30	24.2	3.44
40	24.2	3.44
50	24.1	3.44
60	24.1	3.45
70	24.0	3.46
80	24.0	3.46
90	23.9	3.46
100	23.8	3.47
110	23.8	3.48
120	23.8	3.48
130	23.8	3.48
140	23.8	3.48
150	23.7	3.49
160	23.6	3.50
170	23.6	3.50
180	23.5	3.51
190	23.5	3.51
200	23.4	3.52
210	23.4	3.52
220	23.3	3.53
230	23.3	3.53
240	23.2	3.54
250	23.2	3.54
260	23.2	3.54
270	23.1	**3.55**
280	23.0	3.56
290	23.0	3.56
300	22.9	3.57

Drying Time (min)	Water content (%)	Suction (pF) (Predicted from SWCC)
310	22.9	3.57
320	22.8	3.58
330	22.8	3.58
340	22.8	3.58
350	22.7	3.59
360	22.6	3.60
370	22.6	3.60
380	22.5	3.61
390	22.5	3.61
400	22.5	3.61
410	22.4	3.61
420	22.4	3.62
430	22.3	3.63
440	22.3	3.63
450	22.3	3.63
460	22.2	3.64
470	22.2	3.64
480	22.1	3.64
490	22.0	3.65
500	22.0	3.65
510	22.0	3.66

Table A.5 Measured Suctions at OWC for Sample E

Drying Time (min)	Water content (%)	Suction (pF) (Predicted from SWCC)
0	24.5	3.40
10	24.4	3.41
20	24.4	3.41
30	24.3	3.42
40	24.3	3.43
50	24.3	3.43
60	24.1	3.44
70	24.1	3.45
80	24.1	3.45
90	24.0	3.46
100	23.9	3.46
110	23.9	3.47
120	23.8	3.47
130	23.8	3.48
140	23.8	3.48
150	23.7	3.49
160	23.6	3.50
170	23.6	3.50
180	23.6	3.50
190	23.5	3.51
200	23.4	3.52
210	23.4	3.52
220	23.4	3.52
230	23.3	3.53
240	23.3	3.53
250	23.2	3.54
260	23.1	3.55
270	23.0	3.56
280	23.0	3.56
290	23.0	3.56

Drying Time (min)	Water content (%)	Suction (pF) (Predicted from SWCC)
300	22.9	3.57
310	22.9	3.57
320	22.8	3.58
330	22.7	3.59
340	22.6	3.60
350	22.6	3.60
360	22.5	3.61
370	22.5	3.61
380	22.4	3.61
390	22.4	3.62
400	22.4	3.62
410	22.3	3.63
420	22.2	3.64
430	22.2	3.64
440	22.2	3.64
450	22.1	3.65
460	22.0	3.65
470	22.0	3.66
480	22.0	3.66
490	21.9	3.66
500	21.9	3.67
510	21.8	3.68
520	21.7	3.68

Table A.6 Measured Suctions at OWC for Sample F

Drying Time (min)	Water content (%)	Suction (pF) (Predicted from SWCC)
0	24.5	3.40
10	24.3	3.42
20	24.3	3.43
30	24.2	3.44
40	24.0	3.45
50	24.0	3.46
60	24.0	3.46
70	23.9	3.47
80	23.9	3.47
90	23.8	3.48
100	23.7	3.49
110	23.7	3.49
120	23.6	3.50
130	23.5	3.51
140	23.5	3.51
150	23.4	3.52
160	23.4	3.52
170	23.3	3.53
180	23.3	3.53
190	23.2	3.54
200	23.1	3.55
210	23.1	3.55
220	23.0	3.56
230	23.0	3.56
240	22.9	3.57
250	22.8	3.58
260	22.7	3.59
270	22.7	3.59
280	22.7	3.59
290	22.6	3.60

Drying Time (min)	Water content (%)	Suction (pF) (Predicted from SWCC)
300	22.6	3.60
310	22.5	3.61
320	22.4	3.62
330	22.4	3.62
340	22.3	3.63
350	22.3	3.63
360	22.2	3.64
370	22.1	3.65
380	22.1	3.65
390	22.0	3.66
400	22.0	3.66
410	21.9	3.67
420	21.8	3.67

Table A.7 Theoretical Suction at OWC (Lake Hefner)

Drying Time (Minute)	Suction @ 1.5cm (pF)	Suction @ 2.5cm (pF)	Average (pF)
0	3.22	3.22	3.22
10	3.22	3.22	3.22
20	3.22	3.22	3.22
30	3.22	3.22	3.22
40	3.23	3.22	3.22
50	3.24	3.22	3.23
60	3.25	3.22	3.23
70	3.26	3.22	3.24
80	3.28	3.22	3.25
90	3.30	3.22	3.26
100	3.33	3.22	3.28
110	3.35	3.22	3.29
120	3.38	3.23	3.30
130	3.41	3.23	3.32
140	3.43	3.23	3.33
150	3.46	3.23	3.35
160	3.49	3.24	3.36
170	3.52	3.24	3.38
180	3.54	3.25	3.39
190	3.57	3.25	3.41
200	3.60	3.26	3.43
210	3.62	3.26	3.44
220	3.65	3.27	3.46
230	3.67	3.28	3.47
240	3.70	3.28	3.49
250	3.72	3.29	3.50
260	3.74	3.30	3.52
270	3.76	3.31	3.54
280	3.79	3.31	3.55
290	3.81	3.32	3.57
300	3.83	3.33	3.58

Table A.8 Theoretical Suction at OWC (Ardmore)

Drying Time (Minute)	Suction @ 1.5cm (pF)	Suction @ 2.5cm (pF)	Average (pF)
0	3.40	3.40	3.40
10	3.40	3.40	3.40
20	3.40	3.40	3.40
30	3.40	3.40	3.40
40	3.40	3.40	3.40
50	3.40	3.40	3.40
60	3.40	3.40	3.40
70	3.40	3.40	3.40
80	3.40	3.40	3.40
90	3.41	3.40	3.40
100	3.41	3.40	3.41
110	3.41	3.40	3.41
120	3.42	3.40	3.41
130	3.43	3.40	3.41
140	3.43	3.40	3.42
150	3.44	3.40	3.42
160	3.45	3.40	3.42
170	3.46	3.40	3.43
180	3.47	3.40	3.43
190	3.48	3.40	3.44
200	3.49	3.40	3.45
210	3.50	3.40	3.45
220	3.51	3.40	3.46
230	3.52	3.40	3.46
240	3.54	3.40	3.47
250	3.55	3.41	3.48
260	3.56	3.41	3.48
270	3.57	3.41	3.49
280	3.59	3.41	3.50

Drying Time (Minute)	Suction @ 1.5cm (pF)	Suction @ 2.5cm (pF)	Average (pF)
290	3.60	3.41	3.50
300	3.61	3.41	3.51
310	3.62	3.41	3.52
320	3.64	3.41	3.53
330	3.65	3.42	3.53
340	3.66	3.42	3.54
350	3.68	3.42	3.55
360	3.69	3.42	3.56
370	3.70	3.42	3.56
380	3.71	3.43	3.57
390	3.73	3.43	3.58
400	3.74	3.43	3.59
410	3.75	3.43	3.59
420	3.76	3.44	3.60
430	3.78	3.44	3.61
440	3.79	3.44	3.61
450	3.80	3.45	3.62
460	3.81	3.45	3.63
470	3.82	3.45	3.64
480	3.83	3.46	3.64
490	3.84	3.46	3.65
500	3.86	3.46	3.66
510	3.87	3.47	3.67
520	3.88	3.47	3.67
530	3.89	3.47	3.68
540	3.90	3.48	3.69
550	3.91	3.48	3.69
560	3.92	3.49	3.70

Table A.9 Suctions at the State Close to Saturation for Sample G

Drying Time (min)	Measured Suction (kPa)	Measured Suction (pF)	Theoretical Suction (pF)
0	3.7	1.57	1.57
10	4	1.60	1.57
20	4.7	1.67	1.58
30	5.4	1.73	1.61
40	6.1	1.79	1.64
50	6.7	1.83	1.68
60	7.3	1.86	1.72
70	8	1.90	1.77
80	8.9	1.95	1.82
90	10.9	2.04	1.87
100	12.8	2.11	1.92
110	14.6	2.16	1.97
120	16.5	2.22	2.02
130	18.7	2.27	2.07
140	20.9	2.32	2.12
150	23.4	2.37	2.17

Table A.10 Suctions at the State Close to Saturation for Sample H

Drying Time (min)	Measured Suction (kPa)	Measured Suction (pF)	Theoretical Suction (pF)
0	3.4	1.53	1.53
10	3.9	1.59	1.53
20	4.5	1.65	1.54
30	5.2	1.72	1.57
40	5.7	1.76	1.60
50	6.6	1.82	1.64
60	7.1	1.85	1.69
70	7.7	1.89	1.73
80	8.4	1.92	1.78
90	9.3	1.97	1.84
100	10.1	2.00	1.89
110	11.0	2.04	1.94
120	11.8	2.07	1.99
130	12.7	2.10	2.04
140	13.7	2.14	2.09
150	14.7	2.17	2.13
160	15.9	2.20	2.18
170	17.1	2.23	2.23
180	18.4	2.26	2.27
190	21.3	2.33	2.31
200	23.0	2.36	2.35

Table A.11 Suctions at the State Close to Saturation for Sample I

Drying Time (min)	Measured Suction (kPa)	Measured Suction (pF)	Theoretical Suction (pF)
0	3.2	1.51	1.51
10	3.6	1.56	1.51
20	3.9	1.59	1.52
30	4.2	1.62	1.55
40	4.5	1.65	1.58
50	4.8	1.68	1.62
60	5.3	1.72	1.67
70	5.7	1.76	1.72
80	6.2	1.79	1.77
90	7.8	1.89	1.82
100	8.4	1.92	1.87
110	9.1	1.96	1.92
120	9.5	1.98	1.97
130	10.1	2.00	2.02
140	10.9	2.04	2.07
150	11.5	2.06	2.12
160	12.2	2.09	2.16
170	13.1	2.12	2.21
180	13.8	2.14	2.25

Table A.12 Suctions at the State Close to Saturation for Sample J

Drying Time (min)	Measured Suction (kPa)	Measured Suction (pF)	Theoretical Suction (pF)
0	6.0	1.78	1.78
10	6.3	1.80	1.78
20	6.6	1.82	1.78
30	7.3	1.86	1.78
40	7.7	1.89	1.79
50	8.2	1.91	1.79
60	8.4	1.92	1.80
70	9.0	1.95	1.81
80	9.4	1.97	1.83
90	9.8	1.99	1.84
100	10.3	2.01	1.86
110	10.7	2.03	1.88
120	11.1	2.05	1.90
130	11.3	2.05	1.93
140	11.8	2.07	1.95
150	12.0	2.08	1.97
160	12.5	2.10	2.00
170	12.9	2.11	2.02
180	13.5	2.13	2.04
190	14.0	2.15	2.07
200	14.7	2.17	2.09
210	15.4	2.19	2.12
220	15.9	2.20	2.14
230	16.5	2.22	2.16
240	17.2	2.24	2.19
250	17.9	2.25	2.21
260	18.5	2.27	2.24
270	19.2	2.28	2.26
280	19.8	2.30	2.28

Drying Time (min)	Measured Suction (kPa)	Measured Suction (pF)	Theoretical Suction (pF)
290	20.6	2.31	2.30
300	21.4	2.33	2.33
310	22.4	2.35	2.35
320	23.0	2.36	2.37
330	23.8	2.38	2.39
340	24.6	2.39	2.41

Table A.13 Suctions at the State Close to Saturation for Sample K

Drying Time (min)	Measured Suction (kPa)	Measured Suction (pF)	Theoretical Suction (pF)
0	6.8	1.83	1.83
10	7.3	1.86	1.83
20	8.4	1.92	1.83
30	9.4	1.97	1.83
40	9.5	1.98	1.84
50	10.6	2.03	1.84
60	11.1	2.05	1.85
70	12.1	2.08	1.86
80	12.8	2.11	1.88
90	13.2	2.12	1.89
100	13.9	2.14	1.91
110	14.5	2.16	1.93
120	15	2.18	1.95
130	15.6	2.19	1.98
140	15.9	2.20	2.00
150	16.5	2.22	2.02
160	17.1	2.23	2.04
170	17.7	2.25	2.07
180	18.1	2.26	2.09
190	18.4	2.26	2.11
200	19	2.28	2.14
210	19.6	2.29	2.16
220	20.3	2.31	2.19
230	20.7	2.32	2.21
240	21.2	2.33	2.23
250	21.7	2.34	2.26
260	22.5	2.35	2.28
270	23.3	2.37	2.30
280	24.1	2.38	2.33

Table A.14 Suctions at the State Close to Saturation for Sample L

Drying Time (min)	Measured Suction (kPa)	Measured Suction (pF)	Theoretical Suction (pF)
0	5.2	1.72	1.72
10	5.6	1.75	1.72
20	5.9	1.77	1.72
30	6.2	1.79	1.72
40	6.4	1.81	1.73
50	6.9	1.84	1.73
60	7.3	1.86	1.74
70	7.4	1.87	1.75
80	7.7	1.89	1.77
90	8.4	1.92	1.79
100	8.7	1.94	1.80
110	8.9	1.95	1.83
120	9.5	1.98	1.85
130	9.8	1.99	1.87
140	10.1	2.00	1.89
150	10.4	2.02	1.92
160	11.1	2.05	1.94
170	11.4	2.06	1.96
180	11.9	2.08	1.99
190	12.4	2.09	2.01
200	12.8	2.11	2.04
210	13.4	2.13	2.06
220	13.8	2.14	2.09
230	14.1	2.15	2.11
240	14.7	2.17	2.13
250	15.3	2.18	2.16
260	15.9	2.20	2.18
270	16.3	2.21	2.21

Drying Time (min)	Measured Suction (kPa)	Measured Suction (pF)	Theoretical Suction (pF)
280	16.9	2.23	2.23
290	17.4	2.24	2.25
300	18.1	2.26	2.27
310	18.8	2.27	2.30
320	19.3	2.29	2.32
330	20.0	2.30	2.34

Table A.15 Theoretical Tensile Stress for the Soil Samples at OWC

Time (min)	Sample A (kPa)	Sample B (kPa)	Sample C (kPa)	Sample D (kPa)	Sample E (kPa)	Sample F (kPa)
0	0	0	0	0	0	0
10	0	0	0	0	0	0
20	0	0	0	0	0	0
30	0	0	0	0	0	0
40	1	1	1	0	0	0
50	2	2	2	0	0	0
60	4	4	4	0	0	0
70	6	6	6	0	0	0
80	9	9	9	1	1	1
90	12	12	12	1	1	1
100	15	15	15	2	2	2
110	19	19	19	3	3	3
120	23	23	23	4	4	4
130	26	26	26	5	5	5
140	31	31	31	6	6	6
150	35	35	35	8	8	8
160	39	39	39	9	9	9
170	43	43	43	11	11	11
180	48	48	48	13	13	13
190	52	52	52	15	15	15
200	56	56	56	17	17	17
210	61	61	61	19	19	19
220	65	65	65	21	21	21
230	69	69	69	24	24	24

Time (min)	Sample A (kPa)	Sample B (kPa)	Sample C (kPa)	Sample D (kPa)	Sample E (kPa)	Sample F (kPa)
240	74	74	74	26	26	26
250	78	78	78	29	29	29
260	82	82	Crack	31	31	31
270	88	Crack		34	34	34
280	90			36	36	36
290	Crack			39	39	39
300				41	41	41
310				44	44	44
320				47	47	47
330				49	49	49
340				52	52	52
350				55	55	55
360				58	58	58
370				60	60	60
380				63	63	63
390				66	66	66
400				69	69	Crack
410				71	71	
420				74	74	
430				77	77	
440				80	80	
450				82	82	
460				85	85	
470				88	88	
480				91	91	
490				93	93	
500				Crack	96	
510					Crack	

Crack: Tensile stress begins to go down at the point of crack

Table A.16 Theoretical Tensile Stress for the Soil Samples Close to Saturation

Time (min)	Sample G (kPa)	Sample H (kPa)	Sample I (kPa)	Sample J (kPa)	Sample K (kPa)	Sample L (kPa)
0	0	0	0	0	0	0
10	0	0	0	0	0	0
20	1	1	1	0	0	0
30	2	2	2	0	0	0
40	4	4	4	0	0	0
50	6	6	6	1	1	1
60	8	8	8	2	2	2
70	11	11	11	3	3	3
80	14	14	14	4	4	4
90	16	17	17	5	5	5
100	19	19	19	7	7	7
110	22	22	22	8	8	8
120	25	25	25	10	10	10
130	Crack	27	28	12	12	12
140		30	30	14	13	14
150		33	33	15	15	16
160		35	35	17	17	18
170		38	Crack	19	19	19
180		40		21	21	21
190		Crack		23	23	23
200				25	25	25
210				27	27	27
220				29	28	29
230				31	30	31

Time (min)	Sample G (kPa)	Sample H (kPa)	Sample I (kPa)	Sample J (kPa)	Sample K (kPa)	Sample L (kPa)
240				33	32	33
250				35	34	35
260				36	36	37
270				38	Crack	39
280				40		41
290				42		43
300				44		44
310				46		Crack
320				Crack		

Crack: Tensile stress begins to go down at the point of crack

Table A.17 Strain and Stress for Sample A

Time (min)	Strain Gauge 1 (Micron)	Strain Gauge 2 (Micron)	Stress 1 (kPa)	Stress 2 (kPa)
0	1	0	0	0
10	4	9	1	3
20	7	21	2	6
30	10	48	3	14
40	17	69	5	21
50	23	66	7	20
60	39	81	12	24
70	48	90	14	27
80	67	93	20	28
90	79	120	24	36
100	89	129	27	39
110	97	138	29	41
120	110	144	33	43
130	125	147	38	44
140	130	153	39	46
150	142	159	43	48
160	152	168	46	50
170	166	177	50	53
180	178	183	53	55
190	191	192	57	58
200	203	192	61	58
210	216	186	65	56
220	229	195	69	59
230	243	195	73	59
240	257	207	77	62
250	272	228	82	68
260	283	243	85	73
270	296	258	89	77
280	307	212	92	64
290	280	200	84	60
300	175	198	53	59

Table A.18 Measured Tensile Stress for the Soil Samples at OWC

Time (min)	Sample A (kPa)	Sample B (kPa)	Sample C (kPa)	Sample D (kPa)	Sample E (kPa)	Sample F (kPa)
0	0	0	0	0	0	0
10	2	4	4	0	3	1
20	4	4	9	3	5	3
30	9	6	14	4	6	4
40	13	9	16	4	7	5
50	13	13	18	6	8	7
60	18	16	19	7	10	9
70	21	20	22	9	12	10
80	25	24	24	12	15	12
90	30	27	28	15	18	14
100	33	30	32	18	21	15
110	35	33	37	22	23	17
120	38	35	41	24	25	19
130	41	38	45	26	29	21
140	42	41	47	28	32	24
150	45	44	53	31	35	25
160	48	47	55	34	39	26
170	52	51	59	36	41	27
180	54	53	63	38	43	28
190	57	55	65	38	45	31
200	59	57	69	40	48	33
210	60	62	72	42	52	36
220	64	64	74	44	54	39
230	66	66	75	46	56	43
240	70	69	77	47	59	45
250	75	69	79	50	62	48
260	79	70	55	52	64	51

Time (min)	Sample A (kPa)	Sample B (kPa)	Sample C (kPa)	Sample D (kPa)	Sample E (kPa)	Sample F (kPa)
270	83	45	53	55	66	52
280	85	43	/	56	69	54
290	74	/		58	70	56
300	58			60	71	58
310	/			61	74	59
320				62	75	60
330				64	76	61
340				65	77	61
350				67	79	62
360				69	80	63
370				70	81	63
380				71	82	64
390				73	83	65
400				75	85	53
410				77	86	45
420				78	87	/
430				80	88	
440				81	89	
450				82	91	
460				84	91	
470				86	92	
480				87	93	
490				89	93	
500				88	94	
510				69	84	

Table A.19 Measured Tensile Stress for the Soil Samples Close to Saturation

Time (min)	Sample G (kPa)	Sample H (kPa)	Sample I (kPa)	Sample J (kPa)	Sample K (kPa)	Sample L (kPa)
0	0	0	0	0	0	0
10	3	2	2	2	1	2
20	5	4	3	3	2	4
30	7	6	6	4	4	6
40	10	11	7	6	7	7
50	13	15	8	8	8	10
60	15	19	9	9	9	12
70	17	22	10	11	11	13
80	18	26	12	12	12	14
90	20	29	14	14	13	14
100	22	30	15	15	14	16
110	25	33	17	16	16	17
120	27	35	20	17	17	20
130	27	35	24	18	18	22
140	26	36	27	19	18	23
150	24	36	29	20	18	25
160	/	37	32	21	20	25
170	/	39	32	23	21	25
180		40	30	23	22	28
190		40	/	24	23	30
200		33	/	25	25	31
210		/		26	26	33
220		/		26	28	35
230				27	30	36
240				29	33	37
250				30	37	38

Time (min)	Sample G (kPa)	Sample H (kPa)	Sample I (kPa)	Sample J (kPa)	Sample K (kPa)	Sample L (kPa)
260				31	39	39
270				31	37	40
280				32	35	41
290				33	/	42
300				35	/	42
310				36		36
320				33		35

APPENDIX B

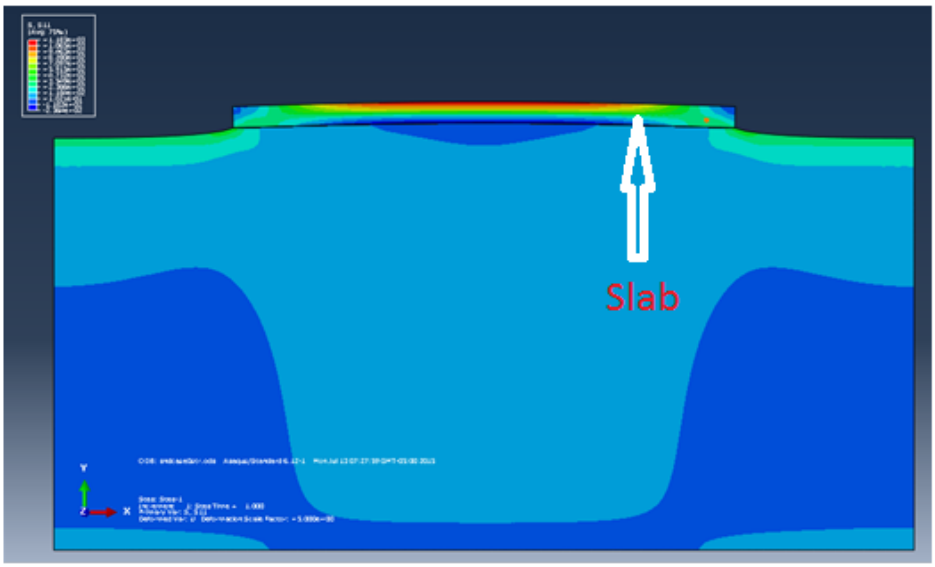

Figure B.1 The Profile of Tensile Stress in the Pavement Slab for Case 1

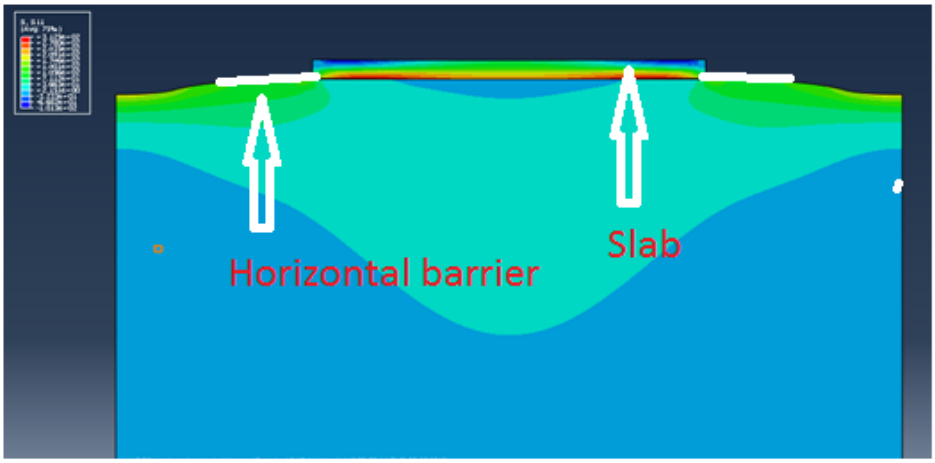

Figure B.2 The Profile of Tensile Stress in the Pavement Slab for Case 2

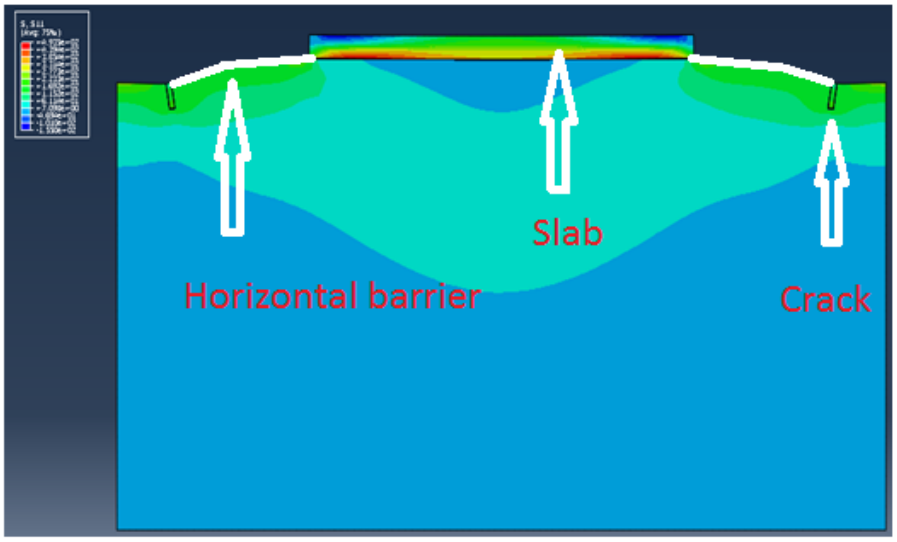

Figure B.3 The Profile of Tensile Stress in the Pavement Slab for Case 3

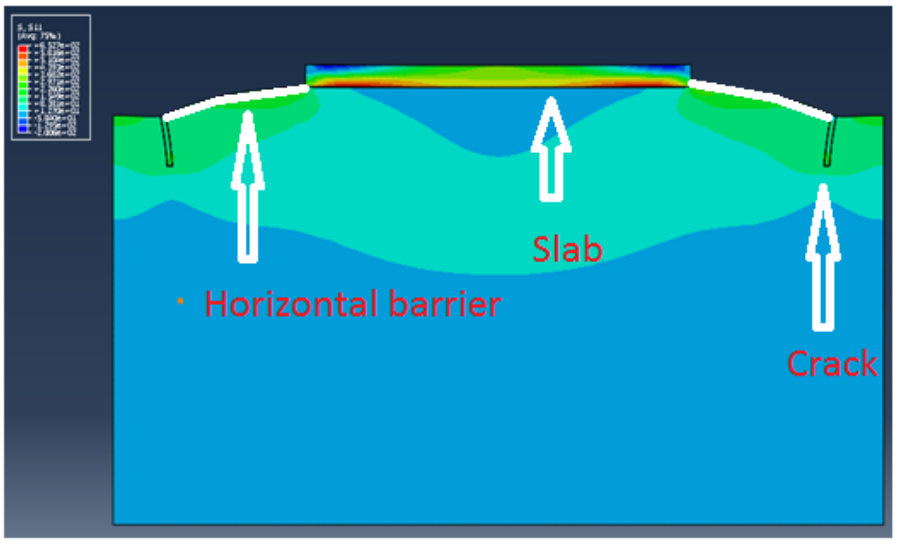

Figure B.4 The Profile of Tensile Stress in the Pavement Slab for Case 4

VITA

LIZHOU CHEN

Candidate for the Degree of

Doctor of Philosophy

Thesis: DEVELOPMENT OF A NEW TENSILE STRESS MODEL FOR EXPANSIVE SOILS

Major Field: Geotechnical Engineering

Biographical:

Education:

Completed the requirements for the Doctor of Philosophy in geotechnical engineering at Oklahoma State University, Stillwater, Oklahoma in December, 2015.

Completed the requirements for the Master of Science in geotechnical engineering at Michigan State University, East Lansing, Michigan in 2007.

Completed the requirements for the Master of Science in geotechnical engineering at Tongji University, Shanghai, China in 1999.

Completed the requirements for the Bachelor of Science in geotechnical engineering at Tongji University, Shanghai, China in 1999.

Experience:

Company: Building & Science Institute in Fujian, China
Time: 04/2000-07/2006, 11/2007-07/2012
Title: Associate department manager, senior engineer, professional engineer

Professional Memberships:

ASCE, Phi Kappa Phi